FACULDADE DE ENGENHARIA DA UNIVERSIDADE DO PORTO

Autonomous Identification and Tracking of Thermoclines

Hugo Miguel Gomes Antunes

Mestrado Integrado em Engenharia Eletrotécnica e de Computadores

Supervisor: Nuno Alexandre Cruz

July, 2019

Resumo

Toda a recolha de dados de características de águas oceânicas é um trabalho árduo e crucial. Árduo tendo em conta à dificuldade de obter esses mesmos dados, dado às condições desfavoráveis. Requer equipamentos que sejam fiáveis nas medições das características desejadas e robustos, isto é, equipamentos que sejam capazes de suportar as condições desfavoráveis e variáveis em termos espaciais e temporais. Devido a essas mesmas mudanças, espaciais e temporais, os métodos tradicionais não se revelam os mais adequados, dado que não têm a capacidade suficiente de amostrar as medidas de características dinâmicas de processos oceanográficos. Deste modo, para obter essas mesmas medidas, a utilização de sistemas robóticos autónomos revela-se importante. Com estes assegura-se uma amostragem mais rápida, mais eficaz e sistemática, não estando sujeita a erros de intervenção humana. A recolha de dados é então um trabalho crucial para perceber e compreender como é que eventuais processos oceanográficos surgem e variam temporal e espacialmente. Assim, este trabalho propõe a implementação de um algoritmo que identifica e rastreia o ponto de maior gradiente de temperatura na termoclina usando um *profiler* vertical autónomo.

A termoclina é a camada de água que separa a camada *mixed layer* da camada *deep-water layer*. Nesta camada ocorre uma mudança brusca de temperatura com o aumento da profundidade. Por isso, o gradiente de temperatura em relação à profundidade é o mais alto em relação às restantes camadas da coluna de água. As características da termoclina estão fortemente relacionadas com a atividade biológica e a propagação de som.

Com o uso de veículos subaquáticos autónomos (AUVs), é possível adquirir grandes conjuntos de dados de forma mais eficiente. Também é possível o processamento de dados em tempo-real com o objetivo de adaptar o comportamento de um veículo e assim proceder à deteção e ao rastreamento de uma característica específica com maior eficácia. Um *profiler* vertical é um tipo de AUV projetado para operar predominantemente na direção vertical. Portanto, é uma plataforma muito bem adaptada para implementar algoritmos de deteção e rastreamento de termoclinas.

Neste trabalho, propomos a implementação de um algoritmo que realiza o rastreamento da termoclina no ponto de maior gradiente de temperatura de uma forma completamente autónoma. Como já foi referido anteriormente, para realizar este *tracking*, usamos um *profiler* vertical já desenvolvido num trabalho anterior. Para obter medidas instantâneas do gradiente de temperatura, aproveitou-se a geometria e a orientação do *profiler* para instalar um conjunto de sensores em diferentes locais do corpo do veículo. Para manter o veículo na região da termoclina usou-se o método de controlo *Extremum Seeking Control* (ESC).

ESC é um método de controlo em que o principal objetivo é colocar a variável de entrada no valor correspondente ao extremo da variável de saída (máximo ou mínimo). Uma das grandes vantagens deste método é que não é necessário saber o modelo do sistema, mas sim saber que existe um extremo local. Assim, este método requer medidas instantâneas do gradiente de temperatura com o propósito de maximizar esse valor. Maximizando o valor do gradiente, este método de controlo gera a profundidade respetiva ao máximo. Por isso, é necessário um veículo que seja capaz de seguir referências de profundidade, requisito devidamente cumprido pelo *profiler*.

Abstract

All data acquired from oceanic water features is hard and crucial work. Its hard due to the difficulty to obtain a specific data given the unfavorable conditions. It requires, therefore, equipment that are reliable in the measurements of the desired characteristics and robust equipment, that is to say, equipment that are capable of withstanding unfavorable and variable conditions in space and time terms. Due to these same space and time changes, the traditional methods do not prove to be the most adequate, because these methods do not have sufficient capacity to sample measurements of the dynamic characteristics of oceanographic processes. Thus, to obtain such measurements, the use of the autonomous robotic systems proves to be important. With these systems it is ensured a faster, more efficient and systematic sampling and is not subject to human error. The data acquisition is then a crucial work to understand how oceanographic process happens and varies in time and space. Therefore, we propose to carry out the detection and tracking of the thermocline with an autonomous vertical profiler.

The thermocline is a water layer that separates the mixed layer from the deep-water layer. In the thermocline, the gradient of temperature with respect to depth is higher than in the rest of the water column. The characteristics of the thermocline are strongly related to biological activity and sound propagation, therefore, there is a great interest in the study of its spatial distribution and dynamics.

With the use of Autonomous Underwater Vehicles (AUVs), it is possible to acquire large set of underwater data very efficiently. It is also possible to process specific data in real time in order to adapt the behavior of a vehicle with greater effectiveness. A vertical profiler is a particular type of AUV designed to operate predominantly in the vertical direction. It is, in this way, a platform very well suited to implement algorithms for the detection and tracking of thermoclines.

In this work, we propose an implementation in which it is possible to carry out the tracking of the thermocline at its point of highest temperature gradient in a completely autonomous way. As already was described, to perform this tracking, we use a small vertical profiler developed earlier. To obtain instant measurements of the vertical temperature gradient, we take advantage of the profiler geometry and orientation to install temperature sensors at different locations of the body. We use Extremum Seeking Control (ESC) scheme to maintain the vehicle in the thermocline region.

ESC is a control method with the main purpose of placing the input variable in a specific value that corresponds to the output variable in an extremum value (maximum or minimum). One of the advantages of this method is that it is not necessary to know an exact model of the system, but mainly that there is a local extremum. Thus, this method requires instantaneous measurements of the temperature gradient with the purpose to maximize this value. The ESC method maximizes the temperature gradient, generating the reference depth corresponding to this maximum. Thus, it is necessary a vehicle capable of following depth references, a requirement duly verified by the profiler.

Agradecimentos

Ao professor Nuno Cruz, um especial agradecimento pela excelente orientação, pelas críticas, bem como por todos os momentos em que prontamente se disponibilizou para partilhar todo o seu conhecimento.

Quero também agradecer a todos os meus amigos que fiz durante estes 5 anos de faculdade por todos os momentos de descontração, amizade e estudo.

Não posso deixar de agradecer também a todos os meus amigos da equipa futebol. Contribuíram com imensos momentos de descontração, mas tenho de lhes agradecer todos os ensinamentos que me deram, bem como uma paciência enorme para comigo.

Agradeço também aos meus amigos mais próximos, que direta ou indiretamente, fizeram parte deste caminho e da elaboração deste projeto.

Por último, agradecer à minha família e de uma forma especial aos meus pais e à minha irmã, por todo o apoio e o acompanhamento ao longo desta etapa e da minha vida. A eles um especial obrigado, este sucesso também é vosso!

Hugo Antunes

"The only way of discovering the limits of the possible is to venture a little way past them into the impossible."

Arthur C. Clarke

Contents

List of Figures

List of Tables

Abbreviations

AUV	Autonomous Underwater Vehicle
CTD	Conductivity, Temperature and Depth
DOF	Degree of Freedom
ESC	Extremum Seeking Control
GDEM	Generalized Digital Environmental Model
HPF	High-Pass Filter
LPF	Low-Pass Filter
PD	Proportional-Derivative

Chapter 1

Introduction

1.1 Context

1.1.1 The Thermocline

The vertical profiles of water temperature have a seasonal variation. Typically, during the winter, the considered profiles have one layer where the temperature is vertically uniform from the surface to bottom [7]. In contrast, during the summer this profile has a multilayer (mixed layer, thermocline, deep water layer) [7]. Figure 1.1 represents the different vertical temperature profiles.

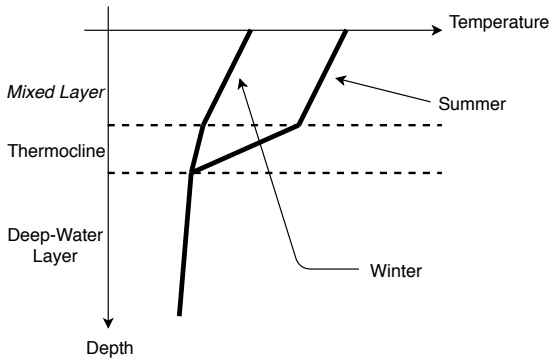

Figure 1.1: Simplified vertical ocean profiles of temperature

The thermocline is the water layer where water temperature decreases rapidly with increasing depth, and it can be found in the oceans and even in rivers and lakes. In other words, in this layer, the vertical temperature gradient is higher than in the rest of the water column. This layer separates the warmer surface from the cold deep water. The depth and thickness of the thermocline vary according to atmospheric conditions, i.e., differ depending on the season.

Above the thermocline, the mixed layer, near the surface, is the layer most influenced by the atmospheric conditions (wind, rain and solar heat), therefore in this layer, the temperature varies throughout the year. Due to the dynamic of the surface waters (wind and wave action), the water is mixed in such a way that the gradient is small. Below the thermocline, the deep-water layer, the variation of temperature with depth is approximately null.

The thermocline is most usually associated to the ocean basins, including both the seasonal occurrences in shallow waters, with very short spatial scales, and the "permanent" thermocline is present all the time in most world's oceans between 200 and 1000 meters of depth [27]. In polar waters, there is no "permanent" thermocline [27]. In fresh water, particularly in large lakes and dam reservoirs, it is also possible to find temporal variations in thermoclines [18].

In the thermocline, the gradient of the speed of sound is negative, in this way, it can reflect active sonar and other acoustic signals, and affects the sound propagation. For this reason, the characterization of the thermocline is essential since it can help in planning military tactics and as well as it plays an important role in underwater communications [12, 32]. This characterization is also relevant in marine biology. The thermocline traps a high-nutrient column of water, essential for marine life [31]. Thus, the characterization of thermoclines has economic interest since it can be used to mapping fishing locations and their's seasonality.

1.1.2 Tracking of Thermoclines

Autonomous underwater vehicles (AUVs) are extremely versatile and have low operational costs [12]. AUVs have different applications, divided into the following areas: commercial, research, hobby, and military. In most current applications, AUVs are programmed to follow geo-referenced paths while collecting relevant data [12]. However, there may be missions where the vehicle is not pre-programmed to follow any reference and goes in search of a particular characteristic. In this way, we propose to use a vertical profiler that searches for the highest temperature variation in the thermocline.

Trough interfaces, graphical or not, humans can choose different tasks for AUVs. These interfaces have a different set of options, such as creating follow-path missions, setting way-points, abort missions, or sending other messages to the vehicles. The vehicles can also send messages to the interfaces, for example, through acoustic communications, that way, the operator can get a sense of the position of the vehicle. However, these communications provide a limited baud rate and range and have a particularly poor performance in coastal/shallow waters.

To detect and characterize the thermocline, the use of AUVs is one of the most used forms. To perform this task, the AUVs include a temperature sensor. Usually, these AUVs integrate a CTD sensor. CTD is an oceanography instrument used to measure conductivity, temperature, and pressure of seawater.

To track and characterize the thermocline, the AUV should be programmed to follow a *yo-yo* pattern [13]. This method requires human intervention, for instance, by introducing the thresholds around the thermocline [38].

1.2 Motivation

The characteristics of the thermocline are strongly related to biological activity and sound propagation, therefore there is a great interest in the study of its spatial distribution and dynamics.

With the use of AUVs, it is possible to acquire large sets of underwater data very efficiently. It is also possible to process specific data in real time in order to adapt the behavior of a vehicle and carry out the tracking of a particular characteristic with greater effectiveness. A vertical profiler is a particular type of AUV designed to operate predominantly in the vertical direction. It is, therefore, a platform very well suited to implement algorithms for the detection and tracking of thermoclines.

In this work, we propose an implementation in which it is possible to carry out the tracking of a thermocline at its point of highest temperature gradient. To perform this tracking, we use a small vertical profiler developed earlier and described in [24]. To obtain instant measurements of the vertical temperature gradient, we take advantage of the profiler geometry and orientation to install temperature sensors at different locations of the body.

1.3 Goals

This work intends to realize the tracking of thermoclines that vary temporal and spatially with a vertical profiler using Extremum Seeking Control. Through this implementation, we propose to recreate a vertical temperature profile with different parameters that represent each layer of the water column, for example, the maximum gradient temperature of the thermocline and respectively its depth.

Through the use of Extremum Seeking Control and the explanation of each block, the tuning of the parameters and their physical meaning will allow other researchers to adapt our implementation of ESC to their specific need in tracking the same, or other extrema.

1.4 Document Organization

The present document describes the work done during the development of an implementation that can control the depth of the profiler using Extremum Seeking Control, the simulations and tests performed, and the conclusions obtained. Chapter 2 provides state of the art in terms of thermoclines representation, data acquisition and sampling and methods for depth control. Chapter 3, initially, describes the assumptions that were considered. Furthermore, the vehicle model and methods or algorithms are presented. Chapter 4 presents our strategy for the development of a parametric model that represents the vertical temperature gradient. Chapter 5 discusses the number of sensors and the separation between them so that the measurements are less subject to error. In chapter 6, we detail the algorithm designed for the implementation of the maximum gradient and, in this way, the control of the vertical position of the profiler. Chapter 7 shows different results of the ESC with the purpose to evaluate the performance of this model-based method. Finally, in chapter 8, the results are discussed, and some suggestions for future work are presented.

Chapter 2

State of the Art

Taking into account that this work seeks to perform detection and tracking of thermoclines, the search of how this objective can be realized is essential. Thus, the search for projects that have already performed this tracking is important. New methods of how to achieve this goal will also be evaluated. However, it is also necessary to analyze different models that represent the water column so that the implementation of thermocline tracking find the parameters that represent each layer. So that the detection and tracking of thermoclines and construction of the model are performed, the vehicle must incorporate a set of sensors. In this way, an analysis of works that use the information of the sensors will be done. This analysis aims to find out how the vehicle's behavior can be adapted in real time and how the measurements of oceanic characteristics are obtained. Figure 2.1 shows the division and interconnection between the different research areas of this work.

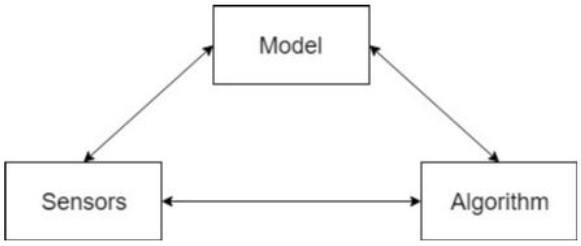

Figure 2.1: Three main areas of research related to this dissertation

2.1 Ocean Temperature Models

There are two approaches of representing the thermocline, through non-parametric or parametric models. The first one by analyzing the profiles obtained by oceanographic institutions [16, 7, 6] or

measures of temperature and depth, usually obtained using autonomous vehicles [13, 38], obtains a vertical profile or graph of temperature against depth.

The other approach, with a set of parameters, can generate a representation of the different oceanic water layers. The objective of this approach is to represent the thermocline and the other layers with a minimum set of parameters without missing detail. Therefore, any parametric representation would allow a dramatic reduction on data warehousing requirements.

2.1.1 Non-parametric Models

The first works used a set of data provided by oceanographic institutions aiming to represent the different layers of the oceanic water [16, 7, 6]. This data can be obtained with underwater vehicles, which have a set of sensors to measure the temperature and depth, like a CTD sensor [13, 12]. Both results show that there is a stratification on the oceanic water. This stratification is more visible during the summer because the first layer of the oceanic water, the mixed layer, is influenced by the air temperature [7]. If the air temperature is cold, this layer has a temperature near to air temperature, and for this reason, a marked decrease for the other layer does not occur.

The majority of the works involving the representation and tracking of the thermocline construct a set of graphs from the observed data, a relation between temperature and depth, and not a parametric model. Figure 2.2 shows an example of a temperature profile measured by an AUV with a CTD sensor.

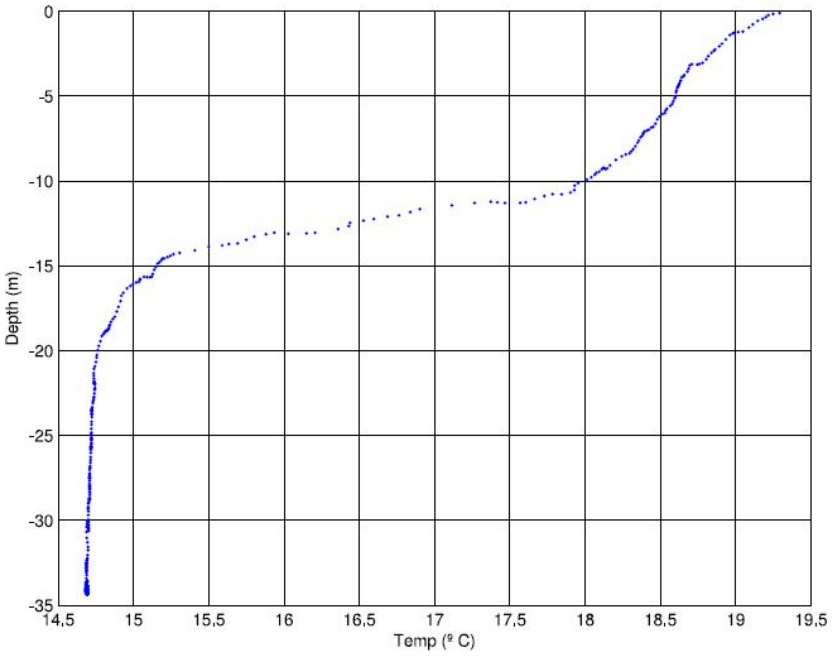

Figure 2.2: Temperature profile measured in mission realized by [13]. At 11-14 meters of depth the thermocline can be identified. Adapted from [13]

2.1.2 Parametric Models

The representation of all layers of the water column by a single function may not be advantageous. With a global function, the necessity to have many parameters, in comparison with the possibility to represent in three different intervals (mixed layer depth, thermocline, and deep water), is a disadvantage. It is not possible to construct a representation of depth as a function of temperature, $Z(T)$, given that for the same temperature, we have different depths. Dividing the water column into three different functions is possible to reduce the number of parameters. However, the continuity between each function and the polynomial capable of representing each function is expected to cause problems. Another problem will be the decision of which points perform the best separation of these three layers (functions).

One of the first attempts to provide that a simple model can represent the thermocline was suggested by [34]. This model was developed to explain the typical shapes of spring and summer temperature profiles in Lake Ontario, Canada. Through physics of the moving water caused by the warming of the coastal surface water, the characteristic values of the parametric models and the shapes of the thermocline were generated.

In [17] is presented functional forms of the temperature profiles provided by Generalized Digital Environmental Model (GDEM). GDEM is a worldwide four-dimensional (latitude, longitude, depth, and time) digital model of temperature and salinity. The temperature and salinity profiles provided by GDEM are compressed into coefficients of mathematical expressions. The temperature model considers three different levels of detail. Eight coefficients represent the top-most layer, the middle layer has seven and a quadratic polynomial represents the bottom-most part of the water column [17].

The parametric model developed by [16] proposes a simple 3-layer piecewise linear gradient model, with a high gradient at the thermocline, and low gradients both above and below. In this work, it was discussed the advantages to represent a vertical profile through low-order or high-order function. With a low-order representation, the coefficients of this function have a physical meaning or feature [16]. This model represents the overall shape of the water column with only six gradient parameters.

Similar geometric representations of a layered structure have been used to model the Yellow Sea [7] and the Beaufort/Chuckchi Sea [9] temperature profiles. The parametric model developed in [7] consists of six layers and six gradients, figure 2.3. Note that the representation of the *T(Z)* in figure 2.3 is a coarse representation of the temperature profile (compare with the measured profile shown in fig. 2.2). This model transforms any profile into a set of five depths (d_1, d_2, d_3, d_4, d_5) and six gradients ($G_T^{(m)}$, $G_T^{(th)}$, $G_T^{(en)}$, $G_T^{(tr)}$, $G_T^{(d1)}$, $G_T^{(d2)}$). In [7] each vertical temperature profile is modeled by the following parameters: sea surface temperature, mixed layer depth, depth of the base of the thermocline, the gradient in the thermocline, and deep layers. Observing figure 2.3, it is visible the possibility to represent a vertical profile temperature in different intervals, in this case, to represent each layer as a function.

The main disadvantage of the models proposed by [7, 16] it is the non-specification of the

highest gradient point in the thermocline. In both models, the gradient that corresponds to the thermocline is a segment. Tracking the highest point of the gradient of the thermocline, it is possible to change this representation and define a model with the maximum gradient of the thermocline with a single point.

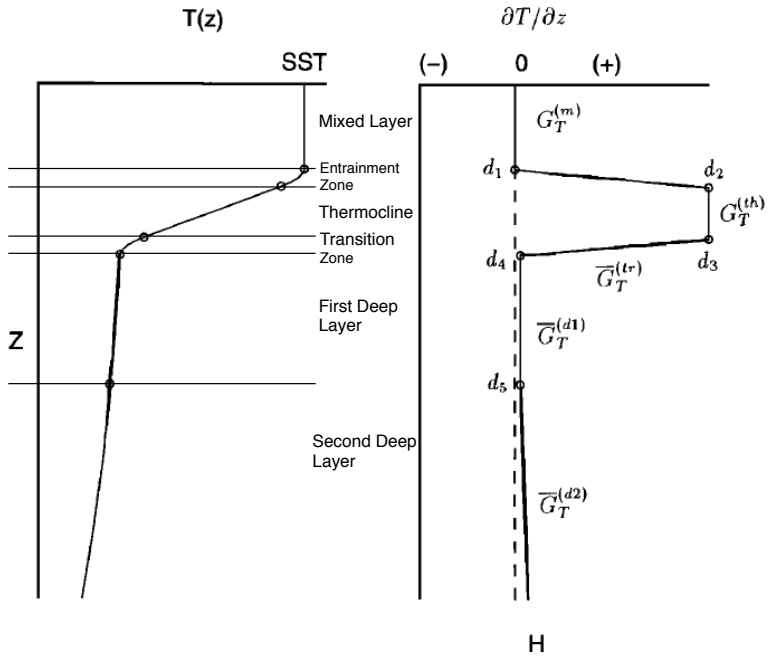

Figure 2.3: The temperature and gradient space representations, adapted from [7]

The work performed in [2], through a genetic programming environment, proposes a model that the desired output is the change in temperature with depth ($\frac{\Delta T}{\Delta Z}$) instead of directly modeling temperature as a function of depth and sea surface temperature. This model is based on average historical data from the World Ocean Atlas, concerning the South East Asian Seas. In the parametric model developed by [2], the vertical profile depends on sea surface temperature, mixed layer depth, thermocline bottom depth, bathymetry, and sea bottom temperature. The relation that represents the variation of the temperature with depth there has no intuition, neither any physical meaning, it just represents the best approximation of the data set.

2.1.2.1 Piecewise

An option to represent the different layers of the vertical temperature profile is to divide the interval into a collection of subintervals and construct for each subinterval an approximating polynomial. This is called piecewise-polynomial approximation [28].

The piecewise-linear interpolation is the simplest piecewise-polynomial approximation. The piecewise-linear consist of joining a set of data points

$$((x_0, f(x_0)), (x_1, f(x_1)), \ldots, (x_n, f(x_n)))$$

by a series of straight lines, as shown in figure 2.4 [28].

A disadvantage of linear function approximation is that probably at the endpoint between two straight lines there is no differentiability, that is, the interpolating function is not "smooth" [28].

An alternative option is to use a piecewise polynomial of Hermite type. The method developed by [33] used this type to construct a piecewise cubic function. If the values of f_i and f_i', for $i = 0, 1, \ldots, n$ are known a cubic Hermite polynomial can be used on each of the subintervals to obtain a function and has a continuous derivative on the interval $[x_0, x_n]$ [33, 28].

However, to use this piecewise polynomial type, for general interpolation, it is necessary to know the derivative of the function being approximated, and this is frequently unavailable [28].

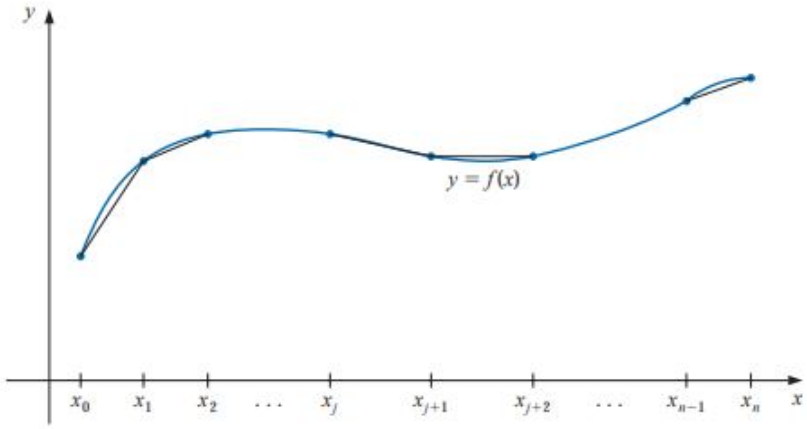

Figure 2.4: Piecewise-linear interpolation, adapted from [28]

2.1.2.2 Spline Curves

The spline curves can determine a smooth curve that approximates a set of points in the plane [23]. Thus, when the smoothness of the interpolation curve is the most significant interest, cubic splines are often the method of choice [33]. Despite producing smooth curves, the spline interpolation generally leads to severe oscillations [33]. Figure 2.5 illustrates this oscillation.

Typically, the construction of a cubic spline curve needs four constants. In this way, it is guaranteed that the interpolant is not only continuously differentiable on the interval but also has a continuous second derivative [28].

2.1.2.3 Polynomial Interpolation

Taking into account that it is possible to develop a representation for each one of the layers (mixed layer, thermocline, and deep-water layer), represent each layer through a polynomial is an option. Each sub-function can be applied to a specific interval. In this case, it can be divided into three sub-functions. A straight line or a second order polynomial can approximate the mixed and deep-water layer, and a cubic function can approximate the thermocline.

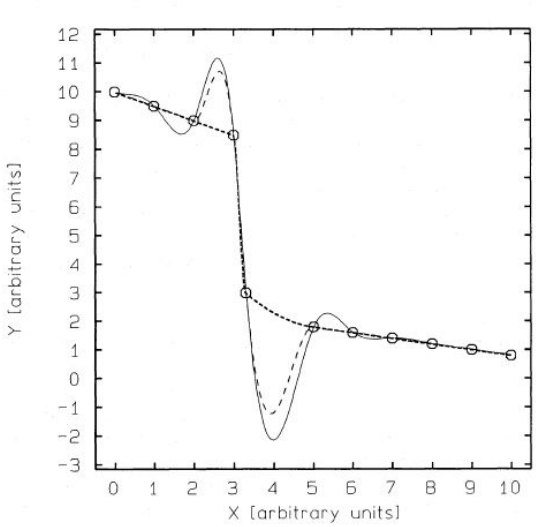

Figure 2.5: Comparison of different interpolation methods. Full-drawn: spline curves, adapted from [33]

Suppose a data set with $n+1$ points $(x_0, x_1, \ldots, x_n)$ and each one point have a arbitrary value $(f_{(x_0)}, f_{(x_1)}, \ldots, f_{(x_n)})$ there is a polynomial, $p_n(x)$ able to interpolate this points [26].

$$p_n(x) = a_0 + a_1 x + a_2 x^2 + \cdots + a_n x^n \tag{2.1}$$

All the values of $f(x_j)$ to each point (x_j), for $j = 0, 1, \ldots, n$ may be written in the following form:

$$AX = B \Leftrightarrow \begin{bmatrix} 1 & x_0 & x_0^2 & \ldots & x_0^n \\ 1 & x_1 & x_1^2 & \ldots & x_1^n \\ \vdots & \vdots & \vdots & \ddots & \vdots \\ 1 & x_n & x_n^2 & \ldots & x_n^n \end{bmatrix} \begin{bmatrix} a_0 \\ a_1 \\ \vdots \\ a_n \end{bmatrix} = \begin{bmatrix} f(x_0) \\ f(x_1) \\ \vdots \\ f(x_n) \end{bmatrix} \tag{2.2}$$

If the matrix A is nonsingular the system of linear equations (2.2) has a unique solution [26].

Figure 2.6 shows a possible representation of the three layers using polynomial interpolation for each layer. The bottom graph of figure 2.6 is the derivative of the polynomial that represents the thermocline. Using this method, we can have an approximation of the temperature gradient of the thermocline through the processing of the acquired data.

2.2 Data Acquisition

Taking into account that to perform the tracking of thermoclines is necessary to obtain temperature measurements, is also important to comprehend how this acquisition is performed.

The main tool to obtain a temperature profile is the CTD [10]. CTD is an instrument that measures conductivity, temperature and pressure (depth). It also allows, indirectly, to compute other

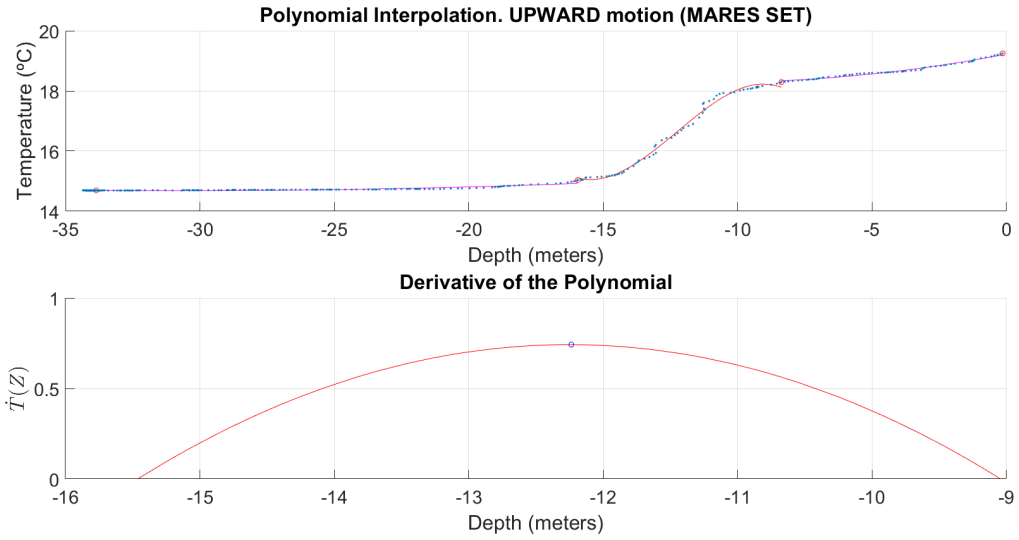

Figure 2.6: Example how to use polynomial interpolation to calculate the peak of the temperature gradient

indirect parameters of the sea water, such as salinity and density [10]. In a traditional approach, the temperature is sampled locally, with a CTD deployed from a research vessel and getting a vertical profile of the water column in specific locations [10].

The following description shows how the data were collected in the 90's [27]. The oceanographer goes to sea for a cruise in a research ship. The ship is stopped when it reaches a preselected location (*stations*), and the oceanographers measure the water properties from surface to deep water. For each station, the measurements are then plotted as "vertical profiles", graphs of temperature or other water property against depth [27]. In [8], another method of how to collect data is described. The coastal monitoring buoy (CMB) was deployed by the U.S Naval Oceanographic Office. Fifteen thermistors are attached to a wire rope extending from the code of CMB to 140 m. These measures are realized every 15 seconds [8].

Lately, AUVs have been used to acquire large sets of underwater data by defining a horizontal trajectory and performing *yo-yo* control in the vertical plane. The range of the *yo-yo* motion is changed depending on the collection of the characteristics in interest and the change of specific parameters in real-time. In [5], the researchers use two AUVs, incorporated with a CTD sensor, to collect the data needed for the study (water temperature of depth).

2.3 Real Time Adaptive Sampling in the Ocean

The real time adaptive sampling allows the ability to adapt to the behavior of the vehicle. Therefore, there are parameters that are changed in real time in function of the measurements of specific data. The real time sampling approach aims to improve the efficiency of the research process or tracking of specific oceanic characteristics.

Next, we present works that use adaptation in real time to perform the identification and tracking of thermoclines.

The projects that look for a thermocline tracking divide the water column into a number of depth bins for error reduction [12, 13, 38, 39, 25]. This division happens due to the necessity to calculate the vertical gradient of temperature. The size of the bin is crucial to avoid errors in the calculated temperature gradient. This size acts as a low-pass filter which may affect the ability to detect gradients [11]. If the bins are too small, only a few points will be measured, then resulting in a large error in gradient estimation, which leads to a wrong thermocline depth [13, 39]. If the bins are too large, the temperature variations will be smooth, and the algorithm will have difficulty to track of thermocline [12].

The information of the depth of the vehicle and the temperature of the water obtained through a CTD sensor is used to change the trajectory of a Slocum Glider [36]. The tracking of the thermocline developed by [13] uses a real-time adaptive sampling to adapt some thresholds such as the gradient of the thermocline and the bottom and top gradient of the thermocline. The algorithm developed by [25] runs an initial deep profiler at the start of the mission to get a complete data set to adjust *yo-yo* depth limits. To perform this tracking, there are other algorithms that adapt the behavior of the vehicle in relation to other oceanic features. In [35] the behavior of the vehicles is adapted according to the speed of sound.

2.4 Tracking of Thermoclines

As described earlier, we are interested in ocean process that exhibits the thermocline region. More, we consider that the vehicle moves through the scalar field to perform pointwise measurements and in this way, that detects the feature in interest, the temperature gradient. Therefore, the following examples refer to the cases where the vehicle has to extract relevant information from data that is streaming and decide the best trajectory to keep tracking of the feature.

The most recent works describing adaptive sampling of thermoclines using AUVs. In these works, the AUV run a *yo-yo* trajectory [13, 12, 38, 39]. On each descent or ascent leg, the algorithm that runs on AUV, with a sensor temperature, detects a set of parameters, such as, the peak of the temperature gradient [38]. Through this peak the vehicle switches ascent or descent trajectory. If the peak is greater than the maximum gradient, previously defined, the algorithm saves the depth correspondent to the depth of the thermocline ($depth_{th}$) and subtracts an extension depth ($dep_{extension}$). When the vehicle arrives at $depth_{th} - depth_{extension}$ the vehicle switches to the descent trajectory. On the other hand, if the peak is smaller than the minimum gradient, also previously defined, the algorithm saves the depth correspondent to the depth of the thermocline and sums an extension depth. When the vehicle arrives at $depth_{th} + depth_{extension}$ the vehicle switches from descent to ascent trajectory [38]. However, if the extension depth, defined by the user, is too small, the detection and tracking of the thermocline will fail because the algorithm may be fooled

by a local maximum of temperature gradient [39]. As already observed, this implementation results in a constant vertical span of the *yo-yo*. However, if sudden changes the thermocline depth happens this algorithm, it may fail this change and thus fail to track of thermoclines.

The work developed by [12] with the acquisition of measurements of the CTD sensor in real time adapts the depth to maintain the vehicle in the vicinity of the thermocline and in this way increasing efficiency in the sampling process [12].

The algorithm developed in [12] and the evolution of this algorithm [13] also use the peak of the temperature gradient. However, this algorithm uses a unique threshold, in each ascent or descent trajectory, to verify the maximum of the vertical temperature gradient (thr_{tc}). If this threshold is exceeded, the vehicle will assume that the thermocline has been detected on the downward or upward motion [13, 12]. When the vertical temperature gradient is lower than a given threshold (thr_{bot}), and the vertical span is traversed, the algorithm changes the motion, downward to upward. The same idea is verified to change upward to downward movement. The condition of the vertical span was implemented to avoid false detections. Even though the algorithm had already detected a marked decrease in the gradient, a safe distance is taken to avoid false detections. When the thermocline is not detected in one of the vertical profiles, the vehicle will extend the vertical span to safety depths (Z_{min} or Z_{max}) [12]. As can already be seen, this algorithm needs the initial configurations, like the following:

- bottom and top depth of the thermocline (Z_{max}, Z_{min})
- vertical gradient of the bottom, middle and top of the thermocline (thr_{tc}, thr_{bot}, thr_{top})
- vertical span (Z_{span})

Comparing the algorithm developed by [38] and [12], the last one needs a previous and detailed study of thermoclines. However, this algorithm has the following option: use no information and let the AUV acquire a full vertical profile to determine the different parameters [13, 12].

The algorithm developed by [25], at the start of the mission performs a preliminary deep profile to calculate the average vertical gradient of temperature. Through this calculation, the thermocline layer is defined as the layer where the gradient exceeds such average and this defines the range of the *yo-yo*. This algorithm performs periodic full profiles with the purpose to ensure a correct tracking even if the thermocline characteristics change (span, location, and gradient). If the vertical excursion is too deep, the full profile average will be biased by this excursion. In this way, results in large vehicle yo-yo around the peak of the thermocline gradient.

2.5 Depth Control

With the purpose to control the AUV on the thermocline is necessary to understand what are the possible references to use in this same control.

Already exists a model that represents the relationship between the force of thrusters of the vehicle and the variation of its position. In this situation, the depth is considered the reference of

the control. This model can represent the dynamic between the force needed to apply to each of the thrusters and the velocity of the AUV. The model that describes the profiler is a 6 DOF model of an underwater vehicle and follows an approach presented in [15].

The control of the profiler developed by [24] is performed by actuation of four thrusters. The control variable is the force that is required for each of the thrusters. Although it is considered that an instant force can be applied to the vehicle, this does not represent reality. This assumption seeks to simplify the model analysis and the determination of controllers and can be justified by the fact that time constants associated with the actuation are smaller than the ones related to the vehicle motion [14].

In [24], the model of the vehicle for its 6 DOF was obtained following the procedures presented in [15]. In [30], the transfer function that relates the input given to the thrusters of the vehicle with the variation of its position in the vertical direction was developed. In this way, to represent the profiler's dynamics and the position controller the implementation developed in [30] was chosen.

Taking into account that one of the objectives of this work is to track the thermocline, the follow-up of reference depths is a method for the AUV to move in the thermocline. In this case, we can consider just one fixed reference or two references, but variable references. Figure 2.7 represents a possible architecture for the position control. Therefore, it is necessary to develop an algorithm that creates depth reference depending of the position of the vehicle. The block **Depth reference** of the figure 2.7 represents this algorithm. The position of the vehicle will be adapted according to depth and temperature gradient. From these two measures, the algorithm generates a new reference. As already was described, there are algorithms that use the information of the temperature gradient to adapt the motion of the vehicle (section 2.4). Thus one of these methods may be an option to the algorithm to be implemented in the block **Depth reference**. The remaining blocks and the feedback scheme of the figure 2.7 represent the control of the vehicle position in order to follow a reference.

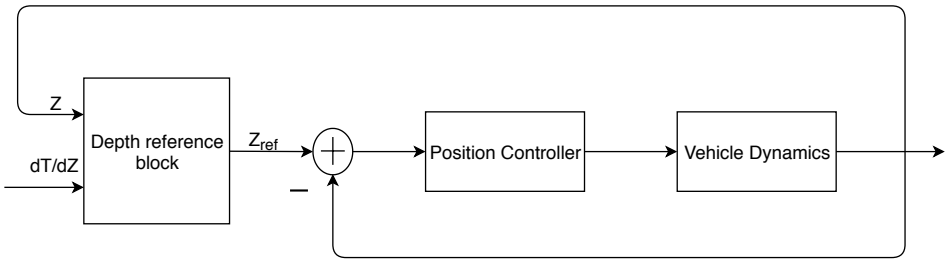

Figure 2.7: Architecture of the position control of the vehicle

2.6 Extremum Seeking Control

Although a model that is capable of representing the temperature gradient is not known, it is known that there is a point where the gradient is maximum. With this acknowledgement, the

Extremum Seeking Control (ESC) is a possible control method to be used to find the maximum of the temperature gradient.

ESC is a non-model-based, adaptive control method that modifies the different parameters of an objective function with the purpose of the output variable reaching its local extremum (maximum or minimum) [20, 22, 37, 3]. The main advantage of this method over conventional adaptive control methods is that the set-points or the reference trajectories haven't to been known a priori [3]. In other words, the plant model is not needed for controller [20, 37]. In this way, in the context of the tracking of the thermoclines, no explicit system model is required, it requires only the measurements of the gradient. To overcome the need to exist a priori known model or set of points, the ESC method uses an external perturbation source as the objective of estimating the gradient of the output variable [1, 3, 37].

ESC has been applied to various problems, for instance, formation flight, anti-lock braking systems, and modeling of bioreactor [1]. It also has applications in Proportional-Integrative-Derivative (PID) parameters turning [19], optimization of the Maximum Power Point Tracking (MPPT) algorithm [4] or ships speed and heading control in the presence of roll [3], etc.

Figure 2.8 shows the structure of the basic ESC scheme for tracking the extremum. The plant of the diagram block, in our case, is the model of the temperature gradient. As already said, this model is unknown. The idea of this scheme is an online optimization of the control input, $\theta = \hat{\theta}$, in such a way that maximize the output variable, $y = \hat{y}$, without knowing the plant ($y = f(\theta)$).

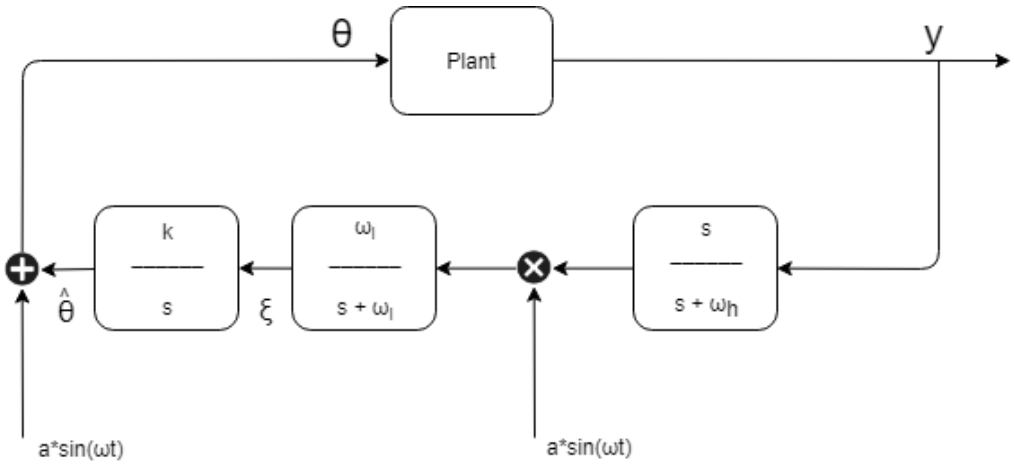

Figure 2.8: Scheme of the ESC loop for a general plant, adapted from [1]

To the signal $\hat{\theta}$, our best estimate of θ^* is added a periodic perturbation, sine signal $asin(\omega t)$. The periodic perturbation will create a periodic response of y, assuming that the plant is quasi-static. If the frequency of the excitation signal ω is slow with respect to the plant's dynamics, our dynamic system can be a static map [22]. The y response is analyzed to detect if the slope is the maximum gradient. The high-pass filter (HPF) removes the mean value of the output. Thus, $asin(\omega t)$ and the response of the HPF will be (approximately) two sinusoids which are

- in phase for $\hat{\theta} < \theta^*$

- out of phase for $\hat{\theta} > \theta^*$ [22]

The figure 2.9 shows the moment when the output variable is in and out of phase with the sine signal. If the signal of the product between the sine wave and the output of the HPF is positive, so we are on the left of the goal (maximum), and the input and output perturbations are in phase. If the product is negative, we are on the right of the maximum, and the input and output perturbations are out of phase.

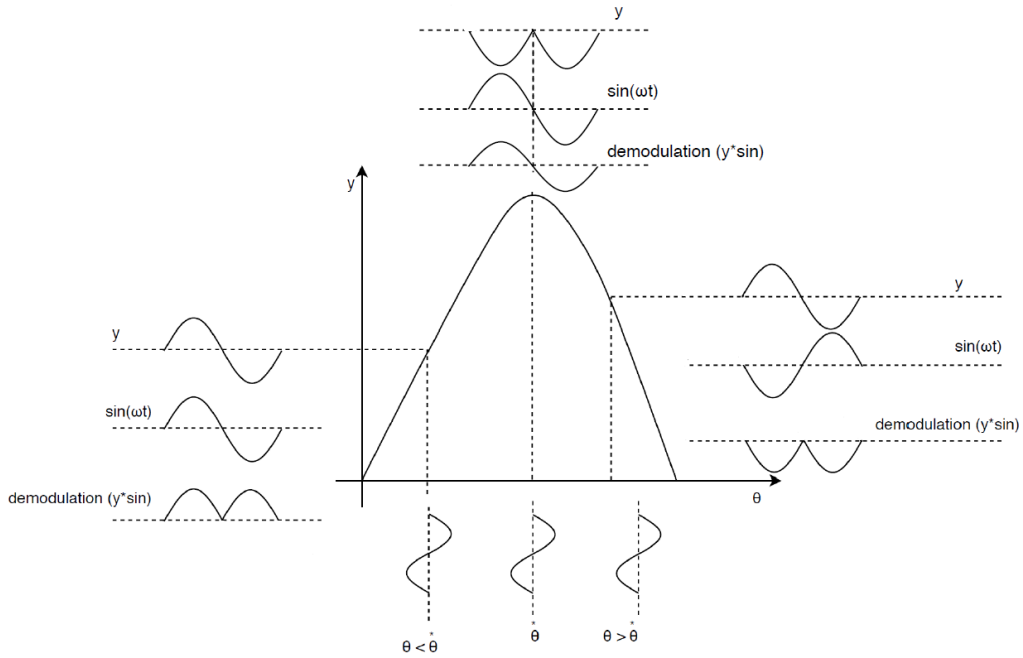

Figure 2.9: Graphic interpretation

The low-pass filter (LPF) extracts the "DC component" of the product of the two sinusoids [22].

The cut-off frequencies of the HPF and the LPF are lower than the frequency ω of the perturbation signal. Thus, the overall feedback systems have three different time scales. The fast time scale corresponding to the plant dynamics, the medium to the periodic perturbation and the lowest time scale corresponding to the filters in the Extremum Seeking Control scheme [20, 22].

Chapter 3

System Overview

In this chapter, it will be presented the description of the problem, as well as a set of assumptions needed to establish the system and an overview of the system. It will be also explained some specifications about the software that was developed.

3.1 Problem Formulation

In this work, we propose an implementation in which it is possible to carry out the tracking of thermocline at its point of highest temperature gradient with an autonomous vertical profiler. Through this tracking, we also want to get the most of possible temperature water characteristics in the different layers. With these characteristics, it is possible to calculate the parameters that can to be used to feed one of the parametric models studied in section 2.1. Due to profiler geometry and orientation, with a distribution of two or more temperature sensors we can calculate the vertical gradient temperature, and in this way, we have instantaneous samples of the variable that we want to maximize.

3.2 Proposed Solution

To track the thermocline with an autonomous process a profiler will be used (Fig. 3.1). The vertical profiler has approximately 1.35 m of length and a mass of 11.3 kg and its main purpose is the navigation in the vertical direction. In order to maintain the profiler in the layer of maximum temperature gradient, we use Extremum Seeking Control (ESC) algorithm. All of the construction, design, requirements, and assumptions about profiler are described in [24]. It will be added new premises, a set of temperature and depth sensors and new functionality, with the finality to tracking the thermocline, on the module Mission Control and Supervision. The model that we want to feed follows the parametric model developed by [7] (Fig. 2.3). Given that we pretend to track the highest point of the temperature gradient, the main difference for the previous model is that the representation of the gradient of the thermocline will be a point, not a segment. The explanation of this difference will be explained in chapter 4.

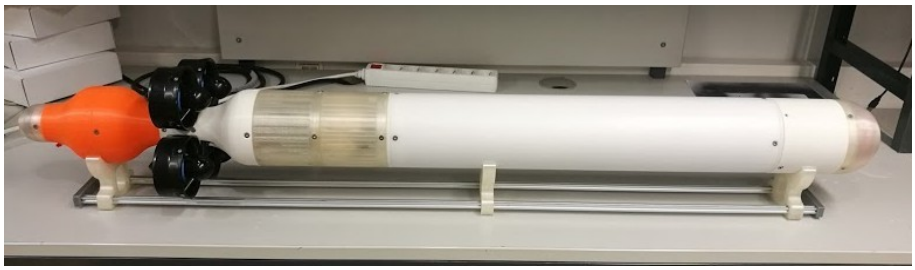

Figure 3.1: Image of the profiler

3.2.1 Assumptions

For the accomplishment of our work, after analyzing the different models of temperature seawater, the following assumptions will be considered:

- the derivative of the vertical temperature profile is monotonic, this is, there are no signal changes in the derivative
- three layer piecewise model (mixed layer, thermocline, deep layer), like the representation of figure 1.1

In this work, we also assume that the algorithm is only capable of tracking thermoclines with vertical spacing greater than 3 meters. The linear system developed by [30] that approximates the 6 DOF model of the vehicle will be used to represent the dynamics of the profiler, as well as the position controller developed by [30]. Because the body of the profiler has a distance of 1 meter, we are limited to this distance to distribute the sensors.

3.2.2 Vehicle Model and Position Controller

The linearization and calculation of the state space of the 6 DOF model of the profiler advanced by [24] was developed in [30].

The following transfer function relates the input given to the thrusters of the vehicle and the variation of its position in the vertical direction:

$$G(s) = \frac{Z(s)}{F(s)} = \frac{0.0860}{s \cdot (s + 0.1029)} \tag{3.1}$$

The position controller was implemented based on the conventional PD, as explained in [30]. The PD controller law obtained is given by:

$$F(s) = K_p \cdot (s + 0.1029) \cdot E(s) \tag{3.2}$$

The value of K_p was chosen in order to have a settling time below 10 s [30]. Taking into account that a sinusoidal signal is added to the reference of the control input variable it is important to verify the response of the system, that represents the profiler's dynamics, to sinusoids.

Figure 3.2 shows that for the K_p determined in [30] there is considerable delay and attenuation if the reference is a sinusoid with frequency equal to 0.2094 rad/s ($T = 30\ s$). For this reason, a more detailed analysis of which is the gain that minimizes the delay and the attenuation in relation to the reference will be presented in section 6.

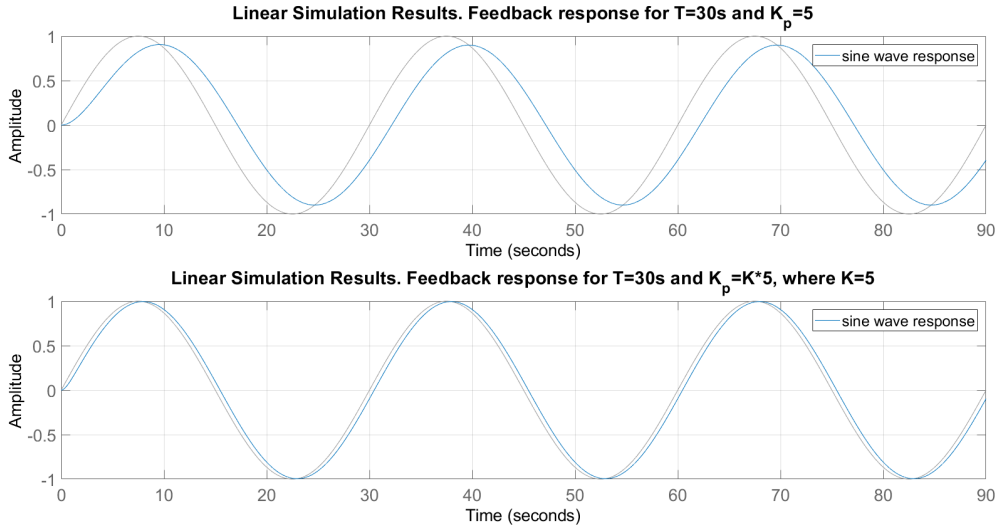

Figure 3.2: Difference between $K_p = 5$ and $K_p = 25$

3.2.3 Software Architecture

Taking into account that it is necessary to develop an algorithm for tracking the thermocline and that this implies that the data of the sensors have to be acquired, these processes will be separated in different modules. With this division, the software that will be developed consists of three separate processes, as shown in figure 3.3: Mission Control and Supervision, Data Processing and Data Acquire.

One of these processes will have to be responsible for the control and the supervision of the mission. In this process an algorithm responsible for the new maneuver, tracking of the thermocline will be developed. When the user chooses the mission plan, the process Mission Control and Supervision runs an algorithm that looks for a characteristic that the user is interested. The new algorithm to be developed is responsible for reading the parameters shared by process Data Processing and controlling the depth of the profiler.

In parallel, it is necessary to read and acquire information from the sensors. For this reason, these two different tasks will be divided, one responsible for the read and processing data and another responsible for the acquire measures of the sensors. For data exchange between these processes, the process Shared Memory will be developed.

The process Data Acquisition should acquire data from all the sensors distributed in an underwater profiler and share these measurements to other processes.

The process Data Processing is responsible for logging the data read from the sensors. With these measurements, the process should calculate the gradient temperature.

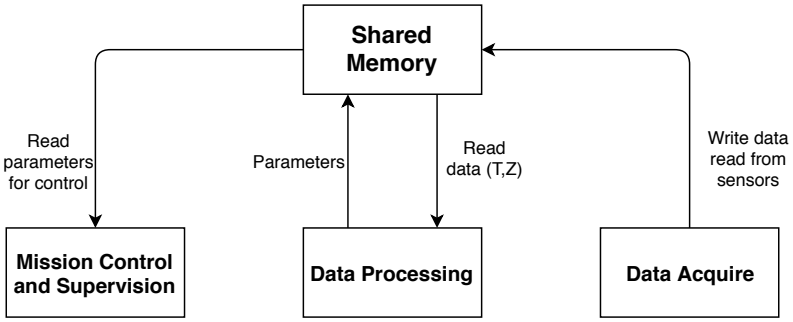

Figure 3.3: Software modules, adapted from [24]

3.2.4 Methods, Tools and Algorithms

To track the thermocline, it will be necessary to calculate a vertical gradient temperature. In this way, the algorithm will have to be able to read and process the information of the sensors. The relationship between the algorithm responsible for the tracking of thermoclines and the vertical gradient temperature is shown in figure 3.4. The feedback of the algorithm responsible for this tracking is performed through the sensors measurements and posteriorly, the calculation of the gradient, that depends on the position of the vehicle.

ESC is a control method with the main purpose of placing the input variable in a specific value that corresponds to the output variable in a extremum value (maximum or minimum). One of the advantages of this method is that is not necessary to know an exact model of the system, but mainly that there is a local extremum. This overcomes a great challenge in thermocline tracking with other mode-based methods - deriving a proper model. The method requires the measurement of the variable to maximize, which we obtain directly by distributing temperature sensors along the profiler body. With the profiler and the previous measures, we can calculate the vertical gradient temperature, and in this way, we have the variable that we want to maximize.

ESC method maximizes the temperature gradient, generating the reference depth corresponding to this maximum. Thus, it is necessary a vehicle capable of following depth references, a requirement duly verified by the profiler.

Comparing the schemes of figure 2.8 and 3.4, it is possible to observe some differences. The scheme of figure 3.4 follows a new approach shown in [21] in relation to the structure described in [22]. The scheme developed by [21] considers a delay (Φ) on the sinusoid that multiplies with the filter response and doest not consider the low-pass filter. However, we consider a new approach, the moving average filter. This block has the purpose to reduce the oscillation provided by sine waves. The difference between a scheme that has this block and another that does not have this block will be discussed in chapter 6.

Although we want a method fully autonomous, some amount of mission configuration is unavoidable. The following parameters are an example of the configurations. For vehicle and mission safety the following parameters are configured:

- top and bottom depth

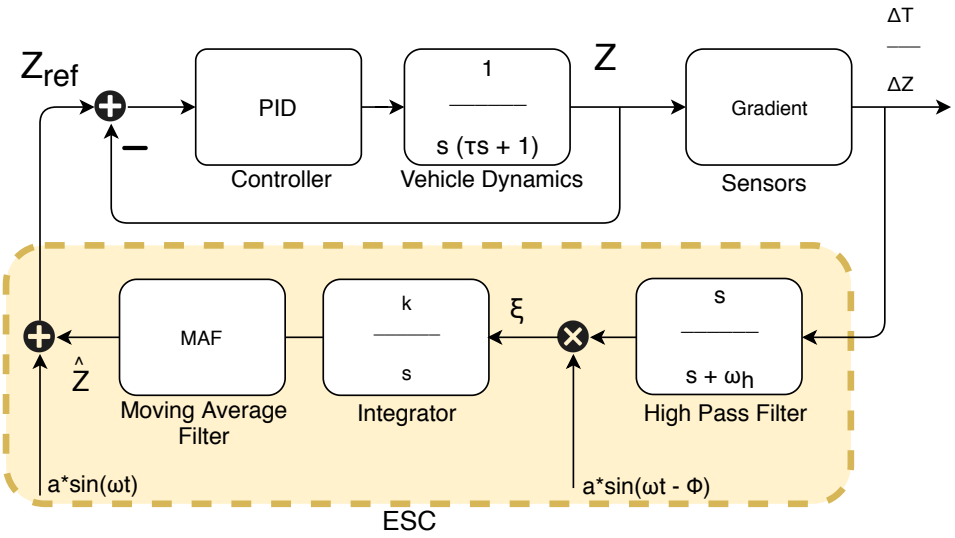

Figure 3.4: ESC scheme to tracking the maximum of the gradient of thermoclines

- time for the mission

The configuration of the top and bottom depths has the purpose of limiting the space traveled by the vehicle in the *yo-yo* trajectory. The time for the mission has a similar objective. If the algorithm does not track and detects thermoclines during this time, the vehicle backs to surface.

Figure 3.5 describes the sequence of each state of the algorithm that will be developed for track and detect thermoclines. In the beginning, the user defines some mission configurations for instance, depths that limits the motion of the vehicle. After, the vehicle will perform four vertical temperature profiles between the bottom and top depths defined in **Configuration**. After all four profiles are completed the algorithm that detects and tracks thermoclines, **Tracking**, will be executed. In this algorithm the Extremum Seeking Control was developed.

In order to have an alternative algorithm in which it does not directly perform the ESC, a new approach has been developed. This approach is represented in figure 3.5 with a dashed line. In this algorithm, the vehicles comes to the surface after to perform all four profiles. Then, the first depth reference was chosen. This reference can be choose by user or calculated autonomously. If it is calculated autonomously the reference depth corresponds to a depth corresponding to 40% of the maximum gradient detected in the four profiles. When the vehicle reaches this reference, the ESC is executed.

When the ESC method is performed, it is possible to calculate some parameters that represent the features of the thermocline, for example, the highest gradient and its depth. Thus, the feedback of the parametric model is performed.

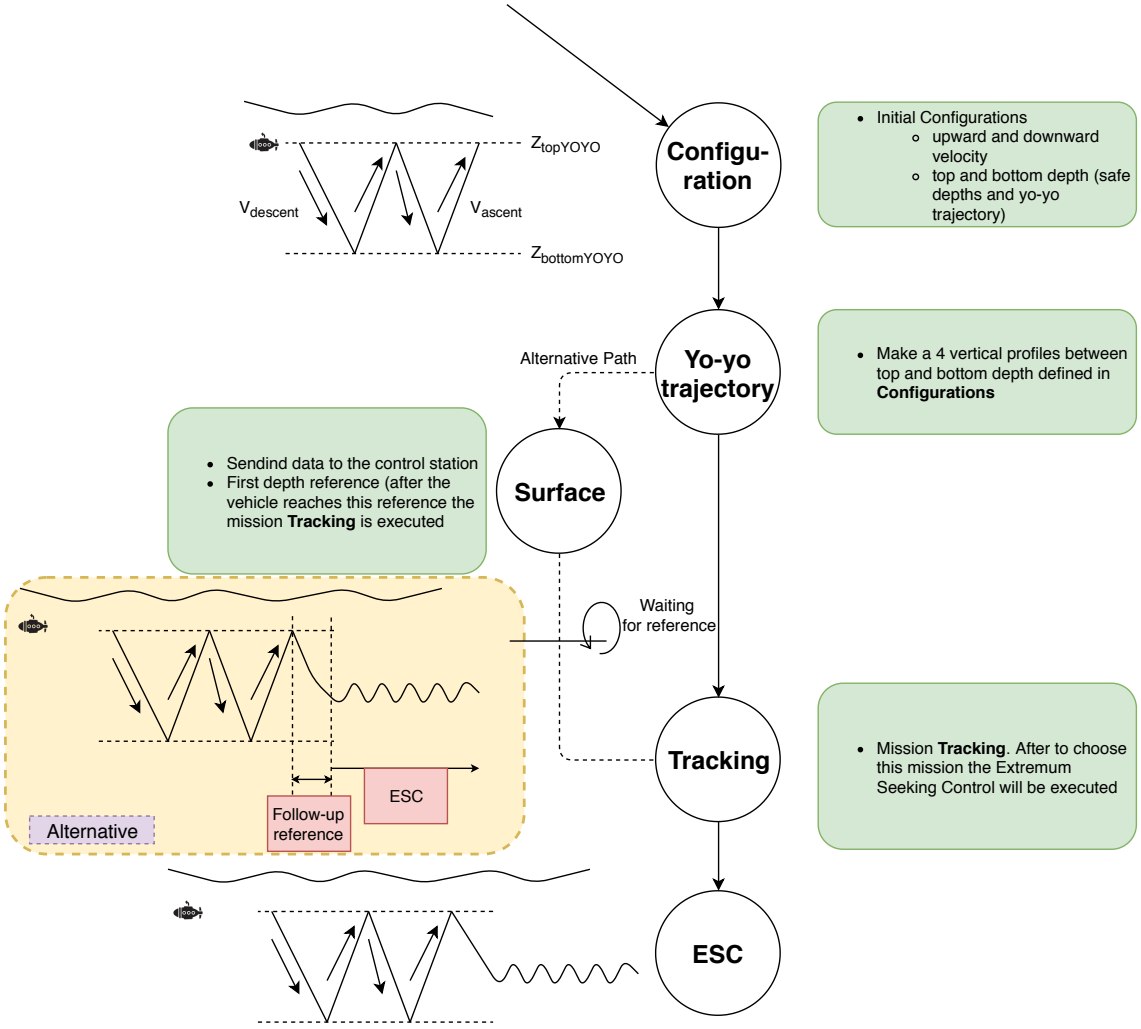

Figure 3.5: Algorithm responsible to maneuver tracking thermoclines using ESC

Chapter 4

Parametric Model

As already was explained, using ESC, it is not necessary to know the model that represents the gradient of the thermocline as a function of depth. However, to that this implementation recreates a model of the water column, a dataset was analyzed (temperature and depth) in order to see how, from the implementation of the ESC, we can create this model or parameters that represent the different layers of the water column.

Taking into account the analysis performed in section 2.1, there are two possibilities of representing the temperature gradient (Fig. 4.1). Observing figure 4.1, we conclude that both models divide the temperature profile into three different levels (mixed layer depth, thermocline, deep-water layer). With these models, we have been able to choose the bottom and top depth of the thermocline, as well as the indicative gradient that we are in the thermocline. The advantage of each model presented in figure 4.1 will be debated in this chapter.

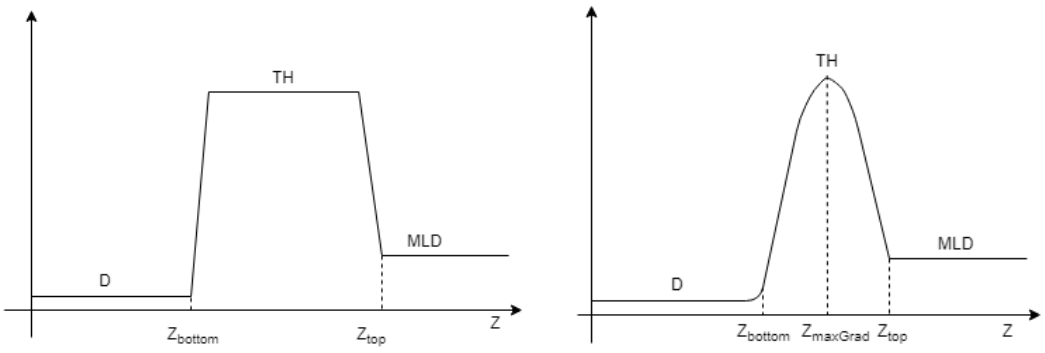

(a) Model 1

(b) Model 2

Figure 4.1: Different options to parametric model. D means deep-water layer, TH the thermocline and MLD means mixed-layer depth

4.1 Vertical Temperature Profile - Ideal vs Real

After to analyze different vertical temperature profiles, it was decided that three layers can represent the vertical profile. Taking into account the data taken from MARES AUV [12] we chose the vertical profile represented by a blue line in figure 4.2 as ideal. The data taken from the MARES AUV are the plots represented in orange and yellow, figure 4.2. To facilitate the use of data from work [12], the name of this dataset will be MARES SET.

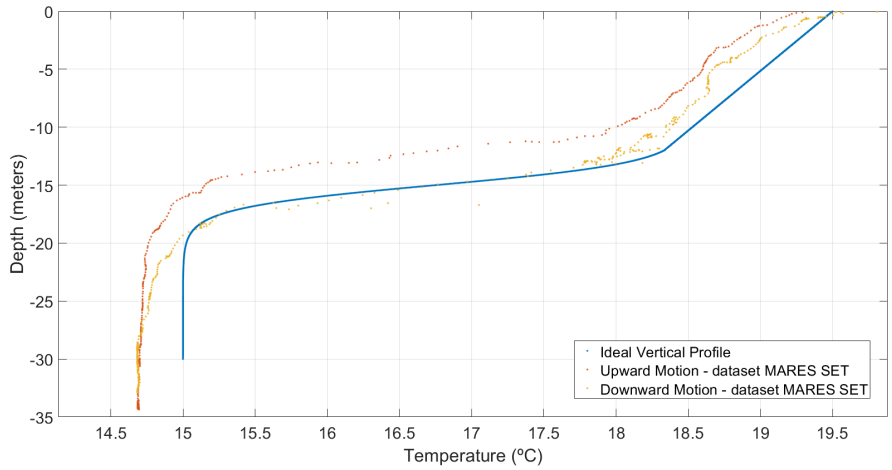

Figure 4.2: Vertical temperature profiles: Ideal vs Real

For the ideal model, the two straight lines represent the mixed layer depth and deep-water layer. The thermocline can be represented by a tangent sigmoid or a logarithm sigmoid. The difference between these two functions consists of spacing and inclination and is shown in figure 4.3.

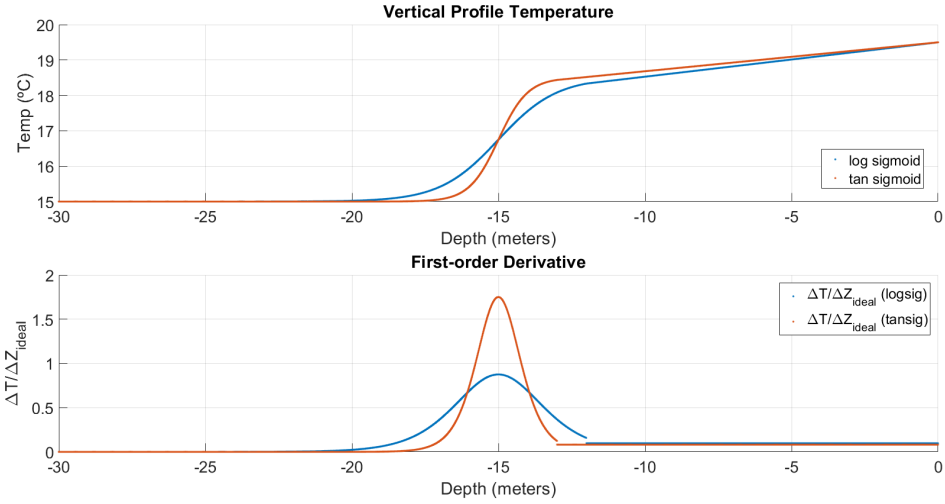

Figure 4.3: Difference between tangent sigmoid and logarithm sigmoid

With the idea of approaching the ideal profile to reality, it was considered to add noise to the data. This noise simulates both the water dynamic of the system and the sensor measurement error.

The noise added to the data is proportional to the derivative $\frac{\Delta T}{\Delta Z}$. In this way, the error is more visible in the mixed layer depth and thermocline.

4.2 Methods

After creating a set of data capable of simulating the real environment of temperature and depth measurement in an aquatic environment, we proceed to construct a model through the derivative of temperature as a function of depth.

4.2.1 Analysis and Pre-processing of Data

To construct a gradient model, we first develop an algorithm that calculates the approximation of first-order derivatives. The Matlab `diff` tool was used. This tool does the following:

$$\Delta X = x_{i+1} - x_i, \tag{4.1}$$

for each $i = 1, 2, \ldots, N$.

The approximation of the first-order derivative of the temperature with depth was calculated as follows.

$$\Delta T = T_{i+1} - T_i \tag{4.2}$$

$$\Delta Z = Z_{i+1} - Z_i \tag{4.3}$$

$$\frac{dT}{dZ} = \frac{\Delta T_i}{\Delta Z_i} \tag{4.4}$$

Figure 4.4 shows the result of the first-order derivative of the dataset MARES SET (upward motion of figure 4.2) and the dataset created in the previous section (ideal vertical profile of figure 4.2). The result of the first-order derivative of the ideal vertical profile (top of Fig. 4.4) shows that it is possible to differentiate three different layers. Analyzing figure 4.4, it is possible to observe that for depths between 20 e 30 m there is no variation of the gradient. Depths between 12.5 (approx) and 20 m there is a dispersion of the approximation of the first-order derivative, which illustrates that there was a transition of a layer. Finally, for depths between the surface and 12.5 m, the result indicates that there is a small variation of the gradient. However, it is difficult to define depths and gradient values for each of the layers. Thus, it is impossible to find the parameters that may feed the parametric model. The result of the first-order derivative of the dataset MARES SET also shows that it is not possible to extract information to differentiate the three layers.

After obtaining the approximation of the first-order derivative of the dataset MARES SET and observing that there were very large derivative values, it was necessary to perform a pre-processing of the data. The measurements of this data set can be affected by sea currents or if the vehicle collides with small objects.

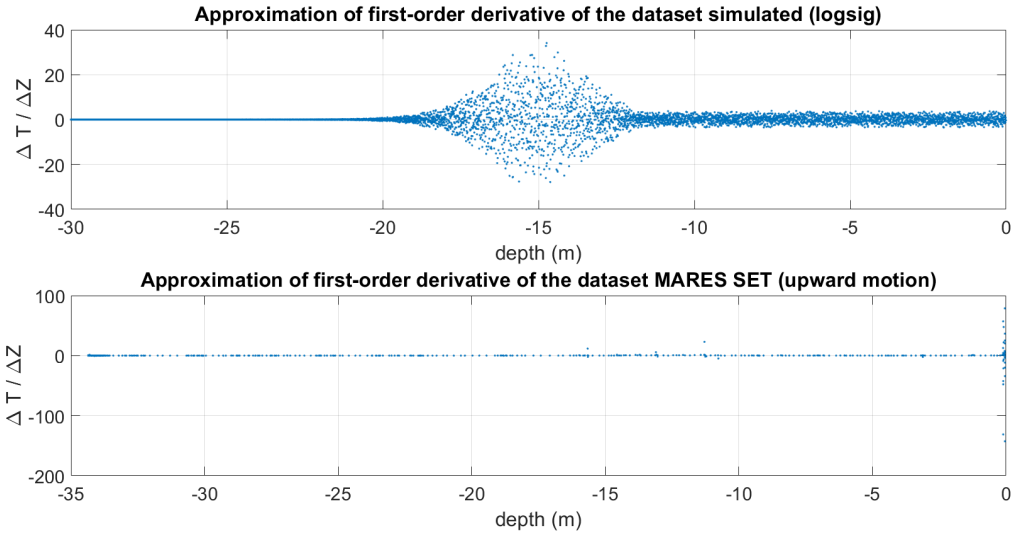

Figure 4.4: First-order derivative using a single sensor

It is considered an error when the following temperature measured is higher or smaller 0.5 °C than previous, or the depth measures is also greater or lesser than 0.5 m. A gradient value of the variable that approximates the first-order derivative, $\frac{dT}{dZ}$, is considered an error when the absolute value is greater than 2.

The last thresholds it was considered because:

- Observing figure 4.2, the maximum variation of the temperature to depth of the dataset MARES SET is 3 $^{\circ}C$ by 5 m (0.8 $^{\circ}C/m$). Thus, considering that the measurements were performed at a short time, it also considered that there does not happen a variation greater than 0.02 $^{\circ}C/m$ for 10 cm for this time. ($\frac{0.02}{0.01} = 2^{\circ}\ C/m > 0.8$)
- Given that in the work [12] was used a single sensor and that the data logging was done in a short time we are certain that the remaining thresholds are robust both to the error of the sensors as to the dynamics of the aquatic environment

Figure 4.5 shows the result of the pre-processing of dataset MARES SET (upward motion). It is still not possible to extract useful information to feed the parametric model.

To be able to take advantage of the first order derivative approximation, a moving average filter was applied. This filter is intended to increase the smoothing of the output curve. However, if the number of points chosen for the calculation of this filter is too large, we can soften the curve further, and in this way, we are subject to lose important information or modify this information. If the number of points is small, the conclusion is the same. Equation 4.5 represents the derivative at point $z(i)$ (mean above $\frac{n}{2}$ points up to $\frac{n}{2}$ below). This formula was used to implement the moving average filter.

$$\frac{\Delta T}{\Delta Z}_{|Z=Z(i)} = \sum_{i-n/2}^{i+n/2} \frac{T_{i+1} - T_i}{Z_{i+1} - Z_i} \tag{4.5}$$

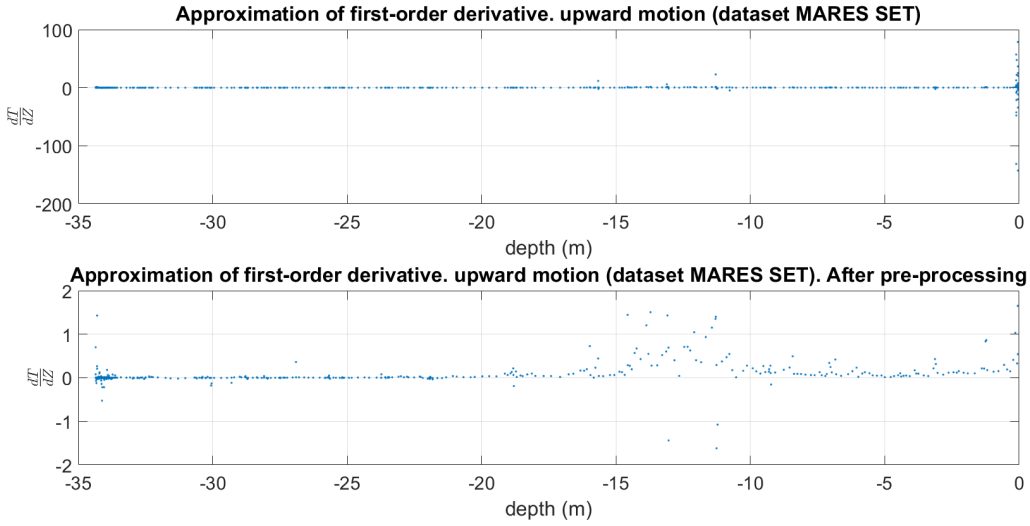

Figure 4.5: Pre-processing of the acquired data

Figure 4.6 shows the application of the moving average filter on $\frac{\Delta T}{\Delta Z}$, with different size of the filter window. These results show a highlighting of the layers. However, it is still difficult to know where we can separate the different layers, and thus, proceed to the tracking of thermoclines. We can observe that the filters with window size 40, 50, and 60 points modify the bottom depth of the thermocline comparing with the remaining filters. These three filters suggest that the endpoint of the thermocline is 18 (approx) meters deep. These filters, in addition to suggesting a different starting point, also soften the gradient value. Comparing the first three filters with the others it is possible to observe that the value of the peak of the gradient is smaller for the last three filters.

To highlighting the different layers a new hypothesis was considered, dividing the depth vector into a specific spacing. The result of the bottom of figure 4.7 presents the possibility of constructing a parametric model through this method. The result shows a more significant differentiation of the different layers in comparison to the previous methods. It also demonstrates that if we can perform measurements with a given spacing, we may obtain better results that all previous methods. This implies that if we have two or more sensors spaced at a given distance we can have the gradient information directly. In this way, while the vehicle tracks the thermocline, we are able to create a set of parameters that identify the different levels of the water column.

With the use of two or more sensors, we achieved the objective of tracking thermoclines with the gradient information. The explanation of the best spacing between the sensors and how many sensors are required to minimize the error for the ideal vertical temperature profile will be explained in a later section. Figure 4.8 shows the result of $\frac{\Delta T}{\Delta Z}$ for the ideal and real vertical profile, using two sensors separated by 1 m.

A good approximation to the gradient model present in figure 4.3 is obtained with the use of two sensors. With this result, we can then conclude that the integration of two or more sensors will be beneficial in comparison to the inclusion of a single sensor. In this way, we were able to perform the tracking of thermoclines using the gradient value and feed the parametric model.

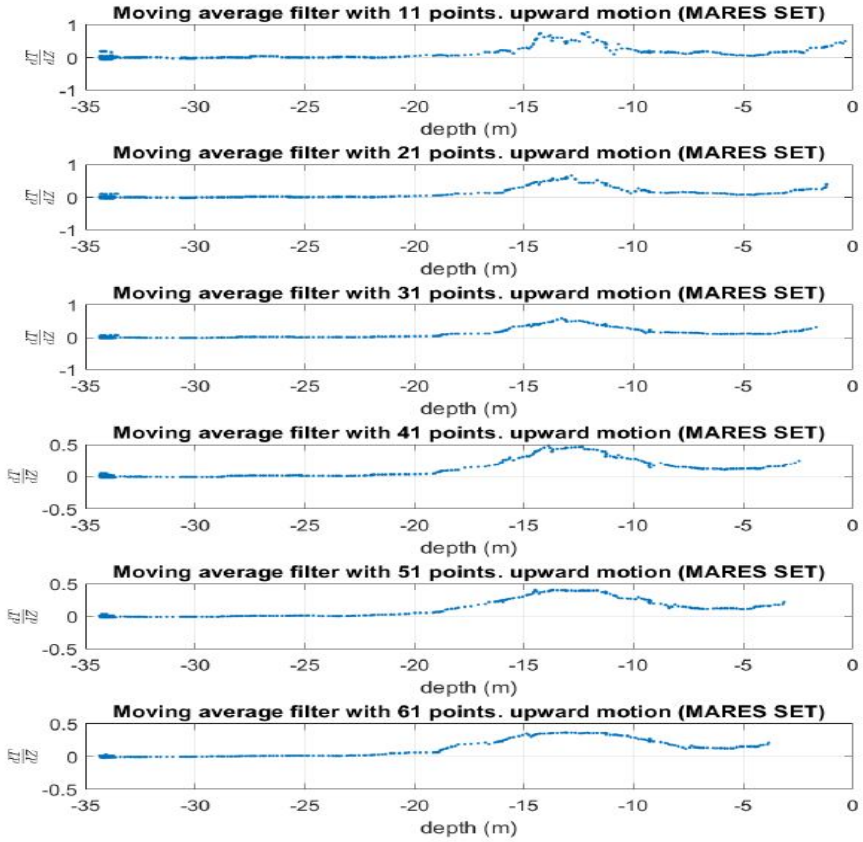

Figure 4.6: Moving average filter

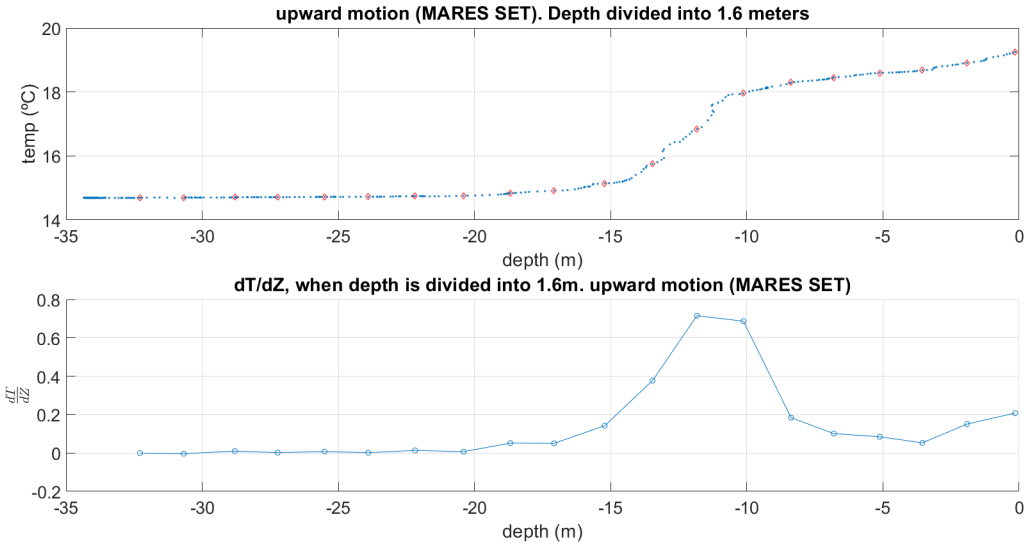

Figure 4.7: Divide the depth into a determining spacing, 1.6m.

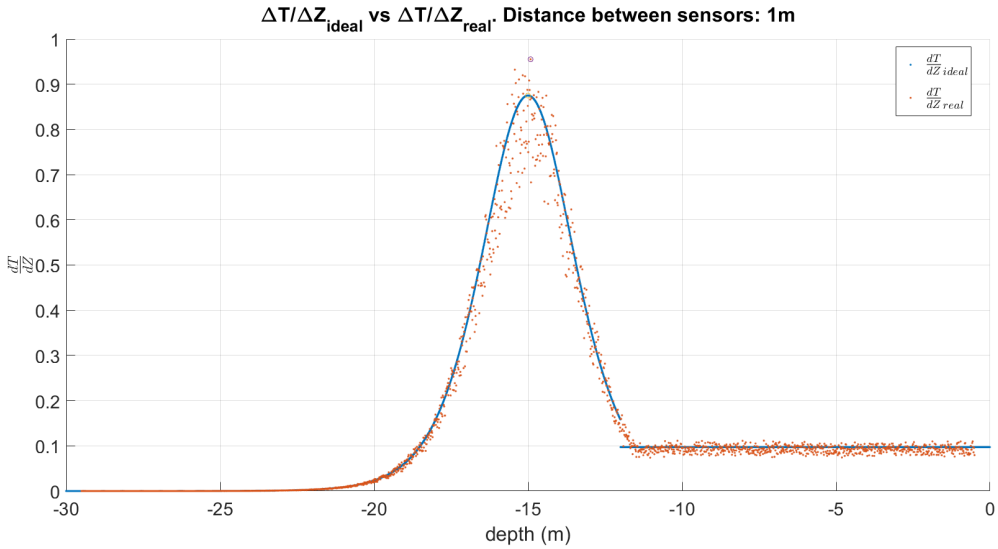

Figure 4.8: Result of the approximation of first-order derivative using 2 sensors

4.2.2 Final Parametric Model

The two possible models of representation of the vertical temperature gradient are present in figure 4.1. The advantages or disadvantages of each of the models will be discussed below.

Starting with the model shown in figure 4.1a, to represent this model, we need five parameters. Three to represent the respective gradient of each layer and two that indicate the top and bottom of the thermocline. The gradient is calculated as the mean of the gradients between the calculated depth parameters.

The disadvantage of this model to the model presented in the figure 4.1b is that with this last model we can detect the maximum gradient and in this way, we get the vehicle to circulate in the point of the higher temperature gradient. However, through a third-degree polynomial approximation of the points (T, Z) between the top and bottom depths of the thermocline, we can have the information of the maximum of the gradient. By calculating the derivative in the algebraic form, we have access to the point of the greatest gradient, and in this way, we already have the possibility of the vehicle to circulate in the point of the greater gradient.

With the model shown in figure 4.1b, we need six parameters to represent this model. Two of these parameters represent the gradient of the layers above and below of the thermocline, and another parameter represents the maximum gradient of the thermocline. The remaining three parameters represent depths. Two of them represent the top and bottom of the thermocline and the remaining parameter corresponding to the depth to the maximum gradient of the thermocline.

4.3 Main Difficulties

In the processing of the data, some difficulties were found. With the analysis made to the dataset MARES SET, it was verified that the results were a little distant to what was expected. Attempts

have been made to mitigate possible reasons for such results to have occurred. The following topics are possible reasons:

- dynamics of the aquatic environment
  - Some similarity between mixed-layer depth and thermocline, which can be explained due to the solar incidence in the first level or the temperature of the same being influenced by the ambient temperature. In this way, the differentiation between layers is difficult to obtain. This implies the application of different methods, such as, a moving average filter or to develop another approach that uses two sensors to obtain the parametric model.
  - Sea currents can affect the movement of the vehicle, and in this way, erroneous measurements are obtained
- errors in measurements
  - Wrong measurements can be obtained when the vehicle collides with objects
  - Sensor measurement error
  - Pressure to depth conversion. This conversion is also influenced by density

Comparing the results of the temperature gradient using a single CTD sensor or including two or more sensors, it was concluded that it is more difficult to obtain this gradient using a single sensor. Thus, implementing an option that integrates two or more sensors on the vertical profiler, it is easier to obtain a gradient model and in this way to find the parameters that feed the parametric model. However, to obtain all the parameters of this model, it is necessary that the profiler performs a deep profile. The ESC method allows the increasing of the amplitude that the profiler performs the tracking of the thermocline. Then, we have an option that tracks and detect the highest point of the gradient and find the parameters that feed the parametric model.

Chapter 5

Distribution of the Sensors

In this chapter, we will discuss the metrics developed to know how many sensors are needed to apply in the profiler and the spacing between them. The objective of these methods is to obtain gradient information with the smallest error relative to the ideal model.

Before proceeding with the explanation of the developed methods, the following assumptions should be considered:

- vertical gradient temperature of the figure 5.1 is the ideal, this means, without considering measurement errors
- consider that we propose to perform the detection and tracking of thermoclines span a minimum of 3 meters
- disposition of the set of sensors limited to 1 meter spacing. Limitation due to the size of the profiler, see figure 5.2
- descent or ascent speed of 1 m/s
- data logging every 15 ms

Some of these premises were already presented in a previous section (section 3.2). The last two assumptions have the purpose to simulate the vehicle motion and the measurements of water temperature and depths. If the vehicle performs a downward motion at 1 m/s and the data logging is performed at 15 ms, the new measure will be performed 15 cm below than the previous.

5.1 Methods

As already was described, the calculation of the gradient will be obtained as a difference of values.

$$\frac{\Delta T}{\Delta Z}_{|Z=Z(i)} = \frac{T_{i+1} - T_i}{Z_{i+1} - Z_i} \tag{5.1}$$

Thus, this difference will be influenced by the error. Intuitively, the use of more sensors reduces the error. Supposing that the sensor error is influenced by ε. Equation 5.2 shows the value

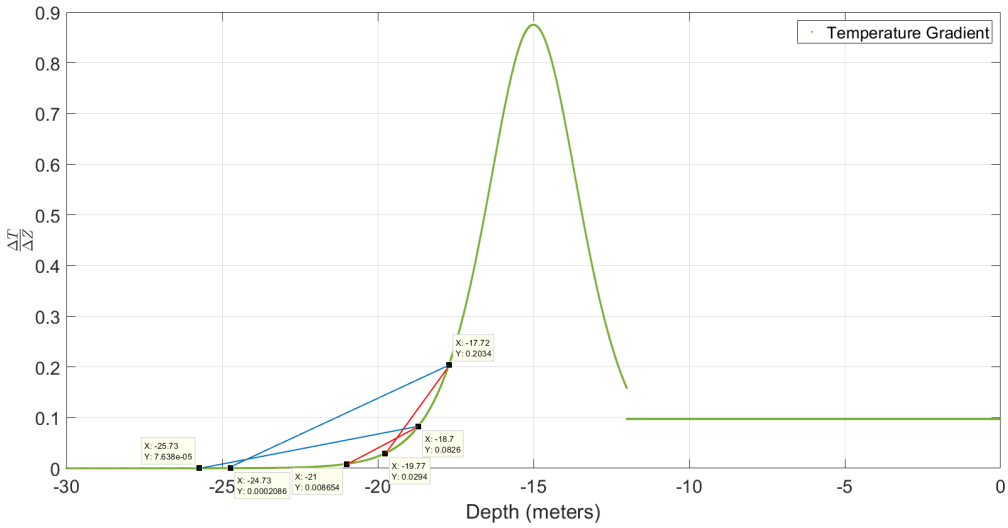

Figure 5.1: Temperature gradient

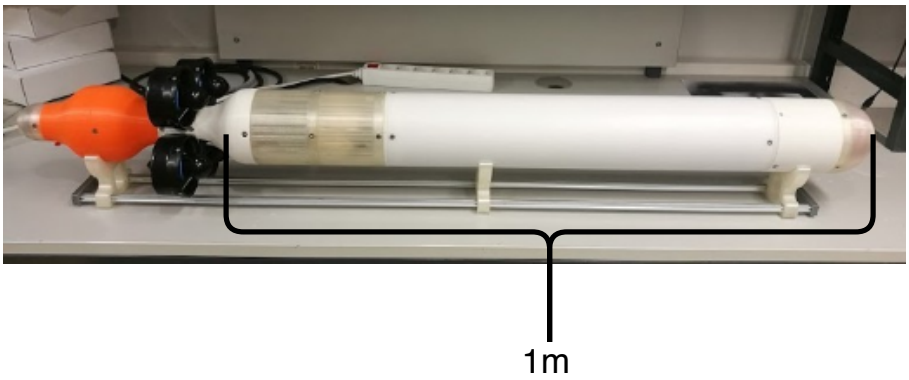

Figure 5.2: Configuration of the profiler

of the derivative influenced by the sensor error.

$$\overline{\frac{\Delta T}{\Delta Z}} = \frac{\overline{T}_{i+1} - \overline{T}_i}{Z_{i+1} - Z_i} = \frac{(T_{i+1} \pm \varepsilon) - (T_i \pm \varepsilon)}{Z_{i+1} - Z_i} \tag{5.2}$$

In the worst case, we have that:

$$\overline{\frac{\Delta T}{\Delta Z}} = \frac{(T_{i+1} - \varepsilon) - (T_i + \varepsilon)}{Z_{i+1} - Z_i} = \frac{\Delta T}{\Delta Z} - \frac{2\varepsilon}{\Delta Z} \tag{5.3}$$

Therefore, by increasing the distance between sensors, we are less subject to the error. However, by increasing this distance, the gradient is smoothed. Analyzing figure 5.1, it is possible to observe this smoothing. The blue lines simulate the gradient measurement with the two sensors spaced 7 meters. The red lines simulate the gradient measurement with the two sensors spaced 2 meters. Comparing these two measurements of the gradient, it is possible to conclude that by increasing the spacing between the two sensors, the gradient will be more smooth. Then, the choice of this distance implies a compromise between the measurement error of the sensors and the error in the calculation of the gradient in relation to the ideal.

The following methods were tested with noise in temperature measurement. This noise is proportional to the derivative $\frac{\Delta T}{\Delta Z}$ of the ideal gradient model (Fig. 5.1).

$$T(i) = T(i) + 0.2 \cdot random(0,1) \cdot \frac{\Delta T}{\Delta Z}(i) \tag{5.4}$$

5.1.1 How Many Sensors?

The maximum distance allowed to place the sensors in the vehicle is 1 meter, and we consider the maximum use of 6 sensors. In this way, in table 5.1 we have the spacings for the different quantities of sensors to be used.

Table 5.1: Spacing between the sensors

Quantity	Spacing (m)
6	0.2
5	0.25
4	0.33
3	0.5
2	1

With the use of two sensors, that is, two measures of temperature (T) and depth (Z), the derivative can be approximated by:

$$a_i \approx \frac{\Delta T}{\Delta Z} = \frac{T_{i+1} - T_i}{Z_{i+1} - Z_i} \tag{5.5}$$

To calculate the derivative when it were used more than two sensors, the least squares linear approximation was used. Equation 5.6 is the linear function that approximates the n measures, where $n = (2,3,4,5,6)$.

$$P(x) = a_0 + a_1 x \tag{5.6}$$

Equation 5.7 shows how to obtain the coefficients a_0 and a_1 of equation 5.6.

$$AX = B \Leftrightarrow \begin{bmatrix} 1 & x_0 \\ 1 & x_1 \\ \vdots & \vdots \\ 1 & x_{n-1} \end{bmatrix} \begin{bmatrix} a_0 \\ a_1 \end{bmatrix} = \begin{bmatrix} f(x_0) \\ f(x_1) \\ \vdots \\ f(x_{n-1}) \end{bmatrix} \tag{5.7}$$

The least squares solution of $AX = B$ is $X = A^{+}B$, where A^{+} is the pseudo-inverse of A, given by $A^{+} = (A'A)^{-1}A'$.

The derivative of $P(x)$ is $P'(x) = a_1$, thus, the element a_1 represents the temperature gradient ($\frac{\Delta T}{\Delta Z}$). This element is calculated at every n measures of temperature and depth. The reference depth of this derivative is half of the distance of the sensors (0.5 m). Each element of a_1 obtained every n measures is compared to the gradient obtained by the `diff` tool of Matlab (Fig. 5.1) for the respective depth.

The following code excerpt shows how the temperature and depth are obtained for each position of the sensors. In this case, the situation of measuring the temperature and depth of the first sensor, in the total of six, is shown.

```
distances  = [0.2 0.25 0.33 0.5 1] %1m

% ascent speed 1.0m/s and logging time 15ms
v    = 1.0; %speed
t    = 15e-3; %logging time
deltaZ = v*t; %distance

%sensor 1, total 6
distance = distances(1); %sensors separated by 0.2m
vehicleBottom  = Z(1); %first depth of the mission (30m, upward motion)
tolerance  = 1e-6;

j = 1;

for i=1:length(Z)
 if abs(Z(i) - vehicleBottom) <= tolerance
  t(1,j) = T(i); %temperature at sensor 1
  z(1,j) = Z(i); %depth at sensor 1
  vehicleBottom  = vehicleBottom + deltaZ; %vehicle motion (more 15cm)
  vehicleTop   = vehicleBottom 5*distance; %position of sensor n (in this case n=6)
  if vehicleTop > Z(end) %arrive at surface
   break;
  end
 end
 j = j + 1;
end
```

To calculate the element a_1, the following method was performed:

```
for i=1:numberOfSensors %sensor 1 to sensor n
 for k=1:numberOfMeasures % measure 1, 2, ..., until length(z(i,:))
  A(i,1) = 1;
  A(i,2) = z(i,k); %depth (x0)
  B(i,1) = t(i,k); %temperature (f(x0))
 end
end

X = A\B;
a = X(:,2); %element a1 P'(x) = a1
```

This method was performed for the quantities of three to six sensors.

To compare the obtained results, it was calculated the absolute difference between the different elements a_1 with the gradient obtained by the `diff` tool. The following excerpt shows the calculation of this gradient. This gradient is influenced by the temperature measurement error.

```
dT = diff(T_ideal);
dZ = diff(Z_ideal);
difference = zeros(length(dT),1);

for i=1:length(difference)
 difference(i) = dT(i)/dZ(i);
end
```

Equation 5.8 calculates the difference between the temperature gradient obtained by sensors and the first-order derivative. This difference is calculated for the different amounts of sensors ($n = 2,3,4,5,6$) along the temperature profile (30 m to 0 m, Fig. 5.1).

$$e(n) = |a_n(i) - difference(Z(i))| \tag{5.8}$$

To compare the error obtained for the different quantities of sensors, the mean of the equation 5.8 was calculated (N measures along the temperature profile).

$$e_{mean}(n) = \frac{\sum_{i=1}^{N} |a_n(i) - difference(Z(i))|}{N} \tag{5.9}$$

The equation 5.10 ponders the error in relation to the average error obtained with 2 sensors.

$$e_{ratio}(n) = \frac{\frac{\sum_{i=1}^{N} |a_n(i) - difference(Z(i))|}{N}}{\frac{\sum_{i=1}^{N} |a_2(i) - difference(Z(i))|}{N}} \tag{5.10}$$

Figures 5.3 and 5.4 show the comparison of results for the different amounts of sensors. Figure 5.3 shows that with more sensors, we are less subject to error. Analyzing figure 5.4, it is possible to observe that the error difference between two and six sensors is less than 20%. Since the difference of the error is minimum between two and six sensors, it was decided to use two sensors. Given that the difference is minimal, the distribution of two sensors also implies fewer adaptations in the profiler and also implies a cost reduction. The distance between the two sensors is discussed in section 5.1.2.

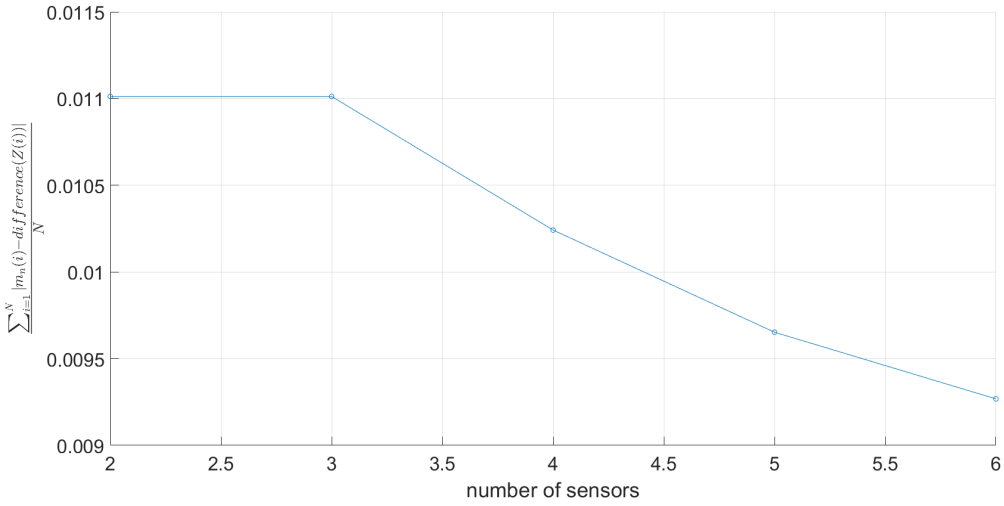

Figure 5.3: Error for the different quantities of sensors

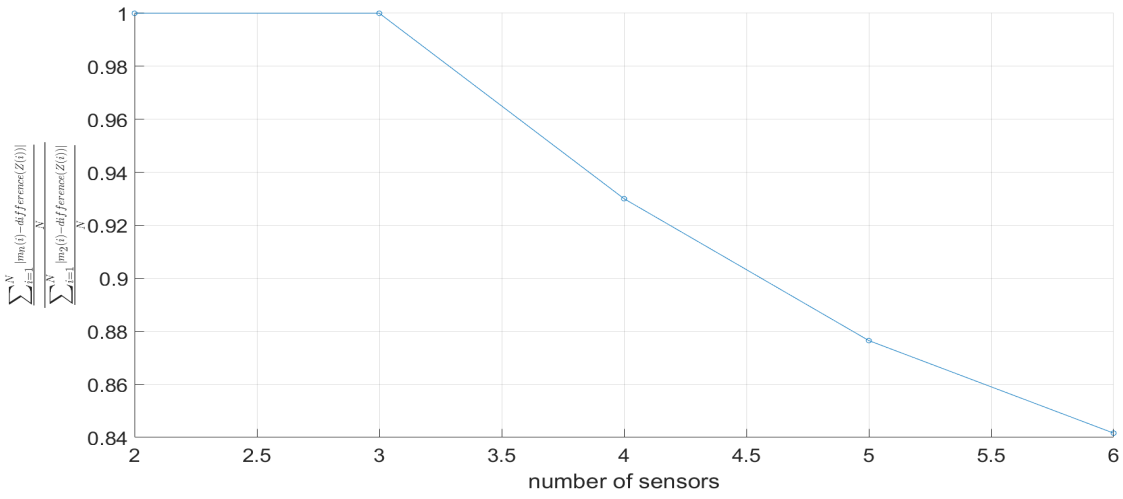

Figure 5.4: Ratio error for the different quantities of sensors

The results of figures 5.3 and 5.4 show that the average error for two and three sensors is the same. Since the position of the middle sensor is central to the sensors placed at the ends, in the least square calculation the value of a_1 is the same. Only the value a_0 changes, i.e., the value of the ordinate at the origin. Thus, we can conclude that using three regularly-spaced sensors yields the same result as using only two sensors at the ends. Moving one of the sensors is what changes the value of the derivative. Figure 5.5 shows that with a different value of Y in the middle sensor, the value of a_1 is the same (compare the element a_1 of $P_1(x)$ and $P_2(x)$). The difference between $P_1(x)$ and $P_2(x)$ is the element a_0. It is also possible to observe that moving the position of the middle sensor, the value of the gradient changes, element a_1 of $P_3(x)$ ($a_1 = 1.0132$).

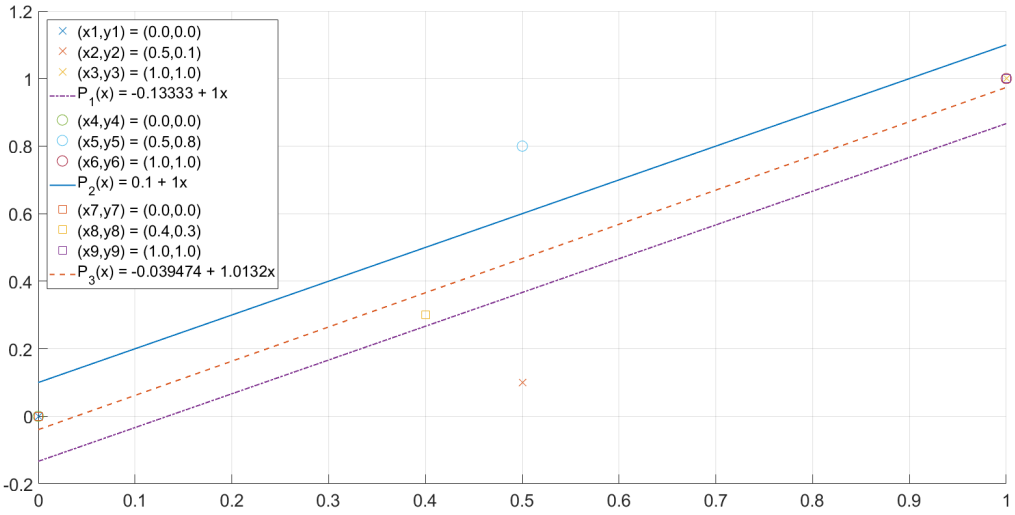

Figure 5.5: Difference between the least square approximation obtained by 2 and 3 sensors

5.1.2 Distance Between Two Sensors

To verify the best possible distance between two sensors, it was considered the possibility of incorporating a wire with temperature and depth sensors. This arrangement aims to ensure that for a given thermoclines span, we know exactly where to place the sensors, i.e., with this spacing, we have the smallest possible error.

The profiles represented in figure 5.6 were considered to represent different shapes of the water column. Thus, it is possible to compare the different results with the purpose to obtain a robust conclusion. As already was described in chapter 4, we consider two different temperature profiles to simulate the real environment. The difference between these two profiles is the thermocline representation. One of these profiles, use logarithm sigmoid (blue trace of Fig. 5.6) and the remaining profile use tangent sigmoid (orange trace of Fig. 5.6). To be more practical to mention these profiles, we will designate the trace in blue as profile 1 and the orange in profile 2. Analyzing the figure 5.6 we verified that the span of the thermocline of the profile 1 is approximately 6 meters.

The profile 2 has a span near to 3.5 meters. For each profile, an error was added as a percentage of the approximation of the first-order derivative.

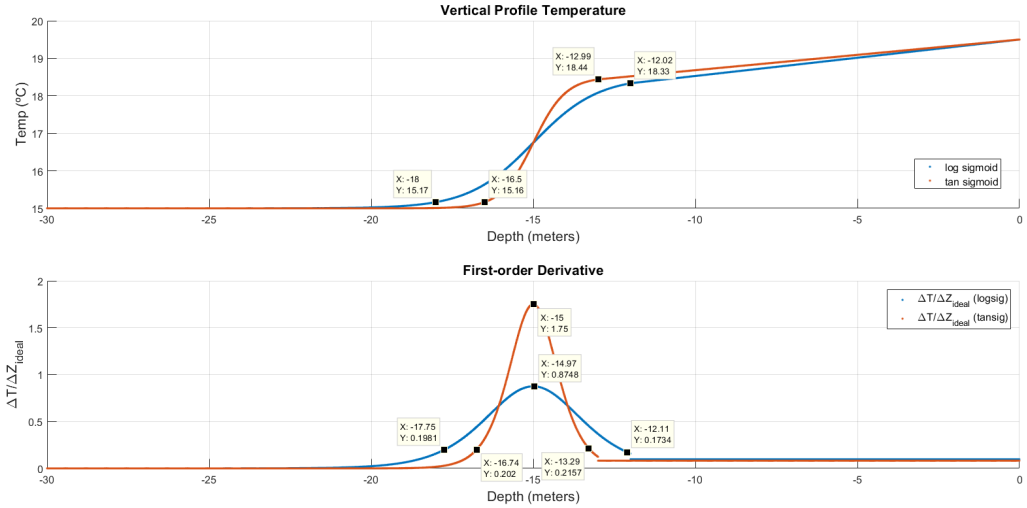

Figure 5.6: Profiles used to calculate the maximum distance that minimizes the error. The bottom figure is the first-order derivative of each profile

As already was explained, the difference between integrating two, three or more sensors is minimum. Therefore, in this method, only two sensors were used. Different distances between the two sensors for each profile of figure 5.6 were used, given that the vertical spacing of the thermocline is different for each profile. Given that the thermocline span of the profile 1 is greater than the thermocline span of the profile 2, greater distances between sensors were used in profile 1. The following distances, in meters, were considered. These are the distances between the two sensors.

- Profile 1
  - 0.25; 0.3; 0.35; 0.4; 0.5; 0.75; 1; 1.25; 1.5; 1.75; 2; 2.5; 3; 3.5; 4; 4.5; 5; 5.5; 6; 6.5; 7
- Profile 2
  - 0.25; 0.3; 0.35; 0.4; 0.5; 0.75; 1; 1.25; 1.5; 1.75; 2; 2.5; 3; 3.5; 4; 4.5

In this method, the error between the maximum derivative of the ideal model (Fig. 5.6) and of the profile that simulates the noise of the sensors measurement was calculated, equation 5.11. The calculation of this error had the purpose to verify what is the distance between two sensors that minimize this error.

$$e = \left| \frac{\Delta T}{\Delta Z}_{max_{ideal}} - \frac{\Delta T}{\Delta Z}_{max_{noise}} \right| \tag{5.11}$$

The error given by the formula in 5.11 was performed for one hundred different profiles, for each value of the distance. Each of these profiles is influenced by a different noise in the temperature measurement. After calculating the error for each profile, the mean of the error was

performed. Figure 5.7 shows that to obtain the smallest possible error in relation to the maximum of the ideal model, the sensors must be separated by 1.75 meters. For profile 2 the distance is 1 m (Fig. 5.8). In our case, due to the size of the profiler, the distance that minimizes the error is 1 m.

Analyzing figures 5.7 and 5.8, it is possible to observe that for the same error there is a greater margin at the right of the distance that minimizes the error, i.e., for the same error it is possible to increase more the distance than to reduce this distance.

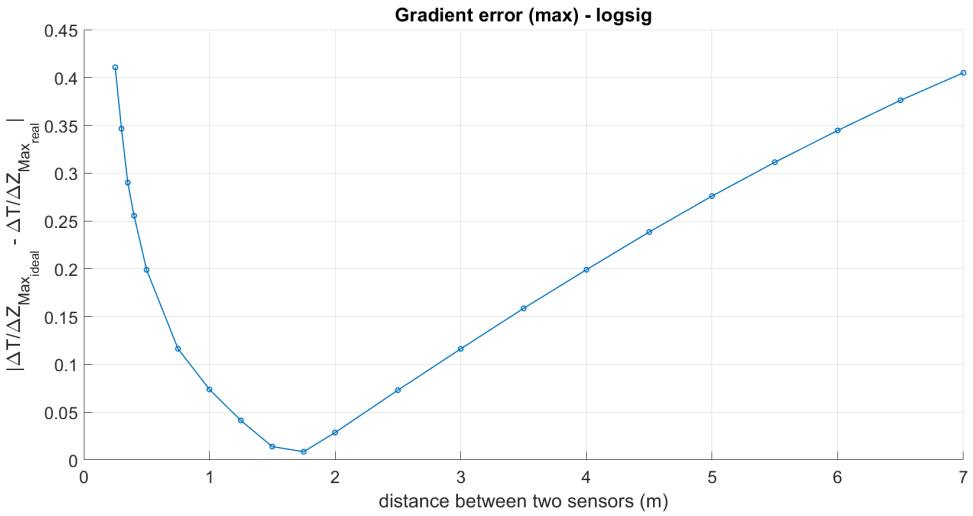

Figure 5.7: Result of the error of the profile 1

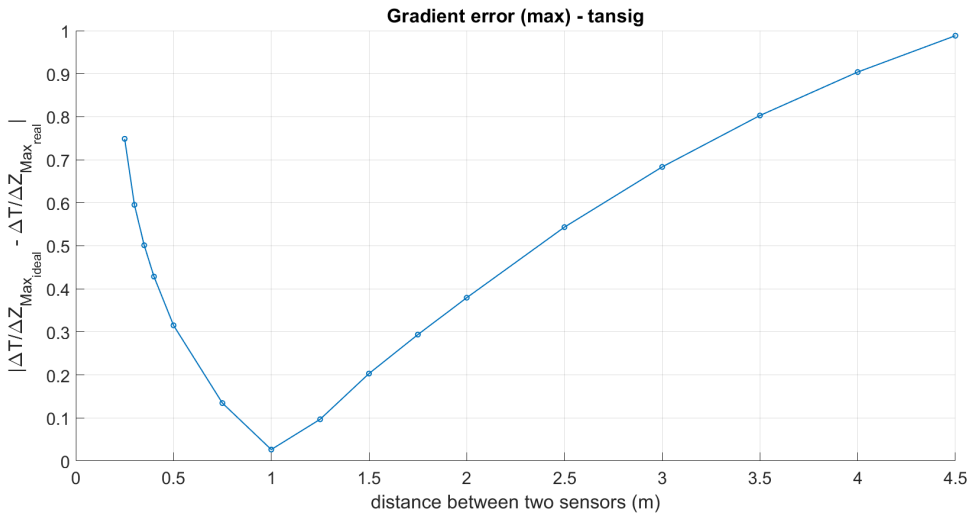

Figure 5.8: Result of the error of the profile 2

5.2 Conclusions

After to develop the method that illustrates that the use of more sensors reduces the error in the measures and another method that illustrates that by increasing the distance between two sensors

the gradient error increases, the following conclusions were obtained:

- if exist a maximum number of sensors, we know that with this quantity, to calculate differences or gradients, we are less subject to the error
- it was concluded that for the same margin in relation to the distance that minimizes the error of the equation 5.11, the distance between two sensors should be increased

Chapter 6

Implementation of the Extremum Seeking Control

During this chapter, the implementation of the ESC will be presented. The different blocks of the ESC scheme will be explained, as well as the physical meanings of the different parameters related to the ESC. Energy consumption issues will also be discussed as well as the stability of the control method.

Figure 6.1 shows the structure implemented in this work. The block **Vehicle Dynamics** represent the vertical profiler. For controller design and tuning, we use the transfer function ($G(s)$) that relates the input given to the thrusters of the vehicle with the variation of its position, in the vertical direction, following the model in [30].

$$G(s) = \frac{Z(s)}{F(s)} = \frac{0.086}{s \cdot (s + 0.1029)} \tag{6.1}$$

With the finality of the profiler to follow references with a minimum delay and low attenuation, in the block **Controller** we consider the position controller proposed by [30] for our profiler. The block **Sensors** is calculated by the difference in temperature of the two sensors placed in the profiler. In our case, these sensors are separated by 1 meter, at the same distance to the vehicle's center of mass. The position of the sensors are illustrated in figure 6.2. The block **MAF** has the purpose to reduce the oscillation, in $\hat{Z}$, provided by sine waves. This block is an implementation of the moving average filter. The other blocks are responsible for the ESC, following the structure described in [22]. After to describe the main purpose of each block, we can conclude that the frequency ω is related to both the profiler dynamics and the periodic perturbation signal. It is also concluded that the phase shift of the ESC (Φ) will be related to the delay of the profiler response to the reference and to the phase shift of the high-pass filter (HPF). Thus, the implementation of the ESC was divided into four main groups:

- Vehicle Dynamics - improvement of the position controller and choice of the ideal frequency to have the least possible delay about the reference
- High-Pass Filter - consequence of the delay of the filter in the system

- Product between HPF and sine wave (demodulation) - determine the delay Φ and verify if the system converges to the optimum (background theory)
- Amplitude and frequency of both sine waves

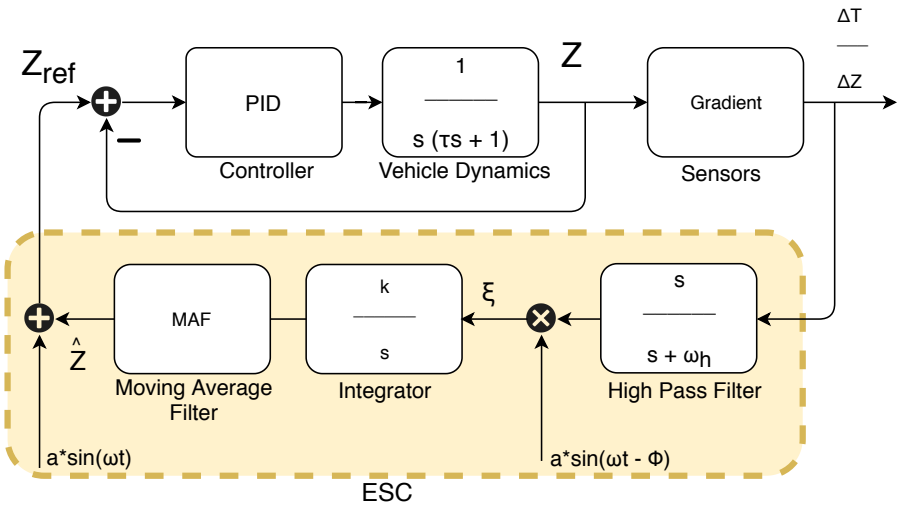

Figure 6.1: ESC scheme to tracking the maximum of the gradient of thermoclines

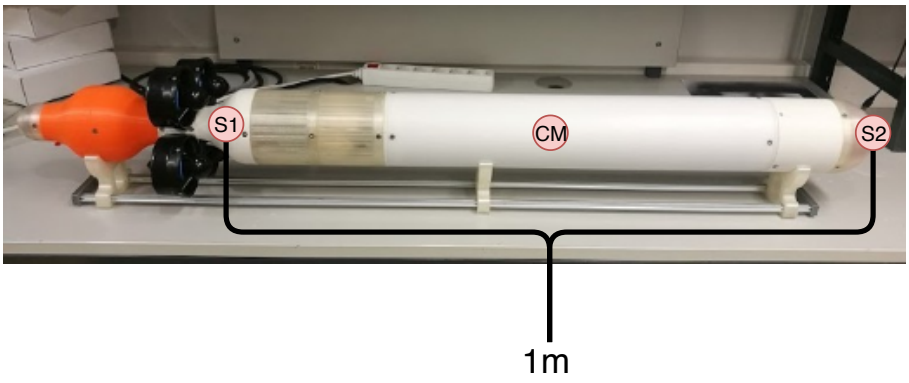

Figure 6.2: Position of the sensors on profiler

In this section, it was considered that the vehicle was to carry out the tracking of a thermocline with a center 15 m and gradient 0.225 $^{\circ}C/m$. The equations 6.2 and 6.3 were the functions used to create the vertical temperature profile present in figure 6.3.

$$\dot{T}(Z) = -\frac{(Z-15)^2 - 15^2}{1000} \tag{6.2}$$

$$T(Z) = \frac{\frac{1}{3}\cdot Z^3 - \frac{1}{2}\cdot 30\cdot Z^2}{1000} + 30 \tag{6.3}$$

The different steps of this implementation were performed in the Matlab Simulink tool.

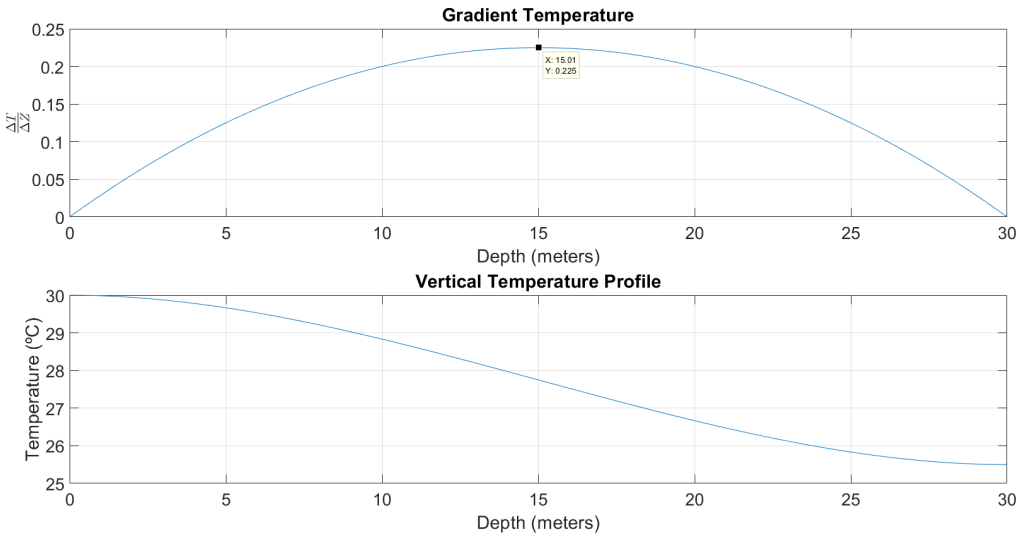

Figure 6.3: Gradient temperature and vertical temperature profile to test the ESC

In order to simplify the language and some explanations, consider the notations present in table 6.1.

Table 6.1: Parameters of ESC scheme

ω_{ESC}	Frequency of both sine waves
Z_{ref}	Depth reference
$\hat{Z}$	Best estimate of the depth
A_1	Amplitude of the sine wave that multiplies with filter response
A_2	Amplitude of the sine wave that sums with $\hat{Z}$
K_{PID}	Gain for the position controller
K_ζ	Gain of the integrator
z_{top}	Maximum depth allowed
z_{bottom}	Minimum depth allowed

6.1 ESC Step 1 - Vehicle dynamics

Taking into account that to the reference of the position of the vehicle is added a sine wave, in this section an analysis of the response of the transfer function $G(s)$ in relation to sinusoidal waves with different periods was realized.

The position controller implemented by [30] was developed in order to have a settling time below 10 s. Thus, for the frequency corresponding to this period, the feedback response to $G(s)$ will have a considerable delay and attenuation. Figure 6.4 shows this delay and attenuation for the feedback response to a sine wave with period equal to 10 s. For this delay to be reduced it would be necessary to increase K_p. This increase implies an increase in the energetic cost, since for small variations of the position the vehicle will respond quickly.

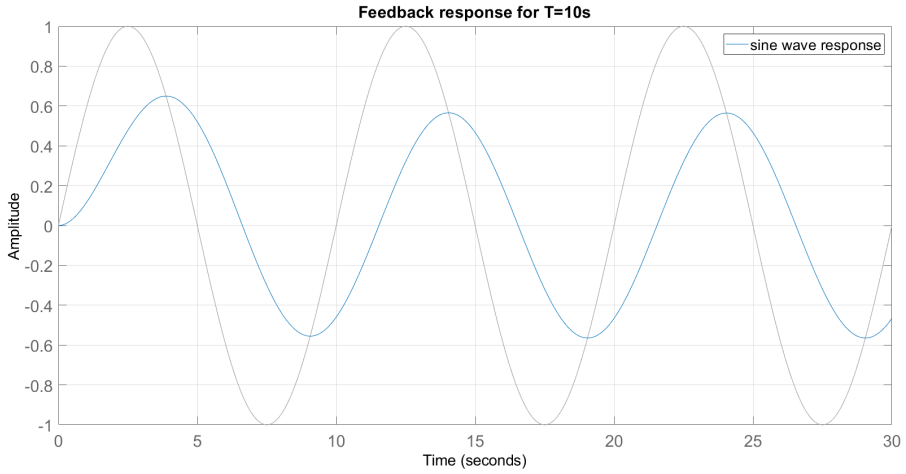

Figure 6.4: Feedback response for T=10s

The increase of the frequency also implies an increase in energetic cost. Knowing that to the reference of the ESC is added a sine wave, the vertical position of the vehicle has the following form:

$$Z = \hat{Z} + A_2 \cdot sin(\omega t) \tag{6.4}$$

So we have to:

$$\dot{Z} = A_2 \cdot \omega \cdot cos(\omega t) \tag{6.5}$$

$$\dot{Z}_{MAX} = A_2 \omega = A_2 \cdot \frac{2\pi}{T} \tag{6.6}$$

Given that the power is proportional to the square of the velocity ($P \propto v^2$), the choice of the frequency and the amplitude imply a change on the energetic cost. Thus, it was considered to use $T = 20\ s$ or $T = 30\ s$ for the ESC period. In figure 6.5, we can verify that to $K_p = 5$, the system has a longer delay and attenuation for the sinusoidal signal with a period of 20 s. In this way, the period of 30 s was chosen.

In order to minimize the delay, it was decided to improve the controller, even though this implies a higher energetic cost. Analyzing figure 6.6, the difference between different position controllers is minimum. Verifying that a delay of 5° has no effect on the convergence of the algorithm (section 6.3.2), $K_{PID} = 5$ was chosen.

6.2 ESC Step 2 - High-Pass Filter

The main goal of the analysis of the block **High-Pass Filter** is to inspect the difference between the speed and delay for different cut-off frequencies. Therefore, the analysis of the filter response and the result of the best estimate of depth ($\hat{Z}$) were performed, i.e., the output of HPF and the output of integrator of figure 6.1 were analyzed, respectively. Given that G(s) has to be faster to

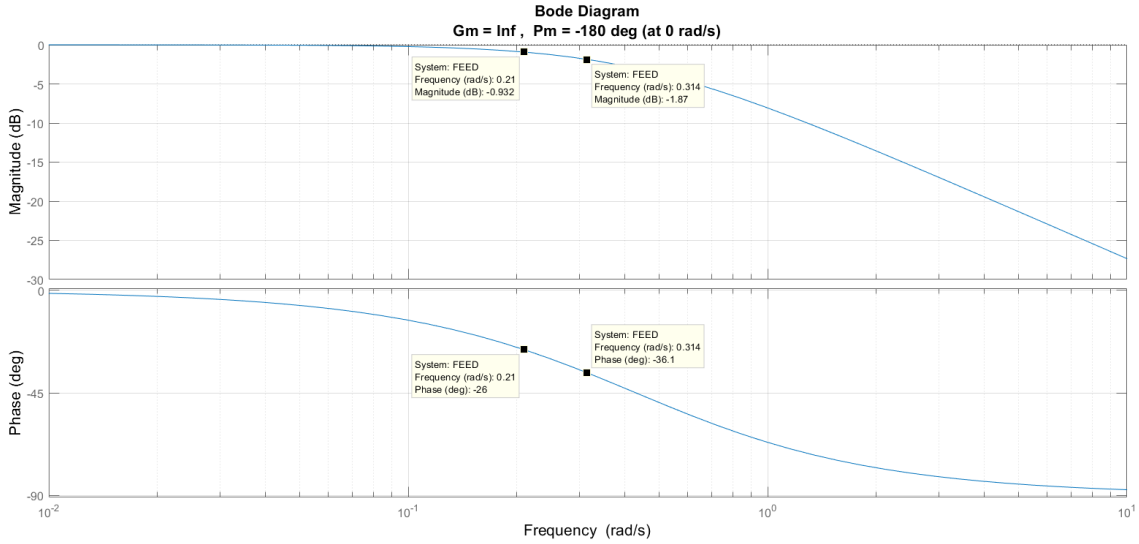

Figure 6.5: Comparison between sinusoidal references with period 20 and 30 seconds

the response of the reference depth than the ESC feedback, ω_h has to be lower ω_{ESC} ($\omega_h < \omega_{ESC}$). Thus, the analysis of the following frequencies was realized:

- $\omega_{h_1} = \dfrac{\omega_{ESC}}{10}$ (1 decade below)
- $\omega_{h_2} = \dfrac{\omega_{ESC}}{100}$ (2 decades below)

Before carrying out the analysis of the result of the filter response in the ESC feedback scheme of figure 6.1, the Bode diagram for the different frequencies was analyzed (Fig. 6.7). With the Bode diagram we can verify that the phase-shift and the attenuation for the frequency ω_{ESC} for each one ω_{h_i} is minimum. In this way, we will only take into account the speed of the filter response.

Figure 6.8 shows that the filter response of ω_{h_2} is slower than the filter response of ω_{h_1}. Since the phase shift is minimum for each of the frequencies, we choose the frequency a decade below the frequency ω_{ESC}, given that the response is faster. Since for ω_{h_2} we are placing a pole closer to the origin, the system gets slower. Thus, for ω_{h_1} the system reaches faster the steady state.

Analyzing figure 6.9, it is possible to observe that for ω_{h_1} the $\hat{Z}$ has lower oscillation. The oscillation in $\hat{Z}$ happens since the system for ω_{h_2} is slower. This oscillation causes the system to reach the steady state more slowly.

6.3 ESC Step 3 - Demodulation

In this section, an analysis of the product between a sinusoidal signal and the output response of High-Pass Filter (HPF) will be performed. This step is denominated by demodulation. Firstly, a set of results that verify the theory behind the ESC (section 2.6) will be demonstrated. After that, an analysis of the delay Φ is performed.

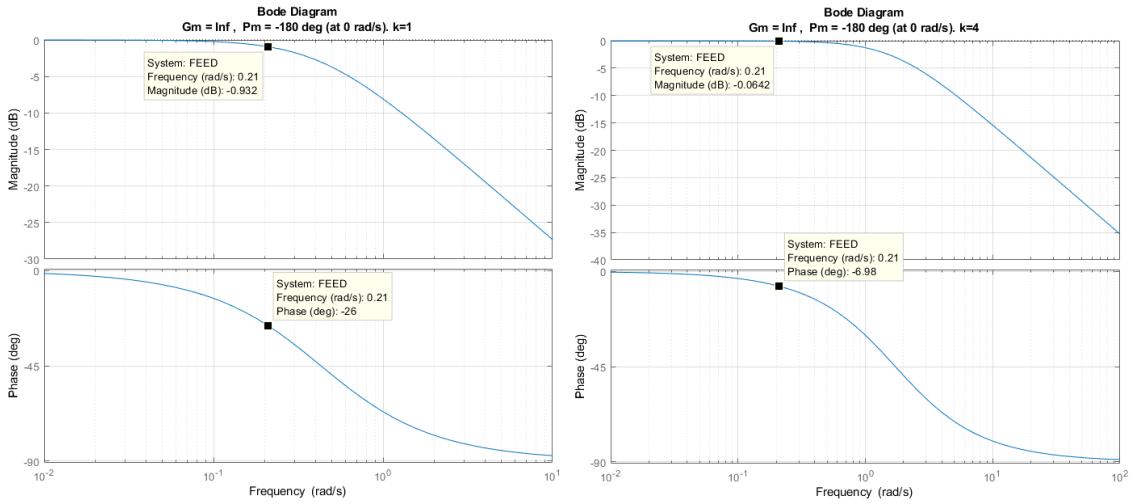

(a) K=4

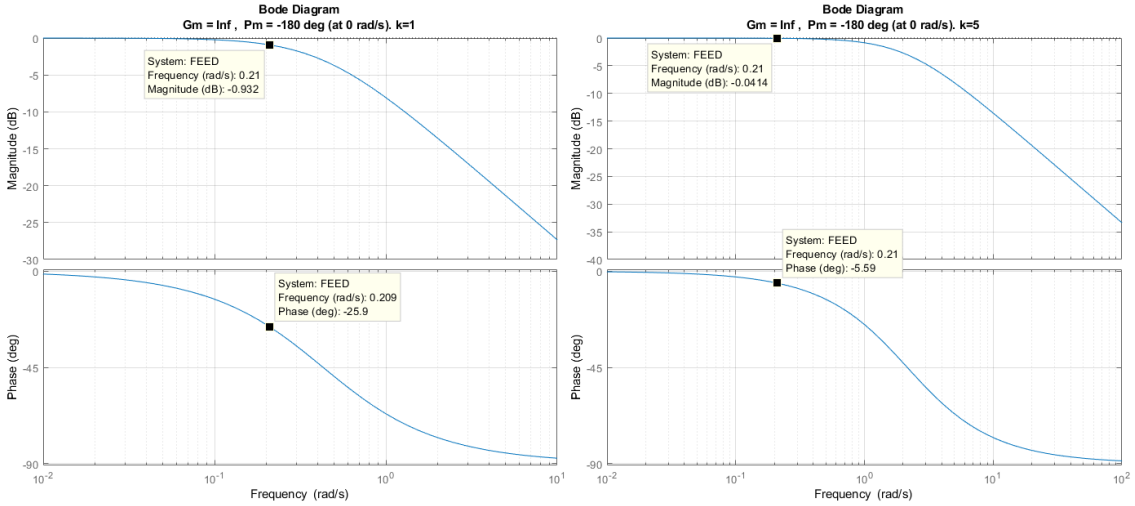

(b) K=5

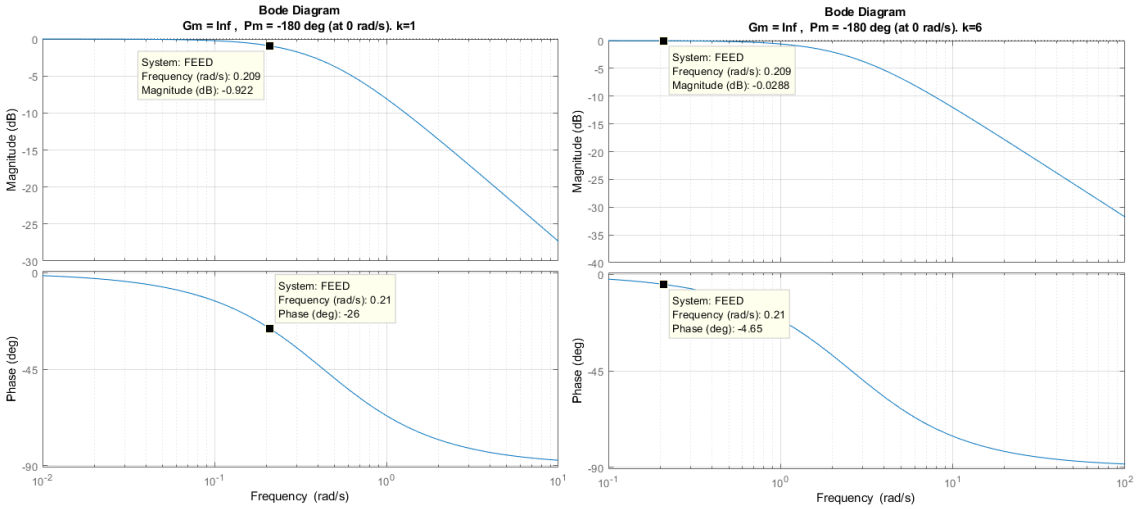

(c) K=6

Figure 6.6: Influence of K in the position controller

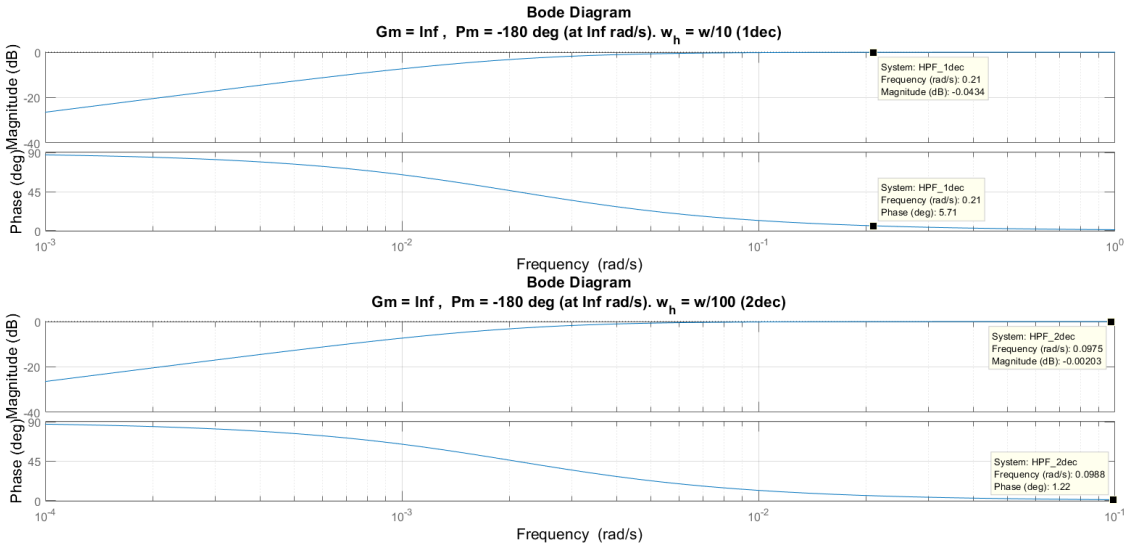

Figure 6.7: Bode Diagram of the High-Pass Filter

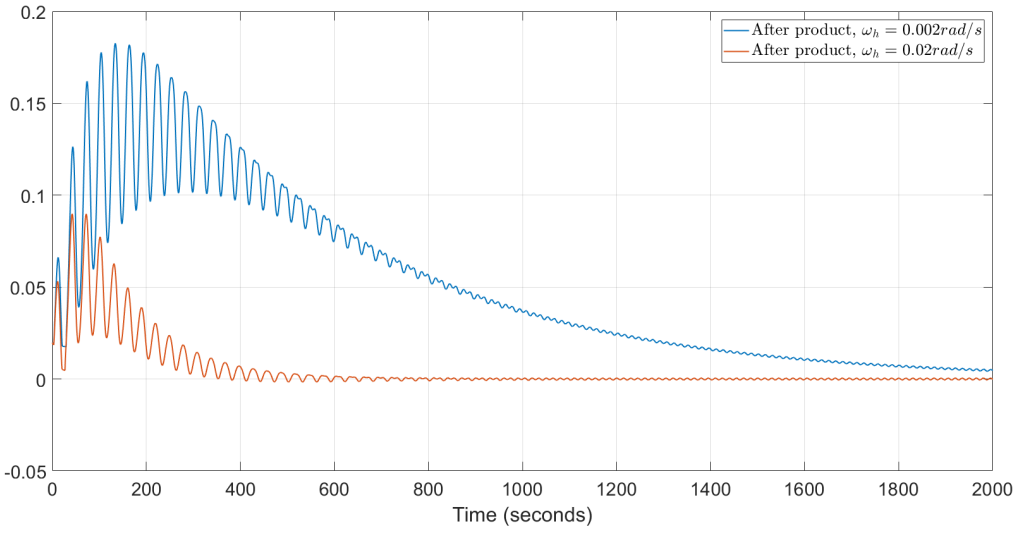

Figure 6.8: Comparison between different cut-off frequencies. Filter response.

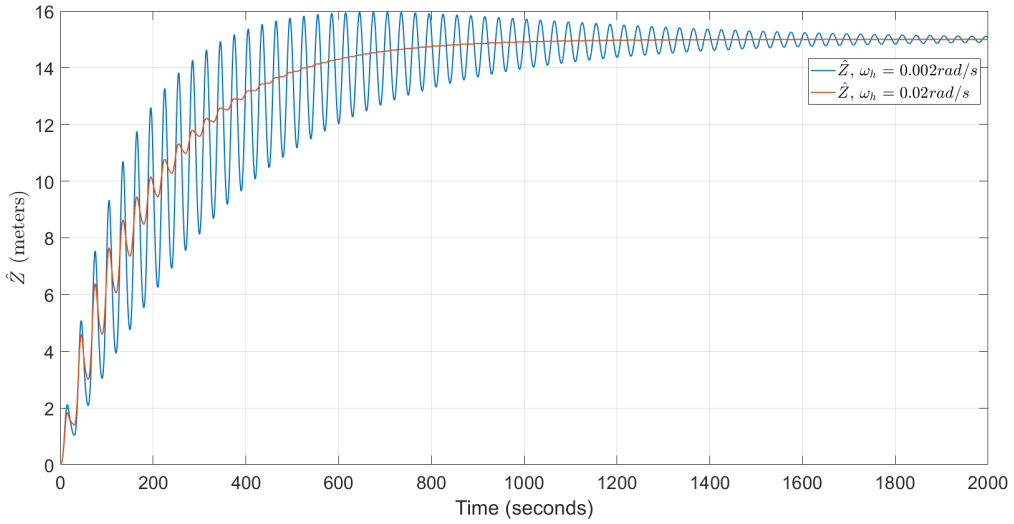

Figure 6.9: Comparison between different cut-off frequencies. Analysis of $\hat{Z}$.

6.3.1 Left or Right of the Optimum, Extremum Seeking Control Response

To illustrate if the system converges to the solution, the result of the product between the HPF and the sine wave was analyzed. For this analysis, the diagram shown in figure 6.10 was used.

In order to simulate $\hat{Z}$, an offset to the sine wave of figure 6.10 was added. This offset simulates the position of the vehicle. Therefore, if we want to verify if it is to the left of the optimum, the offset can be 0 (less than 15), if we want to be on the right, we choose an offset greater than 15. This implies if at the beginning of the mission we started above or below of the respective depth at the maximum gradient.

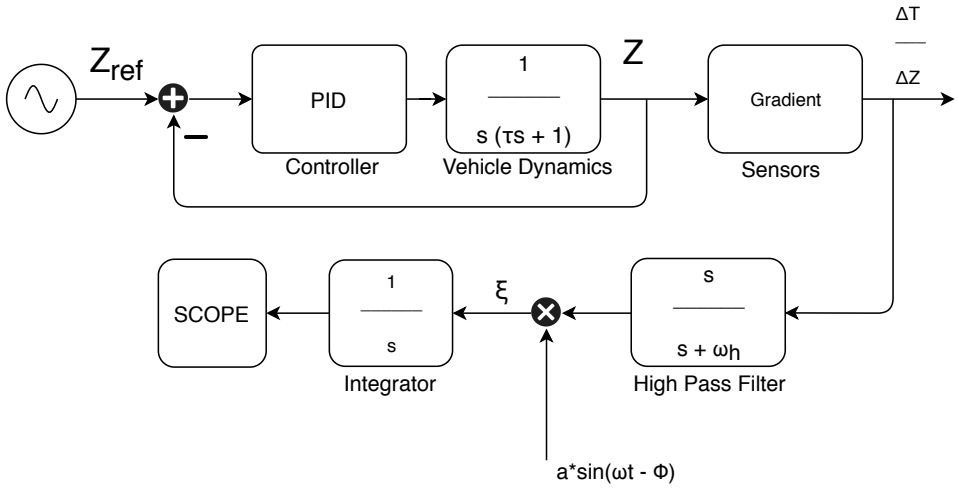

Figure 6.10: Demodulation scheme

Figure 6.11 shows the result of the demodulation and the integration of the demodulation when the simulation starts at the left of the optimal value, offset equal 0. Figure 6.11a shows that the sine wave and the filter response are in phase. In this way, the product between the two previous

signs is positive. As the product is positive, the integration of this signal results in a depth increase. This result can be seen in figure 6.11b.

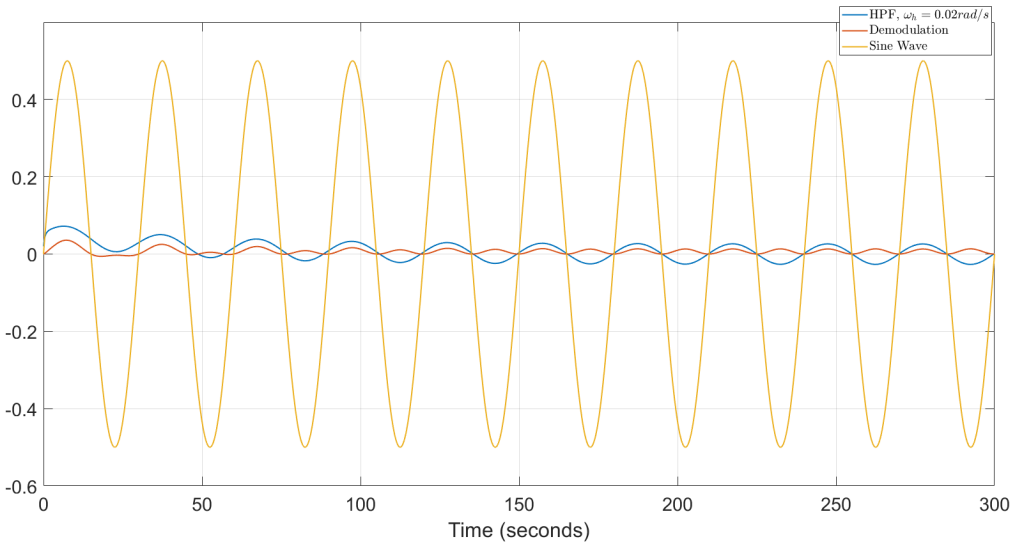

(a) Demodulation, sine wave, and filter response

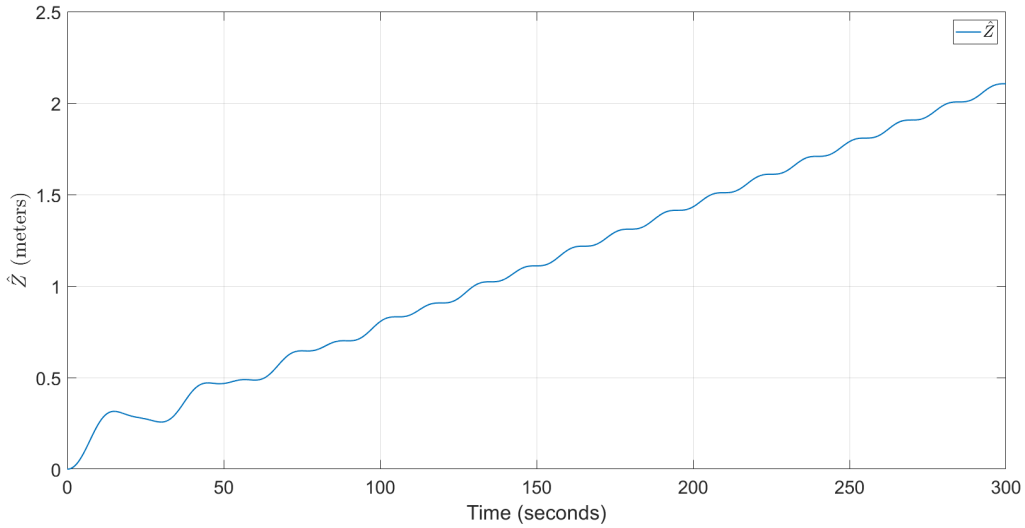

(b) Demodulation integration results

Figure 6.11: Left of the optimum value results

In order for the simulation to start to the right of the optimum value, the following offset was chosen: 20. The results obtained are shown in figure 6.12. Analyzing figure 6.12a, it is possible to observe that the sine wave and the filter response are out of phase. Therefore, the product between them is negative and the integration of this product will indicate that the depth has to be decreased. Figure 6.12b shows this decrease.

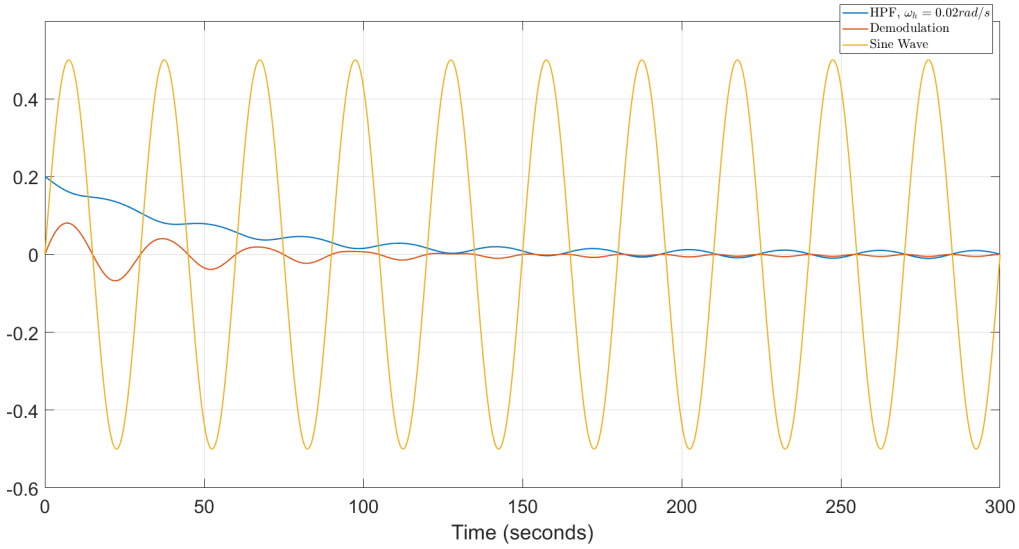

(a) Demodulation, sine wave, and filter response

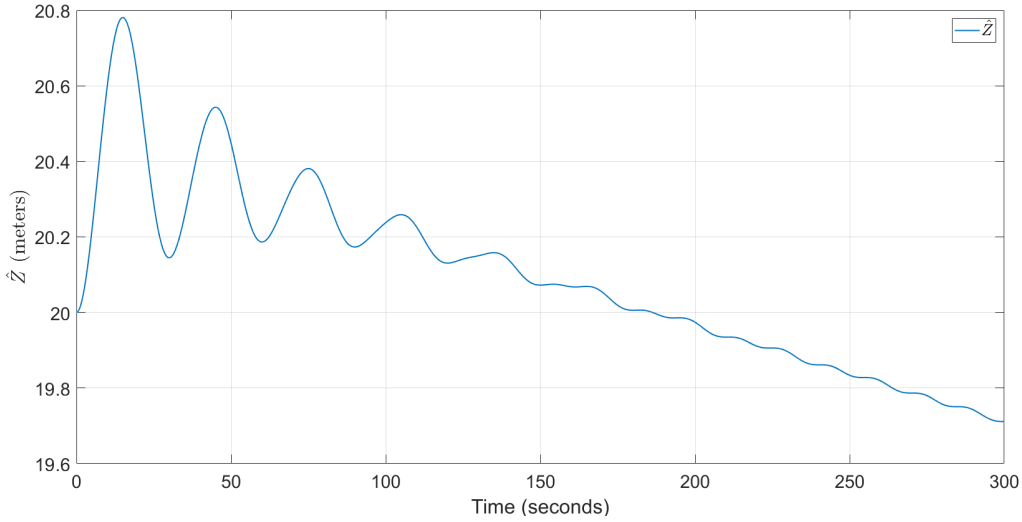

(b) Demodulation integration results

Figure 6.12: Right of the optimum value results

6.3.2 Phase shift of ESC

This section aims to verify what is the physical meaning of Φ in this approach and also verify its effect on the final result of the algorithm.

In this approach, Φ represents the delay of $G(s)$ system in relation to the reference and the phase of the HPF. Thus, for $K'_p = 5 \cdot K_p$, we have the following delay:

$$\Phi_{G(s)} = -5.59^\circ \tag{6.7}$$

$$\Phi_{HPF} = 5.52^\circ \tag{6.8}$$

$$\Phi = \Phi_{G(s)} + \Phi_{HPF} \approx 0, \tag{6.9}$$

where $\Phi_{G(s)}$ and Φ_{HPF} were taken from figure 6.6b and 6.7, respectively. Then, in order to observe the effect of Φ in the implementation of the ESC, we will analyze the difference of the response for $K'_p = K_p$ and $T = 20s$, given that for this controller $\Phi_{G(s)} = -36^\circ$. In figure 6.13 the ESC response for $\Phi = 0$ and $\Phi = -31^\circ$ is compared. It is observed that this interferes in the response time of the ESC, given that, for $\Phi = -31^\circ$ the system reaches faster the steady state. Thus, in this approach of the ESC, we can consider that values of Φ between 0 and -31° have a minimum impact.

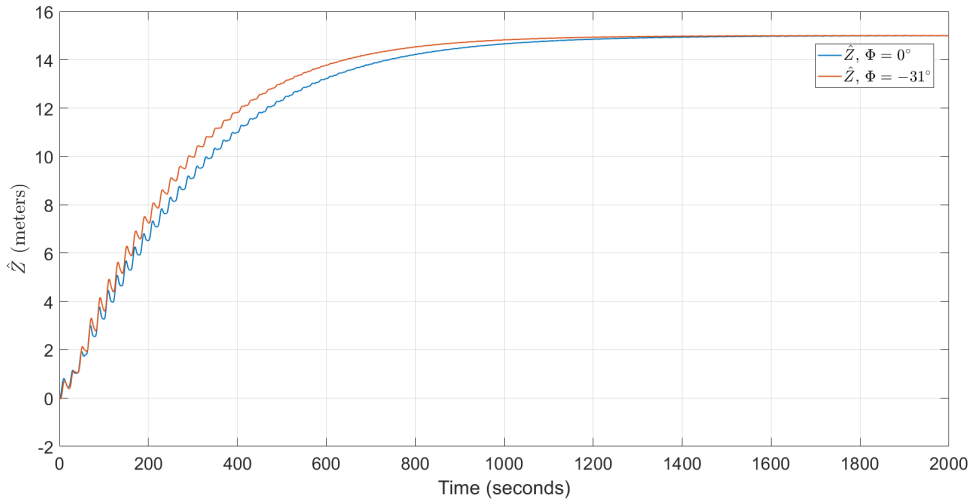

Figure 6.13: Comparison between the ESC response for $\Phi = 0^\circ$ and $\Phi = -31^\circ$

6.4 ESC Step 4 - Sine Wave Analysis

In this section, the influence of the amplitude and frequency of both sinusoids on the ESC response will be discussed.

6.4.1 Frequency

Analyzing the Bode diagram of the figure 6.6b, we observe that increasing the frequency, the phase shift and attenuation also increase. Thus, by increasing the frequency ω_{ESC} the phase shift between the sine wave that multiplies with the HPF and the response of HPF increases. Thus, the product between HPF and the sine wave is affected. This implies that the system is slower to reach the steady state. Figure 6.14 compares the difference of $\hat{Z}$ for different frequencies ($\omega = \omega_{ESC}$ and $\omega = 3 \cdot \omega_{ESC}$) and confirms that the system for $\omega = 3 \cdot \omega_{ESC}$ is slower.

By decreasing the frequency ω, the phase shift is lower. As already was described, decreasing the frequency implies that the system is slower and has a greater oscillation until it reaches the steady state. Figure 6.15 shows the difference of $\hat{Z}$ for different frequencies ($\omega = \omega_{ESC}$ and $\omega = \frac{1}{3} \cdot \omega_{ESC}$). The result of figure 6.15 shows that the system for $\omega = \frac{1}{3} \cdot \omega_{ESC}$ converges to the steady state with more oscillation than to the system with $\omega = \omega_{ESC}$.

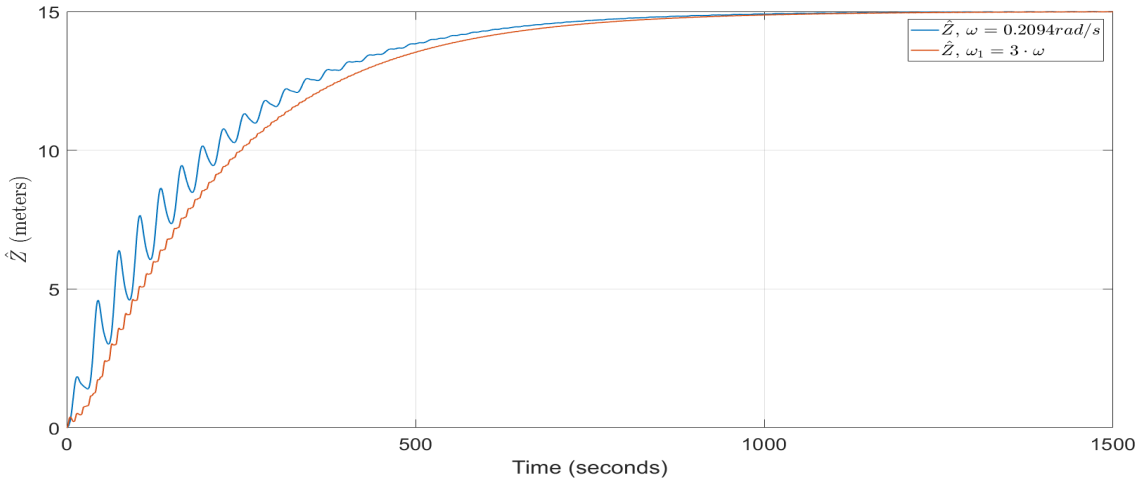

Figure 6.14: ESC response for $\omega_1 = 3\omega$

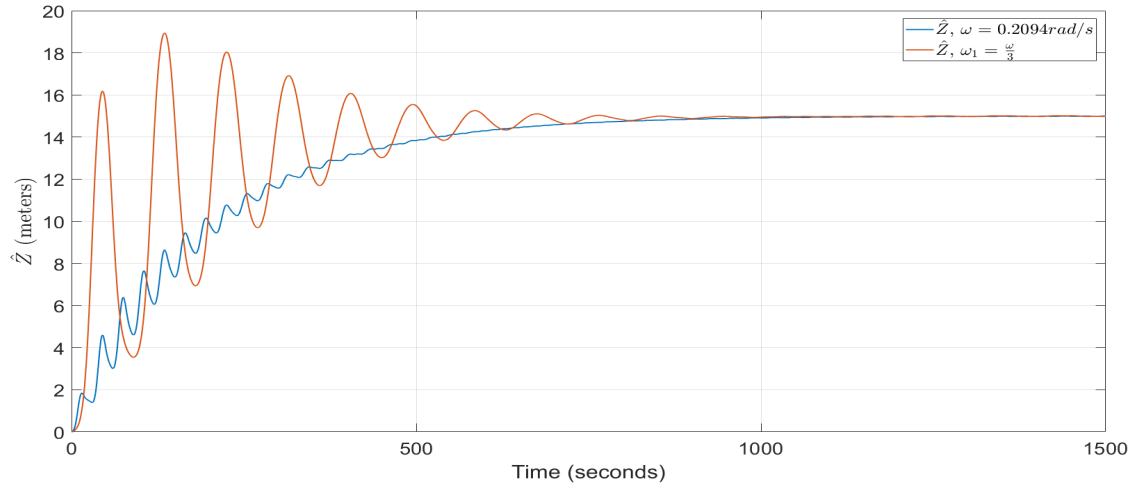

Figure 6.15: ESC response for $\omega_1 = \frac{1}{3}\omega$

6.4.2 Amplitude

The following results show the effect of the amplitude (A_1) of the sine wave that multiplies with output of the filter.

Figures 6.16 and 6.17 compare the $\hat{Z}$ between two schemes with different amplitudes A_1. Figure 6.16 shows that if we increase the amplitude of the sine signal, the scheme converges faster. Conversely, if we reduce the amplitude of this signal, the system slows down (Fig. 6.17).

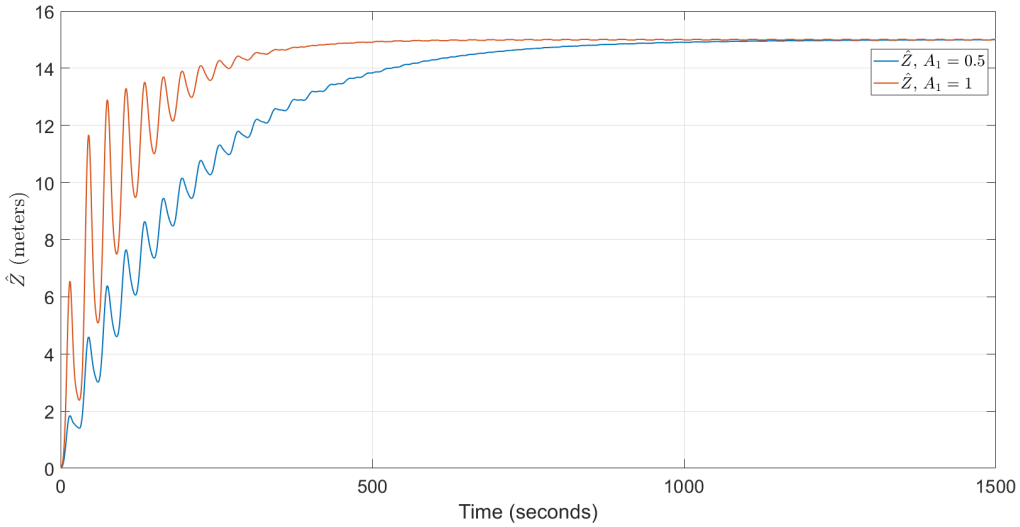

Figure 6.16: Result of $\hat{Z}$ with amplitude $A_1 = 1$

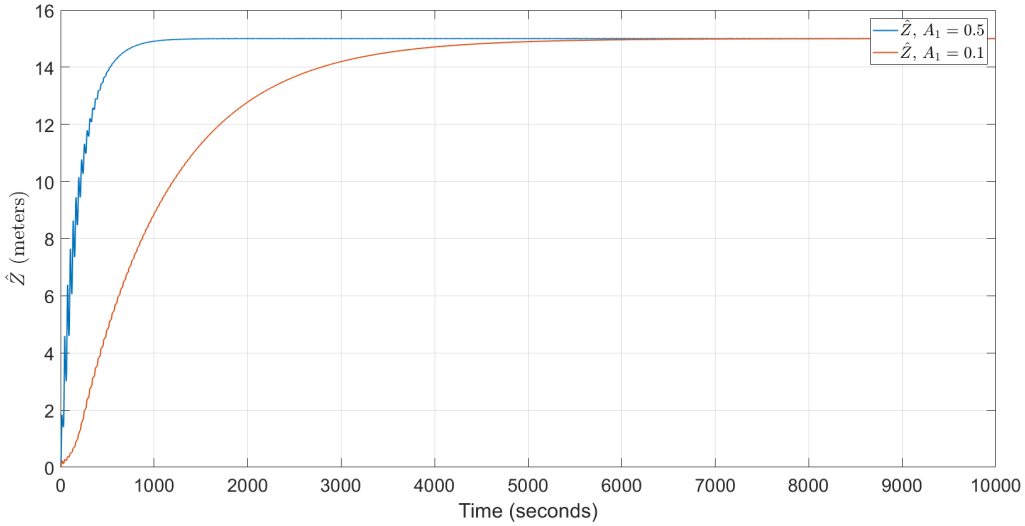

Figure 6.17: Result of $\hat{Z}$ with amplitude $A_1 = 0.1$

Figure 6.18 shows that the relation between the gain K_ζ of the integrator and the amplitude A_1 of the sine wave is inversely proportional. If the amplitude is reduced by half ($A_1' = 0.5A_1$) and if the gain K_ζ is increased to the double ($K_\zeta' = 2K_\zeta$) the result is the same if $A_1' = A_1$ and $K_\zeta' = K_\zeta$.

However, if both parameters increase, the system reaches the solution faster. If both decrease, the system reaches the solution slower.

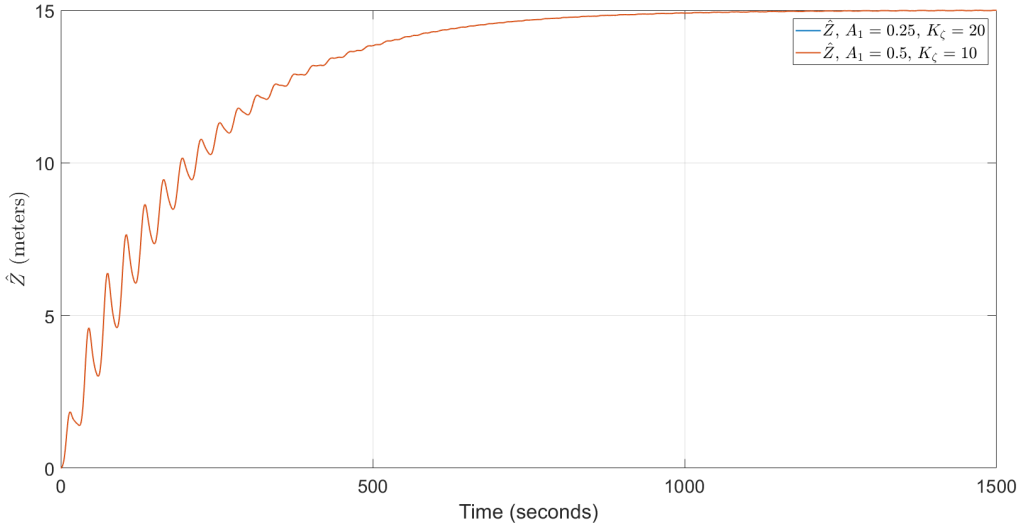

Figure 6.18: Relation between gain K_ζ of the integrator and the amplitude A_1

For the amplitude (A_2) of the sinusoid that sums with the best estimate of the depth, $\hat{Z}$, the conclusions are the same. If the amplitude is reduced, the system is slower, conversely, if the amplitude increases the system is faster. Figures 6.19 and 6.20 show the previous conclusions.

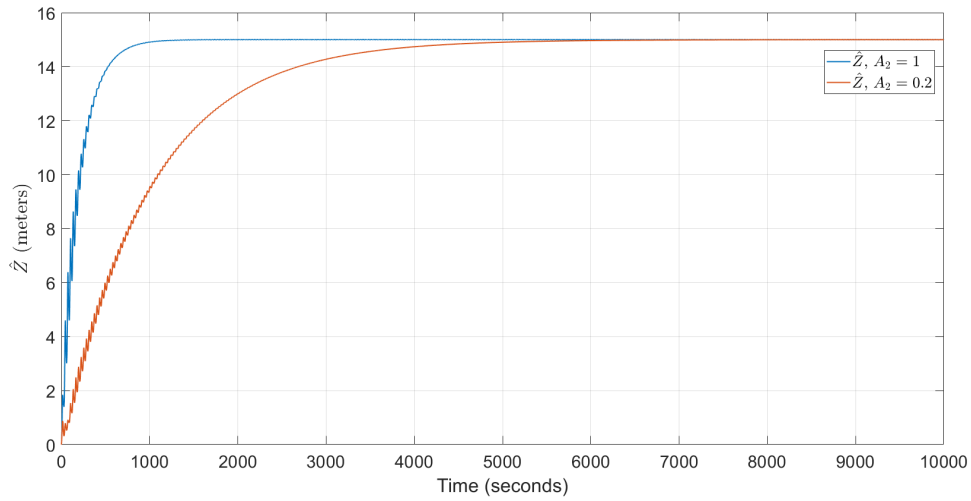

Figure 6.19: Result of $\hat{Z}$ with amplitude $A_2 = 0.2$

All previous results show that if we increase X times the amplitude, the system is X times faster. Although both amplitudes show this relation, the physical meaning is different for each one. The amplitude A_1 is only a multiplicative factor, that is, it makes the system more or less fast. The amplitude A_2 implies the value, in meters, of the variation of Z. For example, if we choose an amplitude equal to 2, the profiler travels a vertical distance of 4 meters. In order to observe the difference of the physical meaning of each sine wave, a simulation was performed, in which

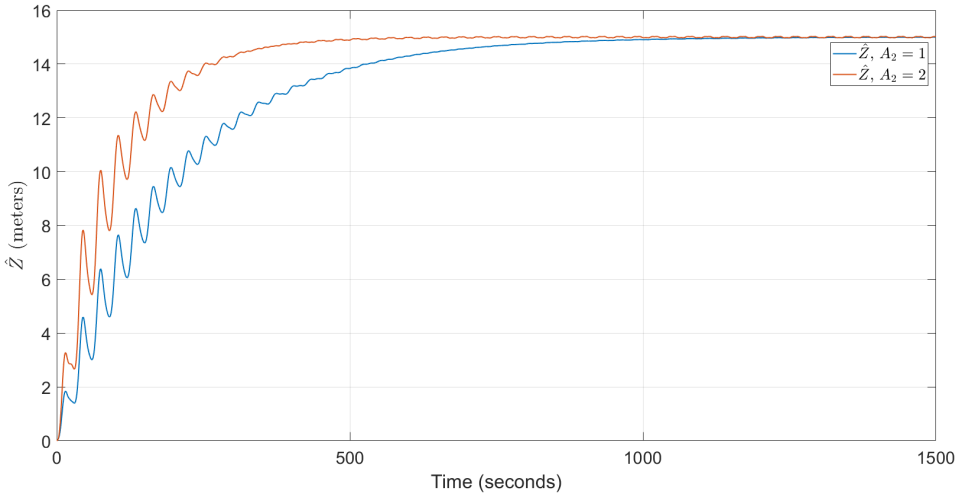

Figure 6.20: Result of $\hat{Z}$ with amplitude $A_2 = 2$

two different schemes are compared. In these schemes only the parameters A_1 and A_2 have been changed. In scheme 1, $A_1 = 0.5$ and $A_2 = 1$ were chosen. In scheme 2, $A_1 = 0.25$ and $A_2 = 2$. These values were chosen so that the convergence time of the algorithm was the same. It can be concluded that these amplitudes have an inversely proportional relation. If we reduce one and increase the other, in the same proportion, the system reaches the steady state at the same time. All previous conclusions can be observed in figure 6.21. We observe that both approaches converge to the depth corresponds to the maximum gradient with the same time. The difference is in the range that the vehicle travels around the peak. Since the frequency ω_{ESC} in the different schemes was not altered, increasing A_2 implies an increase in energy consumption.

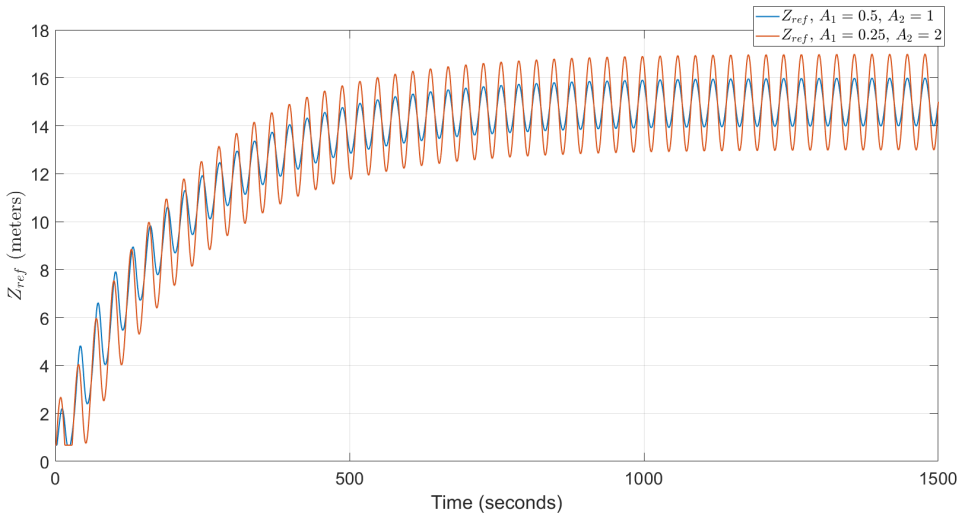

Figure 6.21: The physical meaning of the amplitude of each one sine wave

6.5 Stability of ESC

In order to analyze the stability of this implementation of the ESC, we will take into account the theorems and assumptions proposed in [22]. Figure 6.22 shows the plant used in this implementation.

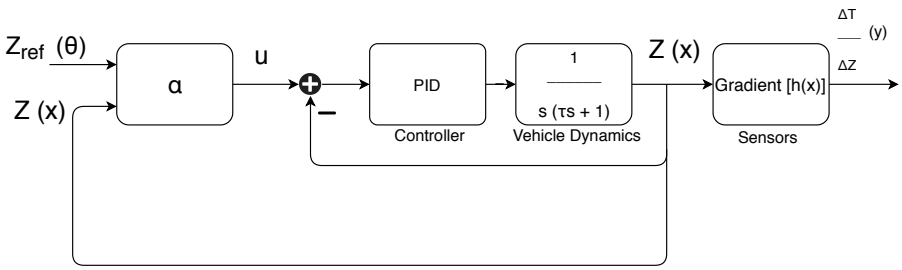

Figure 6.22: Plant

Since the system which simulates the dynamics of the vehicle converges to the reference with a near zero steady state error, the assumptions 2.1 and 2.2 proposed in [22] are verified. Then, when the algorithm reaches the highest point of the gradient, we have that: $Z = Z_{ref}$. The conditions proposed in assumption 2.3 in [22] are verified when the ESC method detects a maximum.

Assumption 2.1. *There exists a smooth function l:*$\mathbb{R} \to \mathbb{R}^n$ *such that*

$$f(x, \alpha(x, \theta)) = 0, \tag{6.10}$$

if and only if $x = l(\theta)$.

Assumption 2.2. *For each* $\theta \in \mathbb{R}$, *the equilibrium* $x = l(\theta)$ *of the system* $\dot{x} = f(x, \alpha(x, \theta))$ *is locally exponentially stable with deacay and overshoot constant uniform in* θ.

Assumption 2.3. *There exists* $\theta^* \in \mathbb{R}$ *such that*

$$(h \circ l)'(\theta^*) = 0, \tag{6.11}$$

$$(h \circ l)''(\theta^*) < 0. \tag{6.12}$$

Theorem 5.1 proposed by [22] says: *considering that the feedback system is under Assumptions 2.1, 2.2 and 2.3, the solution exponentially converges to the neighborhood of the point of the highest gradient for all conditions presented in 6.13, 6.14 and 6.15.*

$$a \in (0, \bar{a}) \tag{6.13}$$

$$\omega \in (0, \bar{\omega}) \tag{6.14}$$

$$\delta \in (0, \bar{\delta}) \tag{6.15}$$

Analyzing the theorem 5.1, we guarantee that the amplitudes chosen are less than the limit, $\bar{a}$. We also guarantee that the frequency ω_{ESC} is less than $\bar{\omega}$. δ is a multiplicative factor between ω and K_ζ, and we also guarantee that for this case it is below the limit. Thus, the stability of this implementation is also guaranteed.

Figure 6.23 shows the result of ESC in the limit of stability when $A_2 = A_1 = 2.75$ and $K_\zeta = 10$.

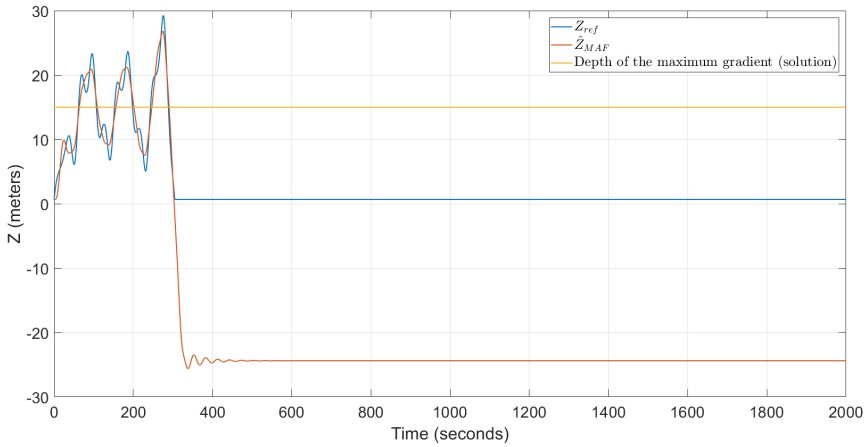

Figure 6.23: Result of ESC with amplitude $A_1 = A_2 = 2.75$

6.6 Moving Average Filter

In order to reduce the oscillation and to make the system faster it was considered the hypothesis to implement a moving average filter. This filter is applied to the output of the integrator (Fig. 6.24). Knowing that the period of both sine waves is 30s, it is possible to eliminate the "AC component", introduced by them at the output of the integrator.

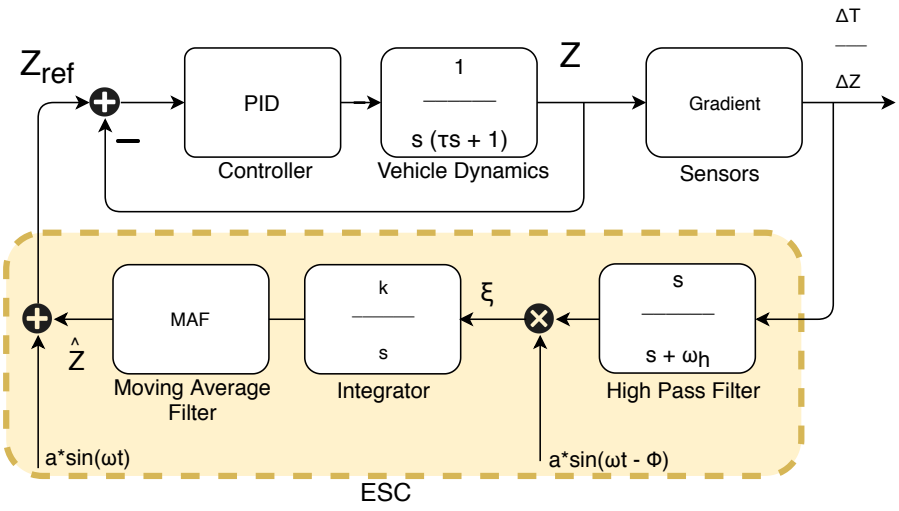

Figure 6.24: ESC scheme with moving average filter

Given that in the Simulink does not exist a function block that implements the moving average filter, it was necessary to develop a function. The following code excerpt simulates the moving average filter.

```
T = 30; %period of the sine wave (w=0.2094 rad/s)
N = T*1e3; %step 1e-3

buffer = [buffer(2:N), u];

y = sum(buffer)/N;
```

We observe in figure 6.25 that the reduction of the oscillation is achieved. Thus, the steady-state error is improved (Fig. 6.26). Although the steady-state error was improved, the speed of the system was not changed. Therefore, the great advantage of this new approach to the ESC general scheme is the reduction of the steady-state error.

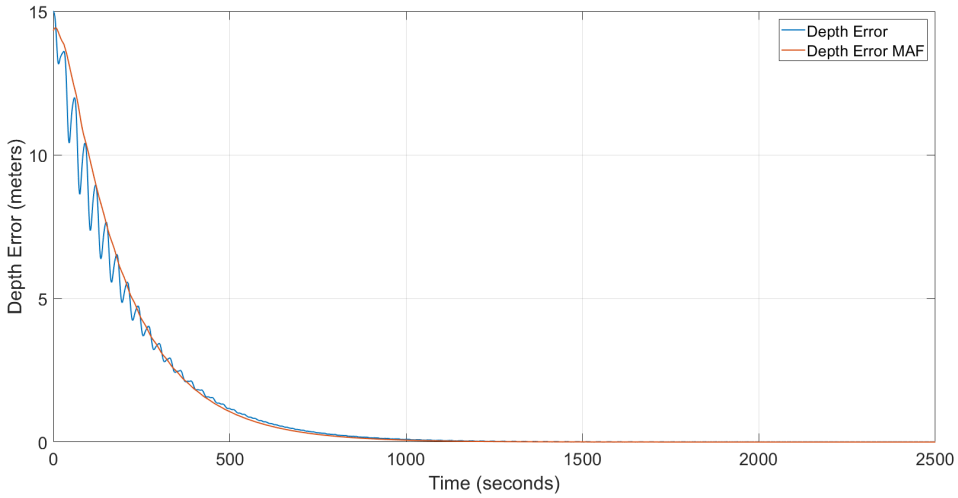

Figure 6.25: Depth error, moving average filter approach

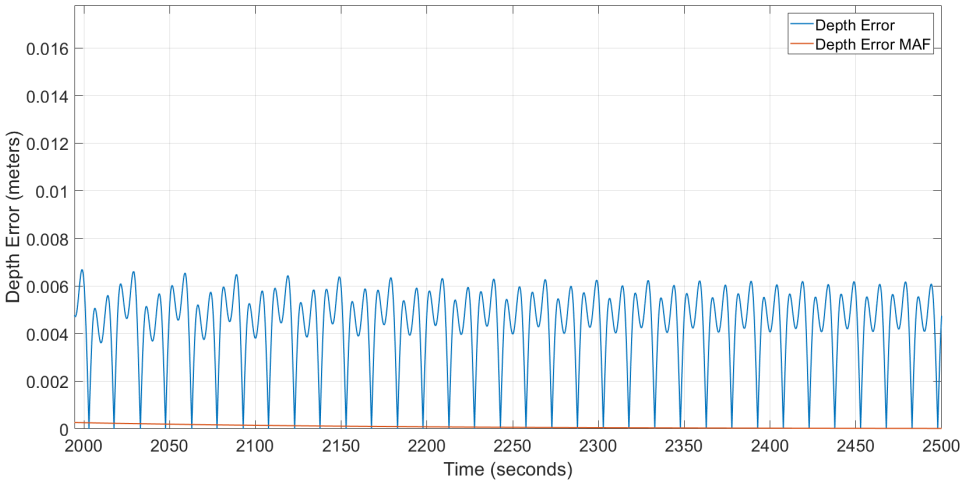

Figure 6.26: Depth error for the last 200 seconds, moving average filter approach

6.7 Power Consumption

This section has the purpose of verifying which is the relation between the power consumption of the vehicle and the number of times the ESC algorithm crosses the depth corresponding to the maximum gradient.

Firstly, we start by analyzing the relation between force and power of the thrusters. This relation is provided by the manufacturer of the thrusters (Fig. 6.27).

Figure 6.27: Performance chart of T100 thruster between Force and Power [29]

The values provided by the manufacturer were used to perform the least square approximation and thus obtain a function that approximates these data (Fig. 6.28).

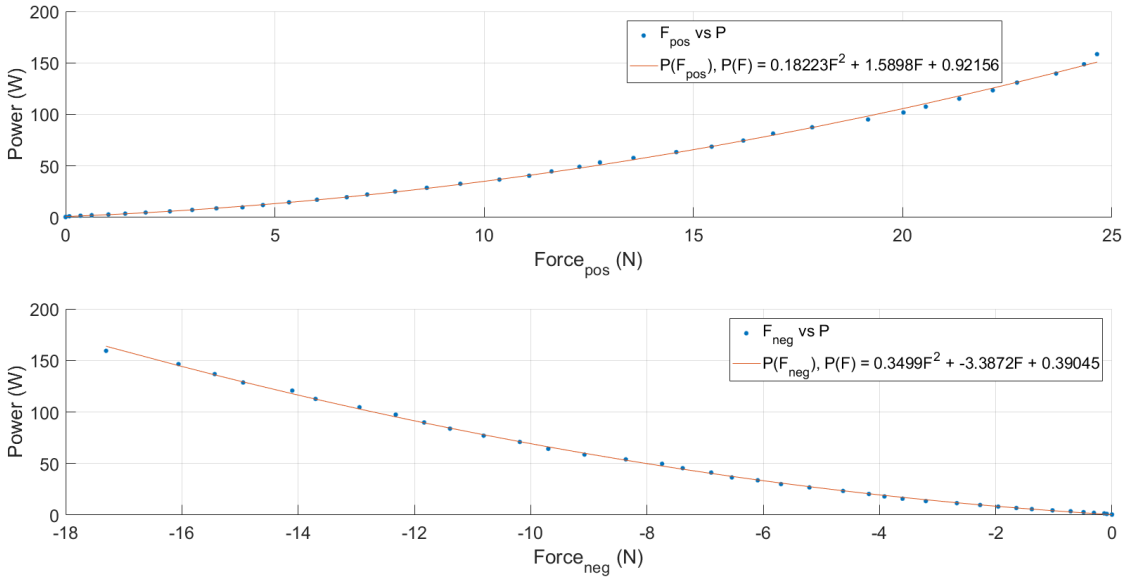

Figure 6.28: Representation of power as a function of force

The force used to move the profiler during a mission can be extracted from the transfer function $G(s)$ (Fig. 6.29). Figure 6.29 also shows how to obtain the energy consumed.

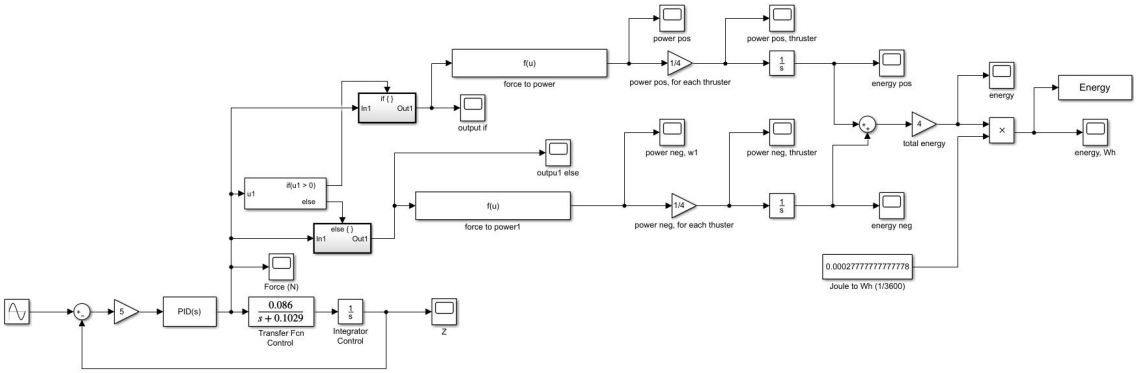

Figure 6.29: Simulink diagram that simulates the energy consumed by the profiler

After explaining the process of obtaining the force spent on a mission, we are ready to analyze the relation between the power consumption and the number of times the algorithm crosses the depth corresponding to the maximum gradient.

In order to obtain some conclusion, the algorithm was simulated for three different frequencies. It is expected that reducing the frequency, the algorithm will cross the point of gradient maximum fewer times. The period of the simulation was 2500 seconds. The results of the energy and the number of times that the algorithm crosses the highest point of the gradient for different frequencies are present in table 6.2.

Table 6.2: Power consumption

T(s)	ω_{ESC} (rad/s)	Energy (Joule)	Cross
90	0.0698	$4.0114 \cdot 10^3$	56
30	0.2094	$5.8514 \cdot 10^3$	131
10	0.6283	$2.992 \cdot 10^4$	385

It was expected that the relation between the increase in frequency and the number of times the algorithm crosses the thermocline would be proportionally direct, that is, if we increase the frequency by 3 times, the number of crosses also increases 3 times. By increasing the frequency, we observe that the number of crosses increases approximately 3 times ($\frac{131}{56} \approx 2.34$, $\frac{385}{131} \approx 2.94$). The ratio of the number of crossings between the first frequency and the second of the table 6.2 is not close to 3, since for smaller frequencies the system oscillation is higher at the beginning and thus reaches the respective depth of the peak gradient earlier. However, if compared in the steady state, this ratio would be exactly 3.

Taking into account that the maximum speed is proportional to ω_{ESC} ($\dot{Z} = A_2 \cdot \omega_{ESC}$) and that the power is proportional to the square of the speed, it is expected that the number of crossings and the energy consumed will have a quadratic relation. Figure 6.30 shows that the relation is approximately quadratic.

Thus, a compromise is required between the amplitude and frequency of the system so that the number of crossings is the largest with the lowest possible consumption.

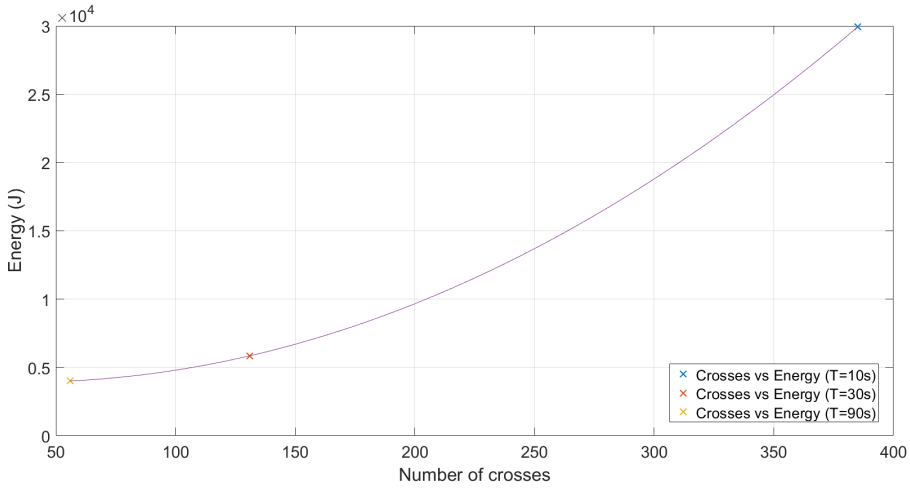

Figure 6.30: Number of crosses of the point of gradient maximum VS Energy (Joule)

6.8 Final Scheme and Parameters

In table 6.3 are present the final parameters for the implementation of the ESC. With these parameters, the algorithm tracks the depth correspondingly to the maximum gradient present in figure 6.3. If the shape of the gradient changes, it may be necessary to adapt some of these parameters. The values of the saturation (lower and upper) are the values that the user configures at the beginning of the mission (z_{bottom} and z_{top}). These parameters are protection values for the vehicle and mission safety.

Figure 6.32 shows the block diagram developed on Matlab Simulink toolbox. In the function block **Saturation** are defined the values of the lower and upper depths. After obtaining the vertical position of the profiler, we simulate the measures of two depths. Given that the sensors are separated by 1 meter, at the same distance to the vehicle's center of mass, adding and subtracting this distance we can simulate two different measures for the depth. In order to simulate the measure of the water temperature, we use the function $T(Z)$ (equation 6.3). To this measure is added noise. This noise simulates the error measurement of the sensors. After obtaining two different measures, it is possible to calculate the gradient through the following difference: $T_2 - T_1$. Given that the value of $T_2 - T_1$ is negative, we multiply by -1 to obtain a positive gradient. The remaining blocks of the diagram are responsible for the ESC and simulation of the vehicle's dynamics. In figure 6.31, it is observed that the algorithm tracks the maximum of the gradient and its depth corresponding to the temperature profile presented in 6.3.

Table 6.3: Final parameters of ESC scheme

ω_{ESC}	0.21rad/s
CM	0.675m
dist	0.5m
z_{TOP}	0.675m
z_{BOTTOM}	30m
Φ	0°
K_ζ	10
K_{PID}	5
A_1	0.5
A_2	1

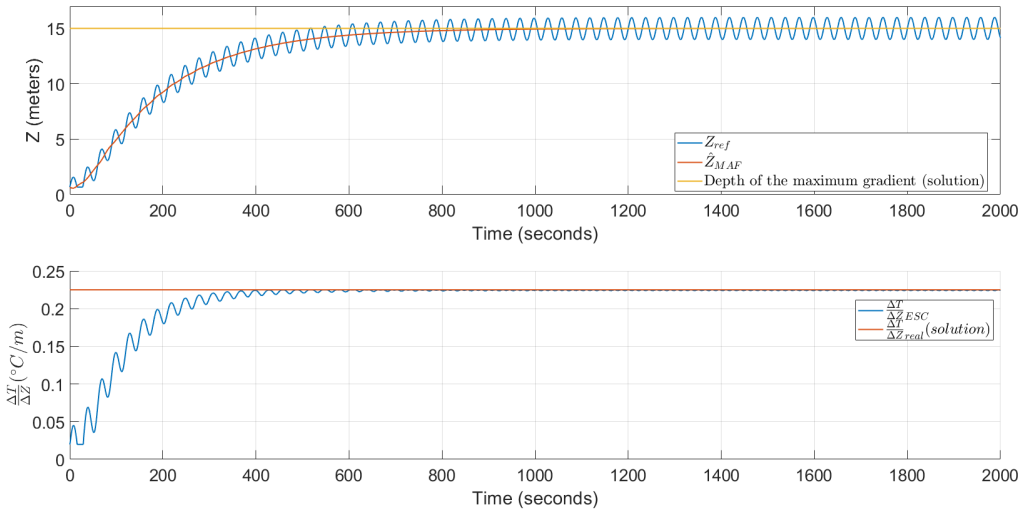

Figure 6.31: ESC simulation

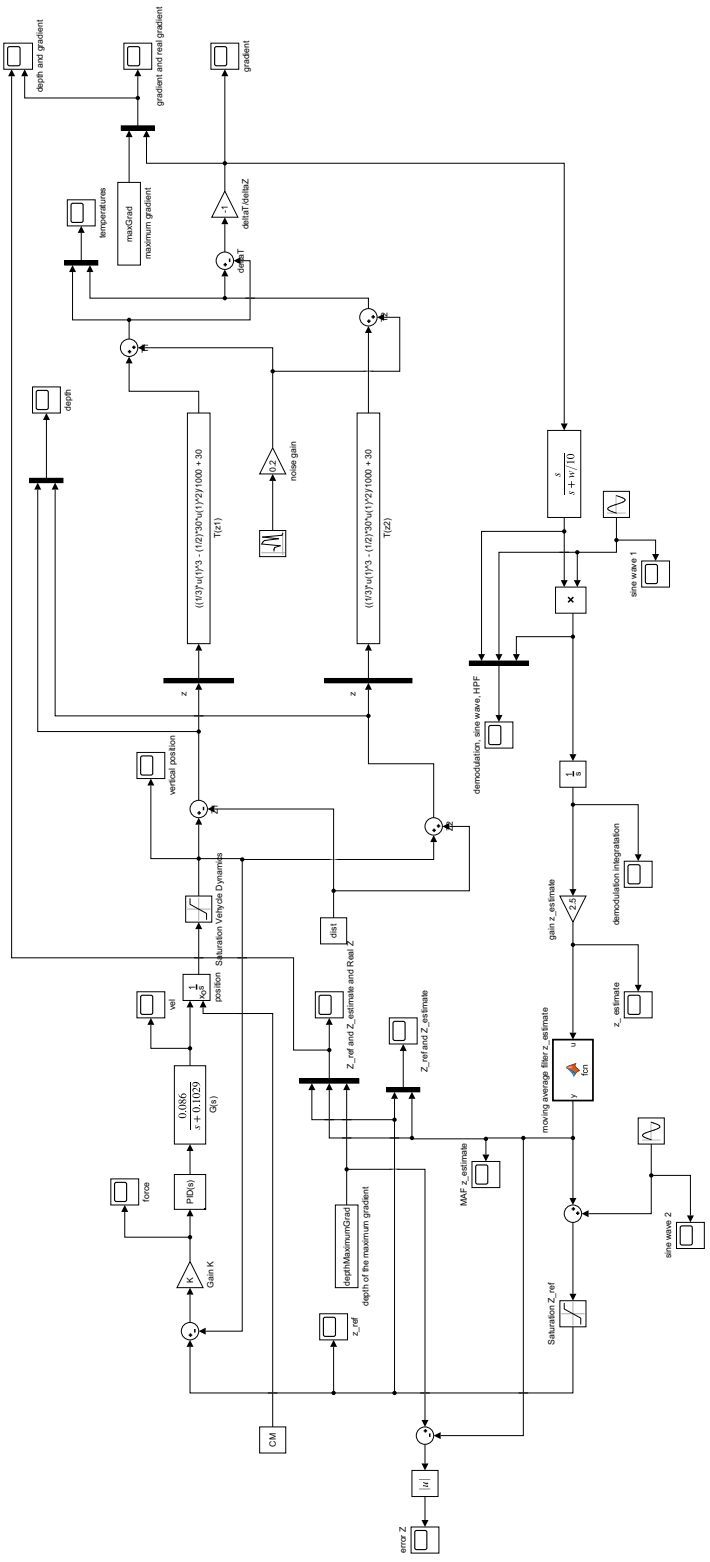

Figure 6.32: Final Simulink diagram

Chapter 7

Simulations

In this chapter, it will be presented and discussed the results obtained from the implementation of ESC on Matlab Simulink toolbox to validate the developed work. In order to validate the strategy and evaluate the performance of the ESC different vertical temperature profiles were created. Thermoclines with static characteristics, and others where the properties (span, location, and gradient) vary in time were considered. Results of this control method will also be demonstrated with data taken from an AUV that incorporated a CTD sensor and perform real-time processing, the MARES AUV [12].

7.1 Static Thermocline in Time and Space

In this section, different simulations for thermoclines static in time will be demonstrated. The shapes of the gradient of the vertical temperature profile of the functions parabola (asymmetric and symmetric) and Gaussian function were considered. The Simulink diagram used to simulate the asymmetric parabola and Gaussian function has a small change. Instead of simulating the measurement of two temperatures, we used a function that simulates the temperature gradient ($\dot{T}(Z)$). In this way, the vertical position of the vehicle is used directly in this function.

7.1.1 Symmetric Parabola

The function that simulates the temperature gradient is presented in figure 7.1. In this way, it is expected that the algorithm reaches a depth equal to 15 m and the gradient equal to 0.225 $^{\circ}C/m$. Figure 7.2 shows that both values are reached. In this configuration there was no change to the parameters presented in table 6.3.

7.1.2 Gaussian Function

Figure 7.3 shows the function that simulates the temperature gradient for this simulation. This gradient has the shape of a Gaussian function. This function was used to simulate higher variations near to the thermocline. However, at the beginning of this function, the variation is too short.

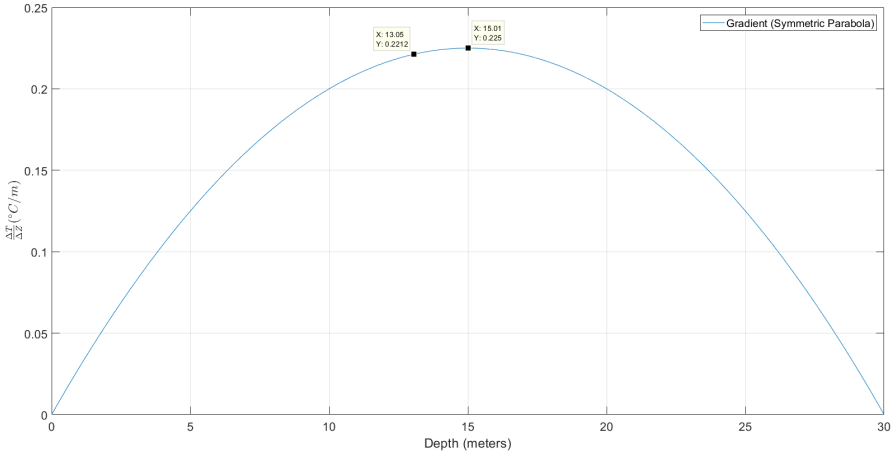

Figure 7.1: Parabolic function that simulates the gradient

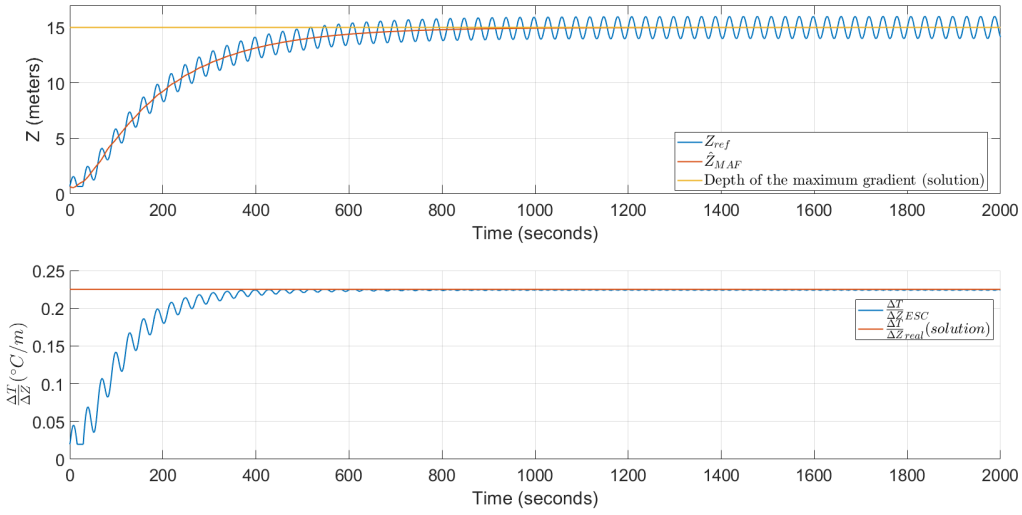

Figure 7.2: Results of the ESC for gradient of figure 7.1

Analyzing figure 7.3, we observe that are necessary more than 5 meters to variate 0.005. Consequently, the amplitude A_2 was increased ($A_2 = 1.5$). Given that the variation at the beginning is too short, the parameter K_ζ also was changed ($K_\zeta = 15$). For this reason, we have the best estimate fastly, and the algorithm tracks the thermocline also quicker. In figure 7.4, it is possible to observe that the maximum gradient shown in figure 7.3 is reached. The depth corresponding to the peak is also reached.

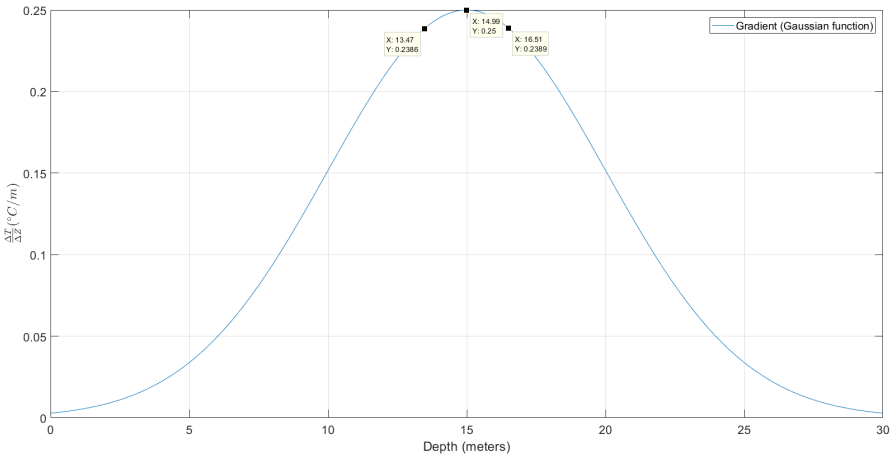

Figure 7.3: Gaussian function that simulates the gradient

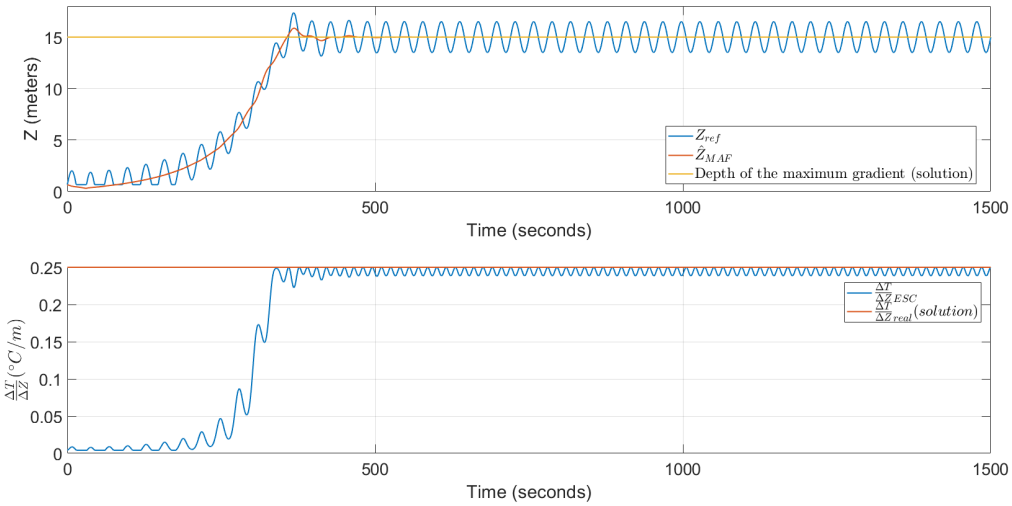

Figure 7.4: Results of the ESC for gradient of figure 7.3

After realizing this simulation, it is possible to observe that the results obtained in figure 7.2 have a difference compared to the results of the figure 7.4. Analyzing figure 7.4, we observe that the ESC tracks at the same time, the peak gradient and its depth. However, observing figure 7.2, the algorithm approaches the gradient peak faster than depth. This difference happens because of the very slow variation of the parabola peak (Fig. 7.1). Observing figure 7.5, it is possible to verify that the variation close to the maximum of the parabola is less than the variation of the Gaussian

function. As we observe, if the amplitude A_2 were equal to 2.6, in the Gaussian function the gradient varies approximately 0.03, whereas the parabola varies 0.005. Given that, the amplitude A_2 for the result of figure 7.2 was 1, it is normal that to this result, the algorithm reaches first peak in relation to corresponding depth.

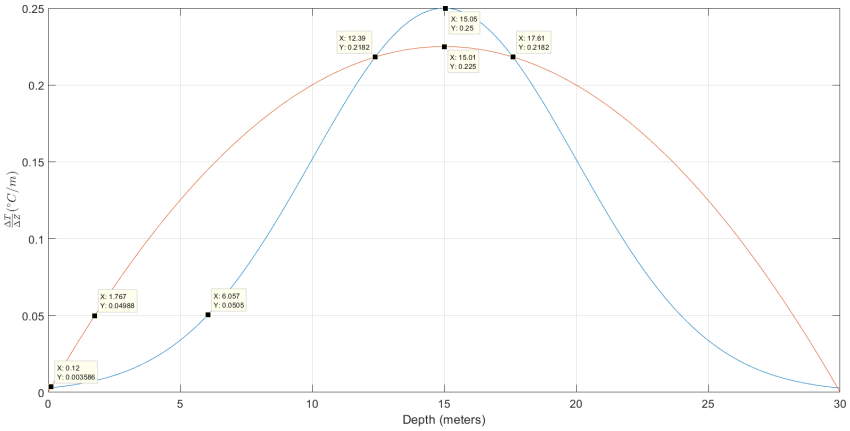

Figure 7.5: Comparison between parabolic function and Gaussian function

7.1.3 Asymmetric Parabola

In order to evaluate the ESC for another shape of gradient model it was chosen a parabolic function which was not symmetrical in relation to its peak. Figure 7.6 shows the shape of the temperature gradient. Observing this figure, it is expected that the algorithm reaches the solution faster. However, it is also expected that for depths above 8 meters it will slow down, since from this depth the variation is minimal up to the corresponding depth of the maximum. Analyzing the figure 7.7, we can observe that the values of the peak and the depth corresponding to this peak are reached. It is also possible to observe the previous conclusions.

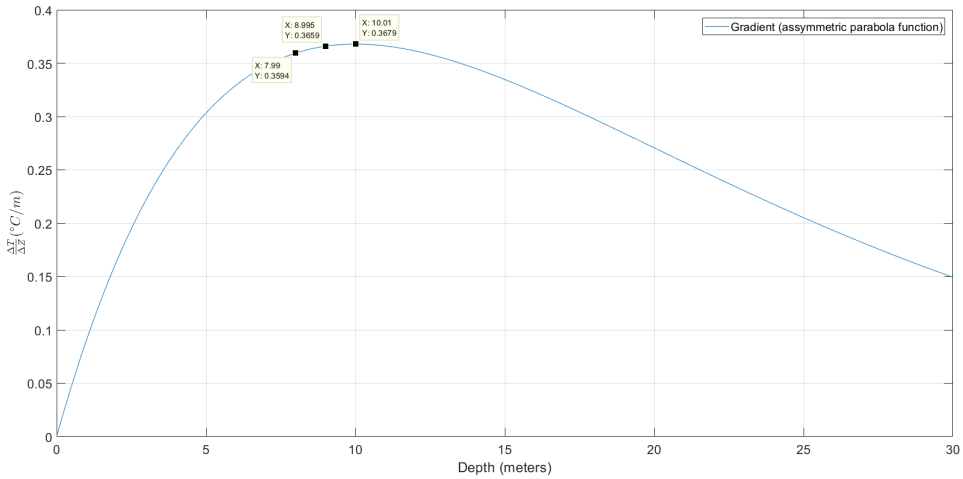

Figure 7.6: Asymmetric parabola that simulate the gradient

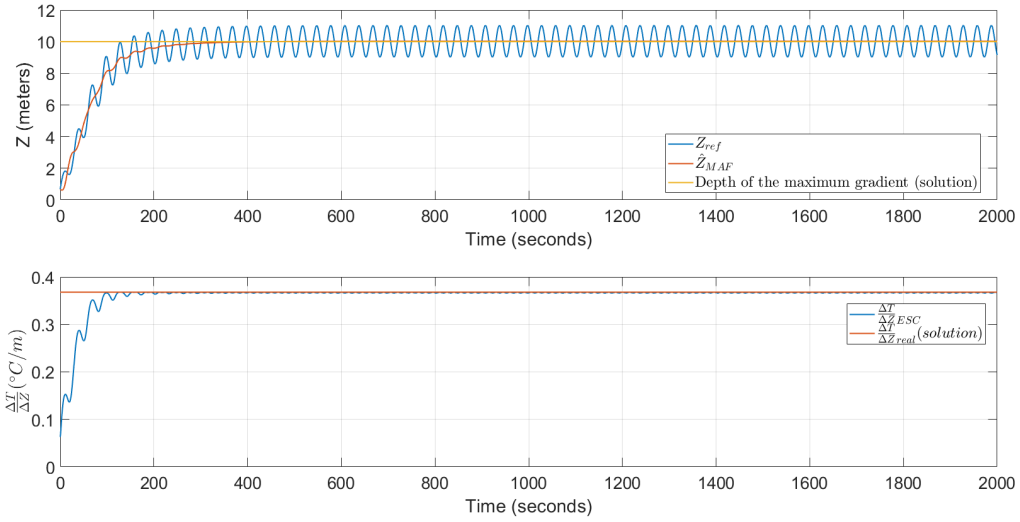

Figure 7.7: Results of the ESC for gradient of figure 7.6

7.2 Varying Thermocline in Time and Space

In order to simulate the variation of properties (span, location, and gradient) of the thermocline it were considered the three functions presented in figure 7.8. In this way, it was considered that during 3000 seconds the thermocline varies from the function $\dot{T}_1(Z)$ to the function $\dot{T}_3(Z)$, passing through the function $\dot{T}_2(Z)$ at the end of 1500 seconds. To obtain the function that varies in time and space, the coefficients (a,b,c) of the different parabolas evolve over time. These coefficients evolve from the coefficients of function $\dot{T}_1(Z)$ to $\dot{T}_3(Z)$, passing through function $\dot{T}_2(Z)$ at the end of 1500s. Equations 7.1 and 7.2 describe the evolution of the three functions.

$$\dot{T}(Z,t) = -\frac{a(t)\cdot Z^2 + b(t)\cdot Z + c(t)}{1000} \tag{7.1}$$

$$T(Z,t) = -\frac{\frac{1}{3}\cdot a(t)\cdot Z^3 + \frac{1}{2}\cdot b(t)\cdot Z^2 + c(t)\cdot Z}{1000} + 30 \tag{7.2}$$

The expressions $a(t)$, $b(t)$, and $c(t)$ have the following form:

$$a(t) = a_1 + a_2\cdot t + a_3\cdot t^2 \tag{7.3}$$

$$b(t) = b_1 + b_2\cdot t + b_3\cdot t^2 \tag{7.4}$$

$$c(t) = c_1 + c_2\cdot t + c_3\cdot t^2 \tag{7.5}$$

Figure 7.9 shows that at the end of 500s the ESC accompanies the depth and gradient values proposed by the variation between the 3 functions of figure 7.8. Thus, we can conclude that the ESC is a control method that can accompany the alterations of the thermocline. The main

advantage in relation to previous works is that there is not needed to change some parameters or thresholds to perform the tracking of thermoclines.

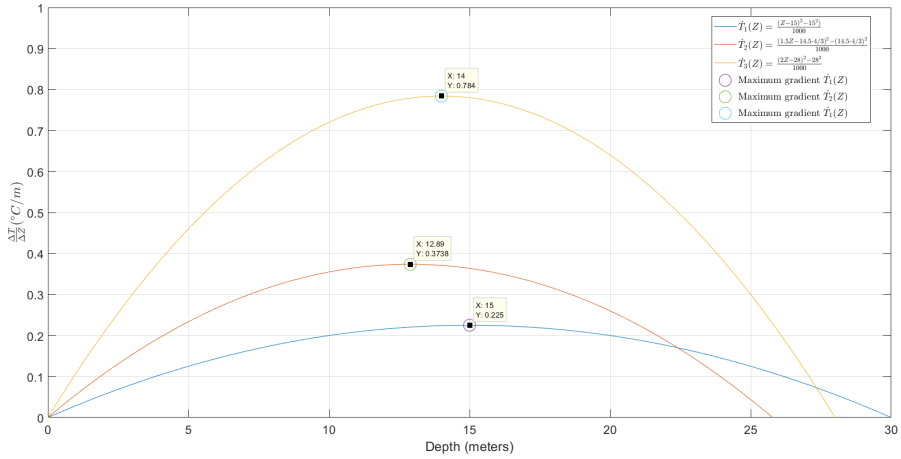

Figure 7.8: Different parabolic functions that simulate time and space variations of the gradient

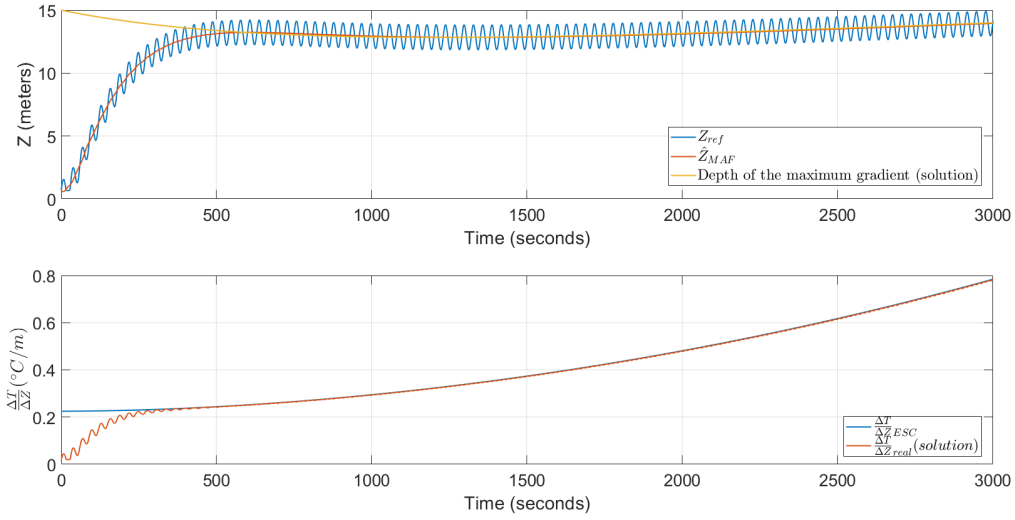

Figure 7.9: Result of the ESC for gradient of figure 7.8

Figure 7.10 shows that the error between the solution and the best estimate depth of ESC ($\hat{Z}$) is close to 0. It is also possible to observe that in a few instants, $\hat{Z}$ crosses the solution.

7.3 Real Thermocline

Two different vertical profiles were obtained using an AUV that incorporated a CTD sensor [12]. One of these profiles was obtained when the vehicle performed a downward motion and the other an upward motion. The top graphic of figures 7.11 and 7.12 show these profiles. Comparing these vertical profiles, it is possible to observe that there was a small spatial variation of the thermocline.

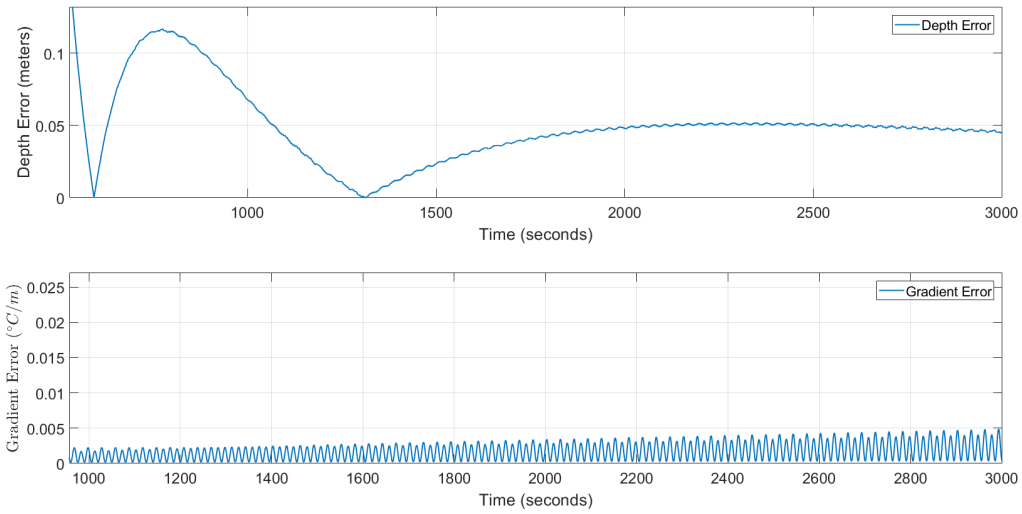

Figure 7.10: Depth error and gradient error for gradient of figure 7.8

Observing figure 7.12, can be identified that for 15 meters we have the center of the thermocline. In figure 7.11, this point seems to be higher up (near to 12.5/13 meters).

As we see in chapter 5, through this dataset the approximation of the first-order derivative is subjected to much noise and has many variations. So that the ESC does not detect a local maximum influenced by abrupt gradient variations, it was decided that the mission begins at depth of 15 meters. Although the thermocline has a small spatial variation, both results of the implementation of ESC show that the maximum gradient is 0.8 $^{\circ}C/m$. In figure 7.11, it is possible to observe that the algorithm tracks and detects the maximum gradient at 13 meters. This result is in agreement with the analysis made before. Figure 7.12 shows that maximum gradient is 15 meters. This result is also goes according to the analysis made for this profile. For both implementations the values of the amplitude A_1 and A_2, and the gain K_ζ were changed. The values used were as follows:

- $A_1 = 0.1$
- $A_2 = 1.25$
- $K_\zeta = 3$

Given that both temperature profiles (top of figures 7.11 and 7.12) is influenced by the sensor error and the aquatic environment, it was needed to adapt the parameters. The increase of amplitude A2 occurred so that the algorithm does not perform the tracking of a local maximum. The decrease of A_1 and K_ζ implies that the system is slower to obtain the solution. By increasing A_2 and decreasing A_1 and K_ζ we have an implementation robust to the dynamic of the aquatic environment and the sensor error.

After. to test the implementation of the ESC for different shapes of the gradient and for real data, we can conclude that this algorithm is robust.

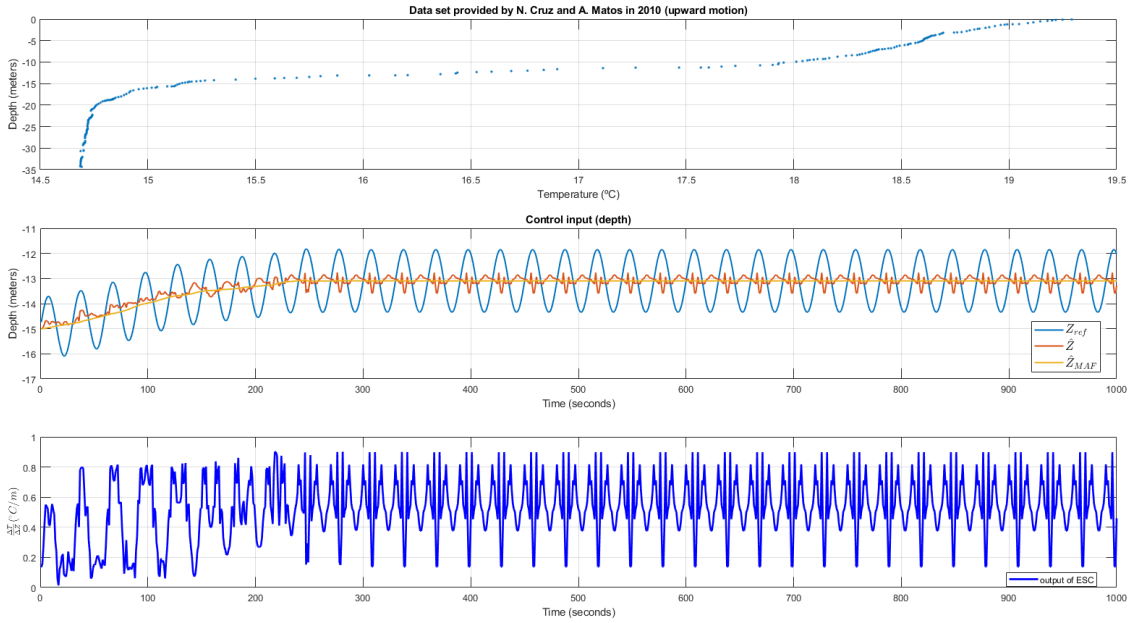

Figure 7.11: Result of the ESC with real data (upward motion)

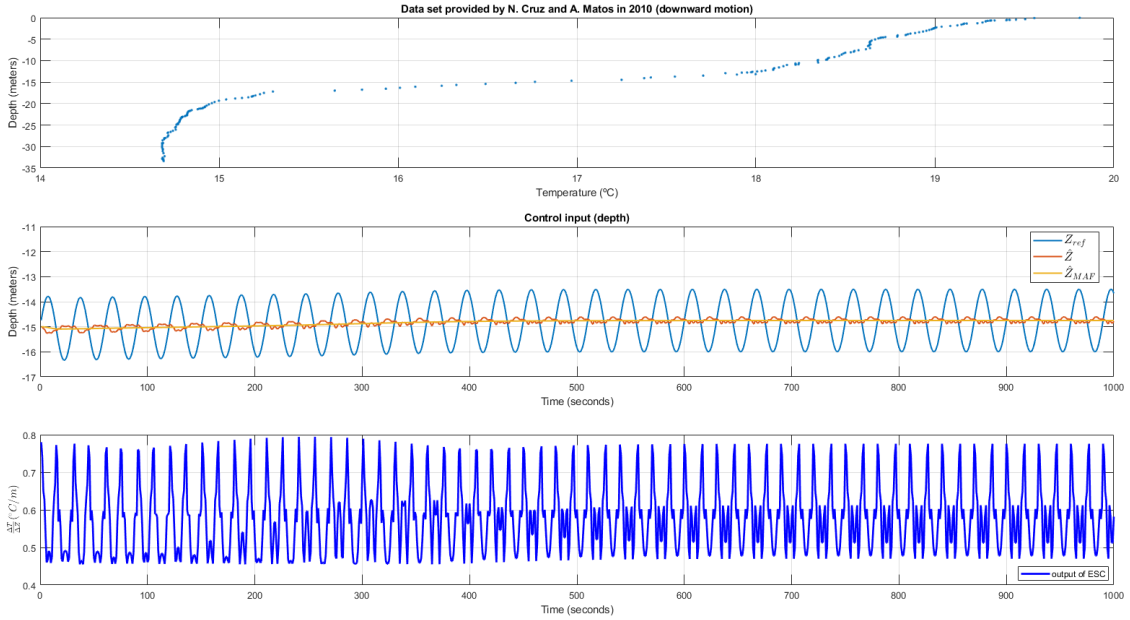

Figure 7.12: Result of the ESC with real data (downward motion)

Chapter 8

Conclusions and Future Work

8.1 Conclusions

This dissertation focused on the implementation of an algorithm that performs identification and tracking of thermoclines at its point of highest temperature gradient in a completely autonomous way. To perform this tracking, a small vertical profiler was used. To obtain instant measurements of the vertical temperature gradient, we taken advantage of the profiler geometry and orientation to install temperature sensors at different locations of the body. In order to maintain the profiler in the layer of maximum temperature gradient, Extremum Seeking Control method was used. One of the advantages of this method is that it is not necessary to know an exact model of the system, but mainly that there is a local extremum. This assumption was verified in this context, given that we know that exists an extremum but we do not know under what conditions this maximum exists. Thus, this overcomes a great challenge in thermocline tracking with other model-based methods - deriving a proper model. The method requires the measurement of the variable to maximize, which we obtain directly by distributing temperature sensors along the profiler body. With the profiler and the previous measures, we can calculate the vertical gradient temperature, and in this way, we have instantaneous samples of the variable that we want to maximize. The ESC method maximizes the temperature gradient, generating the reference depth corresponding to this maximum. Thus, it is necessary a vehicle capable of following depth references, a requirement duly verified by the profiler. Taking into account all of the descriptions previously presented, the implementation of the ESC was essential.

Observing the results of chapter 7, we can conclude that the implementation of this algorithm is robust to different types of thermoclines (span, location, and gradient vary in time). In this way, the main goal of this work was accomplished. Furthermore, the stability conditions were satisfied. A new block has been implemented to the traditional ESC scheme (Fig. 2.8). This block is the implementation of a moving average filter, that has the purpose of reducing the oscillation in $\hat{Z}$ and of reducing the depth error in relation to the solution.

With the discussion of each ESC parameter more conclusions were obtained. It was possible to conclude that by increasing ω and the amplitude of A_2 implies an increase in the energetic

cost. It was also verified that by increase ω, the number of crossings of the maximum point of the thermocline gradient increases. Thus, the user has the necessary information by opting for a mission with a low energetic cost and with the number of thermocline crossings.

The main limitation of the ESC is that the algorithm may be fooled by a local maximum. This situation occurs with the dynamic of the aquatic environment or the sensor error. However, with the discussion of the ESC parameters, we allow that our implementation is robust for these variants. To escape the limitation of the ESC, it is possible to increase the amplitude of A_2 and to decrease the gain K_ζ. Thus, we have an approach in which is slower to obtain $\hat{Z}$ but with more range. An approach that performs four profiles previously, allows obtaining a sense of the depth of the maximum of the temperature gradient and also allows to espace the main limitation of the ESC. This approach implies that the vehicle follows a fixed reference and it is only after reaching this reference that it executes the ESC algorithm.

8.2 Future Work

Although the main goal of this work was reached, it can still be improved. Initially, it would be beneficial to test this algorithm in real environment in order to evaluate the system behavior in this environment. For the algorithm to be robust to real environments, adapting the parameters in real time may be essential. For example, when the thermocline has a minimum variation around the maximum point, increasing amplitude A_2 may help the algorithm to detect the global maximum instead of a local maximum.

Taking into account that we propose an implementation in which it is possible to carry out the tracking of thermoclines, it was not possible to create a parametric model that represents the water column. Through the ESC method, the parameters that are representative of this model are uniquely the maximum gradient and its depth. However, by increasing amplitude A_2 it is possible to obtain more information around to the maximum point.

Through this work, it is possible to perform a multi-vehicle mission, in which the vehicle that performs the ESC method is the reference for the other vehicles. Knowing that is possible to communicate in underwater environments, for example using acoustic communications, the best estimate of depth of the highest poinf of the gradient ($\hat{Z}_{MAF}$) can be the reference for the other vehicles. Thus, the remaining vehicles adapt their depth to that reference. For example, using a vehicle that performs the ESC method, this vehicle sends the message of the depth corresponding to maximum gradient to other vehicle. The last one can adapt its depth at a distance X from the reference. At the beginning of the mission, this distance can be chosen by a user. Through this multi-vehicle mission, it is also possible to compare data relevant to the thermocline, for example, the variation of chlorophyll in a short vertical distance.

The explanation of the role of the different blocks of the ESC, tuning of the different parameters and its physical meaning will allow other researchers to adapt our implementation of ESC to their specif needs in tracking the same goal, or other extrema. For example, if we want to detect a variation of a horizontal gradient, it is necessary to change the function $G(s)$, for a function that

relates the force to the horizontal position. The gradient block of figure 6.1 will depend on the variable that we want to maximize.

8.3 Contribution

An extended abstract of the implementation of the ESC to tracks and detects thermoclines was submitted in May 31st, 2019 to the OCEANS 2019 Seattle conference that will take place in October 27-31,2019. The extended abstract document is present in appendix A. The result of the review will be communicated on (or before) July 12th, 2019.

Appendix A

Attachments

A.1 Extended Abstract Submitted to the OCEANS 2019 Seattle Conference

Autonomous Identification and Tracking of Thermoclines with a Vertical Profiler using Extremum Seeking Control

Extended Abstract

Hugo M. Antunes*, Nuno A. Cruz*†

* Faculty of Engineering, University of Porto, Portugal
† INESC TEC, Porto, Portugal
up201403480@fe.up.pt, nacruz@fe.up.pt

I. Introduction

In this work, we propose to carry out the detection and tracking of the thermocline with an autonomous vertical profiler. The thermocline is a water layer that separates the *mixed layer* from the deep-water layer. In the thermocline, the gradient of temperature with respect to depth is higher than in the rest of the water column. The characteristics of the thermocline are strongly related to biological activity and sound propagation, therefore there is a great interest in the study of its spatial and distribution and dynamics.

With the use of Autonomous Underwater Vehicles (AUVs), it is possible to acquire large sets of underwater data very efficiently. It is also possible to process specific data in real time in order to adapt the behavior of a vehicle and carry out the tracking of a particular characteristic with greater effectiveness. A vertical profiler is a particular type of AUV designed to operate predominantly in the vertical direction. It is therefore a platform very well suited to implement algorithms for the detection and tracking of thermoclines.

In this paper, we propose an implementation in which it is possible to carry out the tracking of a thermocline at its point of highest temperature gradient in a completely autonomous way. There has been previous work where traditional AUVs have been used with the same purpose, using some heuristic guidance methods ([1], [2]). In our case, to perform this tracking, we use a small vertical profiler developed earlier and described in [3]. To obtain instant measurements of the vertical temperature gradient, we take advantage of the profiler geometry and orientation to install temperature sensors at different locations of the body. We use an Extremum Seeking Control scheme to maintain the vehicle in the thermocline region, and we show the tracking performance even when the thermocline characteristics change in time.

II. Algorithm

In order to maintain the profiler in the layer of maximum temperature gradient, we use Extremum Seeking Control (ESC) algorithm.

A. Design

ESC is a control method with the main purpose of placing the input variable in a specific value that corresponds to the output variable in an extremum value (maximum or minimum). One of the advantages of this method is that it is not necessary to know an exact model of the system, but mainly that there is a local extremum. This overcomes a great challenge in thermocline tracking with other model-based methods - deriving a proper model. The method requires the measurement of the variable to maximize, which we obtain directly by distributing temperature sensors along the profiler body. With the profiler and the previous measures, we can calculate the vertical gradient temperature, and in this way, we have the variable that we want to maximize.

The ESC method maximizes the temperature gradient, generating the reference depth corresponding to this maximum. Thus, it is necessary a vehicle capable of following depth references, a requirement duly verified by the profiler.

Figure 1 shows the structure implemented in this work. The block **Vehicle Dynamics** represents the vertical profiler. For controller design and tuning, we use the transfer function that relates the input given to the thrusters of the vehicle with the variation of its position in the vertical direction, following the model in [4]. With the finality of the profiler to follow references with a minimum delay and low attenuation, in the block **Controller** we consider the position controller proposed by [4] for our profiler. The block **Sensors** is calculated by the difference in temperature of the two sensors placed in the profiler. In our case, these sensors are separated by 1 meter, at the same distance to the vehicle's center of mass.

$$\dot{T}(Z) = \frac{(T_2 - T_1)}{Z_2 - Z_1}, \tag{1}$$

where $Z_2 = Z + \Delta Z$ and $Z_1 = Z - \Delta Z$.

The other blocks are responsible for the ESC, following the structure described in [5].

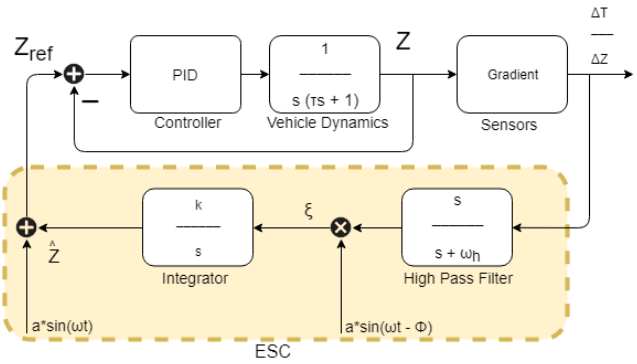

Fig. 1. Extremum Seeking Control scheme

B. Tuning

In the full version of the paper, we describe the design procedure for the different parameters of each block. In particular, we explain the frequency and amplitude of the sine waves, the cut-off frequency of the high-pass filter (HP), and the effect of the product between the sine wave and the HP output.

C. Validation and Performance Evaluation

In order to validate the strategy and evaluate the performance of the ESC, the full paper will have the results of simulations with different vertical temperature profiles. In these simulations we considered thermoclines with static characteristics, and others where the properties (span, location and gradient) vary in time. Results of this control method will also be demonstrated with data taken from an AUV that incorporated a CTD sensor and performed real-time processing, the MARES AUV [1]. Figure 2 shows the result in this case, and it is possible to verify that the profiler maintains an oscillation in the layer corresponding to the thermocline.

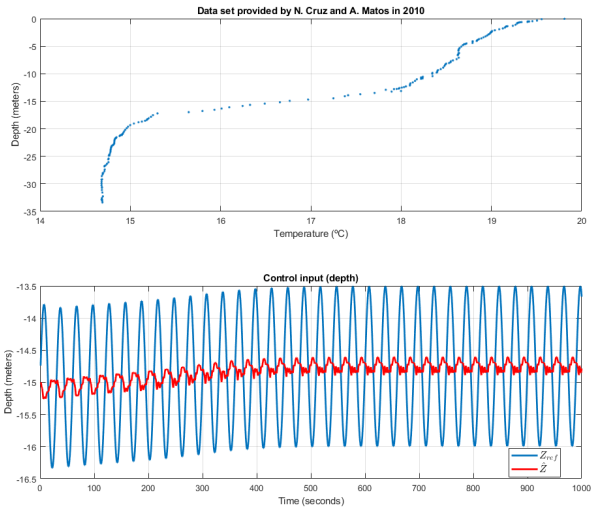

Fig. 2. Result of the ESC with real data

III. Conclusions

In the final section of the paper we will discuss the role of the different blocks of the ESC (Fig. 1), in the thermocline tracking context. The tuning of the different parameters and the stability of the controller will also be discussed.

This discussion, and its physical meaning, will allow other researchers to adapt our implementation of ESC to their specific needs in tracking the same, or other extrema.

References

[1] N. A. Cruz and A. C. Matos, "Reactive AUV motion for thermocline tracking," in *OCEANS'10 IEEE SYDNEY*. IEEE, may 2010.

[2] S. Petillo, A. Balasuriya, and H. Schmidt, "Autonomous adaptive environmental assessment and feature tracking via autonomous underwater vehicles," in *OCEANS'10 IEEE SYDNEY*. IEEE, may 2010.

[3] J. M. M. Monteiro, "Development of an autonomous underwater profiler," Master's thesis, Faculty of Engineering of University of Porto, jul 2017.

[4] P. M. Rodrigues, N. A. Cruz, and A. M. Pinto, "Altitude control of an underwater vehicle based on computer vision," in *OCEANS 2018 MTS/IEEE Charleston*. IEEE, oct 2018.

[5] M. Krstić and H.-H. Wang, "Stability of extremum seeking feedback for general nonlinear dynamic systems," *Automatica*, vol. 36, no. 4, pp. 595–601, apr 2000.

References

[1] Kartik B. Ariyur. *Real-Time Optimization by Extremum-Seeking Control*. Wiley-Blackwell, Oct. 14, 2003. 248 pp. ISBN: 0471468592. URL: https://www.ebook.de/de/product/3617429/kartik_b_ariyur_real_time_optimization_by_extremum_seeking_control.html.

[2] Vladan Babovic and Hong Zhang. "Modeling of Vertical Thermal Structure Using Genetic Programming". In: *7th OMISAR Workshop on Ocean Models, Singapore*. Sept. 2002. URL: https://www.researchgate.net/profile/Vladan_Babovic/publication/29468780_Modeling_of_Vertical_Thermal_Structure_Using_Genetic_Programming/links/0fcfd50bc3b89c9e6d000000.pdf.

[3] Dominik Breu and Thor I. Fossen. "Extremum Seeking Speed and Heading Control Applied to Parametric Roll Resonance". In: *IFAC Proceedings Volumes* 43.20 (Sept. 2010), pp. 28–33. DOI: 10.3182/20100915-3-de-3008.00003.

[4] Steven L. Brunton, Clarence W. Rowley, Sanjeev R. Kulkarni, and Charles Clarkson. "Maximum Power Point Tracking for Photovoltaic Optimization Using Ripple-Based Extremum Seeking Control". In: *IEEE Transactions on Power Electronics* 25.10 (Oct. 2010), pp. 2531–2540. DOI: 10.1109/tpel.2010.2049747.

[5] Sara Cardigos, Renato Mendes, Antonio Sergio Ferreira, Joao Borges de Sousa, and Joao Miguel Dias. "Using LAUVs in highly dynamic environments: influence of the tidal estuarine outflow in the thermocline structure". In: *OCEANS 2018 MTS/IEEE Charleston*. IEEE, Oct. 2018. DOI: 10.1109/oceans.2018.8604504.

[6] Peter C. Chu, Chenwu Fn, and W. Timothy Lu. "Determination of Vertical Thermal Structure from Sea Surface Temperature". In: *American Meteorological Society* (2000).

[7] Peter C. Chu, Charles R. Fralick, Steven D. Haeger, and Michael J. Carron. "A parametric model for the Yellow Sea thermal variability". In: *Journal of Geophysical Research: Oceans* 102.C5 (May 1997), pp. 10499–10507. DOI: 10.1029/97jc00444.

[8] Peter C. Chu and Chung-Ping Hsieh. "Multifractal thermal characteristics of the western Philippine Sea upper layer". In: *Indian Journal of Marine Sciences* 36.2 (June 2007), pp. 141–151.

[9] Peter C. Chu, Qianqian Wang, and Robert H. Bourke. "A Geometric Model for the Beaufort/Chukchi Sea Thermohaline Structure". In: *American Meteorological Society* (1999).

[10] Nuno Cruz. “Adaptive Ocean Sampling with Modular Robotic Platforms”. PhD thesis. Apr. 2016.

[11] Nuno A. Cruz and Anibal C. Matos. “Autonomous tracking of a horizontal boundary”. In: *2014 Oceans - St. John’s*. IEEE, Sept. 2014. DOI: 10.1109/oceans.2014.7003275.

[12] Nuno A. Cruz and Anibal C. Matos. “Reactive AUV motion for thermocline tracking”. In: *OCEANS’10 IEEE SYDNEY*. IEEE, May 2010. DOI: 10.1109/oceanssyd.2010.5603883.

[13] Nuno A. Cruz and Aníbal C. Matos. “Adaptive sampling of thermoclines with Autonomous Underwater Vehicles”. In: *OCEANS 2010 MTS/IEEE SEATTLE*. IEEE, Sept. 2010. DOI: 10.1109/oceans.2010.5663903.

[14] Bruno Ferreira, Miguel Pinto, Anibal Matos, and Nuno Cruz. “Control of the mares autonomous underwater vehicle”. In: *OCEANS 2009 MTS/IEEE BILOXI,MS,USA*. IEEE, Oct. 2009. URL: https://ieeexplore.ieee.org/abstract/document/5422133.

[15] Fossen. *Guidance Control of Ocean Vehicles*. John Wiley & Sons, Aug. 23, 1994. 496 pp. ISBN: 0471941131. URL: https://www.ebook.de/de/product/3597693/fossen_guidance_control_of_ocean_vehicles.html.

[16] S.D. Haeger. “Vertical representation of ocean temperature profiles with a gradient feature model”. In: *’Challenges of Our Changing Global Environment’. Conference Proceedings. OCEANS ’95 MTS/IEEE*. IEEE, 1995. DOI: 10.1109/oceans.1995.526820.

[17] William J. Teague, Michael Carron, and Patrick J. Hogan. “A Comparison between the Generalized Digital Environmental Model and Levitus Climatologies”. In: *Journal of Geophysical Research* 95 (May 1990), p. 18. DOI: 10.1029/JC095iC05p07167.

[18] Brett M. Johnson, Laurel Saito, Mark A. Anderson, Paul Weiss, Mary Andre, and Darrell G. Fontane. “Effects of Climate and Dam Operations on Reservoir Thermal Structure”. In: *Journal of Water Resources Planning and Management* 130.2 (Mar. 2004), pp. 112–122. DOI: 10.1061/(asce)0733-9496(2004)130:2(112).

[19] N. J. Killingsworth and M. Krstic. “PID tuning using extremum seeking: online, model-free performance optimization”. In: *IEEE Control Systems* 26.1 (Feb. 2006), pp. 70–79. DOI: 10.1109/mcs.2006.1580155.

[20] Rudibert King, Ralf Becker, Gerrit Feuerbach, Lars Henning, Ralf Petz, Wolfgang Nitsche, Olaf Lemke, and Wolfgang Neise. “Adaptive flow control using slope seeking”. In: *2006 14th Mediterranean Conference on Control and Automation*. IEEE, June 2006. DOI: 10.1109/med.2006.328753.

[21] Miroslav Krstić. “Performance improvement and limitations in extremum seeking control”. In: *Systems & Control Letters* 39.5 (Apr. 2000), pp. 313–326. DOI: 10.1016/s0167-6911(99)00111-5.

[22] Miroslav Krstić and Hsin-Hsiung Wang. "Stability of extremum seeking feedback for general nonlinear dynamic systems". In: *Automatica* 36.4 (Apr. 2000), pp. 595–601. DOI: 10.1016/s0005-1098(99)00183-1.

[23] Tom Lyche and Knut Mørken. *Spline Methods Draft*. University of Oslo, 2002. URL: http://folk.uio.no/in329/komp.html.

[24] João Manuel Matos Monteiro. "Development of an Autonomous Underwater Profiler". MA thesis. Faculty of Engineering of University of Porto, July 2017.

[25] Stephanie Petillo, Arjuna Balasuriya, and Henrik Schmidt. "Autonomous adaptive environmental assessment and feature tracking via autonomous underwater vehicles". In: *OCEANS'10 IEEE SYDNEY*. IEEE, May 2010. DOI: 10.1109/oceanssyd.2010.5603513.

[26] George M. Phillips. *Interpolation and Approximation by Polynomials*. Springer-Verlag New York Inc., Apr. 8, 2003. 312 pp. ISBN: 0387002154. URL: https://www.ebook.de/de/product/3673779/george_m_phillips_interpolation_and_approximation_by_polynomials.html.

[27] George L. Pickard and William J. Emery. *Descriptive Physical Oceanography – An Introduction.* 5th (SI). Pergamon Press, 1990.

[28] J. Douglas Faires Richard L. Burden. *Numerical Analysis*. BROOKS COLE PUB CO, Aug. 11, 2010. 888 pp. ISBN: 0538733519. URL: https://www.ebook.de/de/product/10947989/richard_l_burden_j_douglas_faires_numerical_analysis.html.

[29] BLue Robotics. *Blue Robotics Thrusters T100*. Accessed: 201-05-29. URL: https://www.bluerobotics.com/store/thrusters/t100-t200-thrusters/t100-thruster/.

[30] Pedro M. Rodrigues, Nuno A. Cruz, and Andry M. Pinto. "Altitude control of an underwater vehicle based on computer vision". In: *OCEANS 2018 MTS/IEEE Charleston*. IEEE, Oct. 2018. DOI: 10.1109/oceans.2018.8604525.

[31] Jonathan Sharples. "Investigating the seasonal vertical structure of phytoplankton in shelf seas". In: *Marine Models* 1.1-4 (Dec. 1999), pp. 3–38. DOI: 10.1016/s0079-6611(99)00002-6.

[32] Martin Siderius, Michael B. Porter, Paul Hursky, and Vincent McDonald and. "Effects of ocean thermocline variability on noncoherent underwater acoustic communications". In: *The Journal of the Acoustical Society of America* 121.4 (Apr. 2007), pp. 1895–1908. DOI: 10.1121/1.2436630.

[33] M. Steffen. "A Simple Method for Monotonic Interpolation in One Dimension". In: *Astronomy and Astrophysics* 239 (Nov. 1990), pp. 443–450.

[34] G T. Csanady. “On the Equilibrium Shape of the Thermocline in a Shore Zone”. In: *Journal of Physical Oceanography - J PHYS OCEANOGR* 1 (Oct. 1971), pp. 263–270. DOI: 10.1175/1520-0485(1971)001<0263:OTESOT>2.0.CO;2.

[35] Ding Wang, Pierre F.J. Lermusiaux, Patrick J. Haley, Donald Eickstedt, Wayne G. Leslie, and Henrik Schmidt. “Acoustically focused adaptive sampling and on-board routing for marine rapid environmental assessment”. In: *Journal of Marine Systems* 78 (Nov. 2009), S393–S407. DOI: 10.1016/j.jmarsys.2009.01.037.

[36] Hans Christian Woithe and Ulrich Kremer. “A programming architecture for smart autonomous underwater vehicles”. In: *2009 IEEE/RSJ International Conference on Intelligent Robots and Systems*. IEEE, Oct. 2009. DOI: 10.1109/iros.2009.5354098.

[37] Lin Xiao, J. C. Alves, N. A. Cruz, and J. Jouffroy. “Online speed optimization for sailing yachts using extremum seeking”. In: *2012 Oceans*. IEEE, Oct. 2012. DOI: 10.1109/oceans.2012.6404876.

[38] Yanwu Zhang, J G Bellingham, M Godin, J P Ryan, R S McEwen, B Kieft, B Hobson, and T Hoover. “Thermocline tracking based on peak-gradient detection by an autonomous underwater vehicle”. In: *OCEANS 2010 MTS/IEEE SEATTLE*. IEEE, Sept. 2010. DOI: 10.1109/oceans.2010.5664545.

[39] Yanwu Zhang, J. G. Bellingham, M. A. Godin, and J. P. Ryan. “Using an Autonomous Underwater Vehicle to Track the Thermocline Based on Peak-Gradient Detection”. In: *IEEE Journal of Oceanic Engineering* 37.3 (July 2012), pp. 544–553. DOI: 10.1109/joe.2012.2192340.